

Syracuse University

SURFACE

Dissertations - ALL

SURFACE

December 2014

A STUDY FOR THE PROPAGATION OF ELECTROMAGNETIC WAVES OVER IMPERFECT GROUND PLANES BASED ON SCHELKUNOFF INTEGRALS

Walid Mohamed Galal Dyab
Syracuse University

Follow this and additional works at: <https://surface.syr.edu/etd>



Part of the [Engineering Commons](#)

Recommended Citation

Dyab, Walid Mohamed Galal, "A STUDY FOR THE PROPAGATION OF ELECTROMAGNETIC WAVES OVER IMPERFECT GROUND PLANES BASED ON SCHELKUNOFF INTEGRALS" (2014). *Dissertations - ALL*. 179. <https://surface.syr.edu/etd/179>

This Dissertation is brought to you for free and open access by the SURFACE at SURFACE. It has been accepted for inclusion in Dissertations - ALL by an authorized administrator of SURFACE. For more information, please contact surface@syr.edu.

Abstract

A new formulation for the analysis of propagation of electromagnetic waves over imperfectly conducting planar surfaces is proposed. The classical approach for the analysis of this problem uses the Sommerfeld formulation. In Sommerfeld formulation, the wave function corresponding to a point source is expanded in terms of the propagation constants of the various waves in the radial direction from the source. This gives rise to the well-known Sommerfeld integrals which are highly oscillatory and slowly-decaying in nature, especially when the source is mounted just on top of a planar boundary between two media of arbitrary conductivity. In addition, the nature of the convergence for these integrals is extremely slow and may not yield stable results. In this dissertation we present an approach, developed originally by Schelkunoff, which expands the wave function in terms of the waves emanating perpendicular to the planar interface, not parallel to it as in Sommerfeld formulation. Expressions are given for both cases of vertical and horizontal electric dipoles on top of a planar interface. The debatable nature of this problem is unavoidable, thus a detailed analytical comparison between the Sommerfeld integrals and the expressions derived here is given. Based on the study given in this dissertation, the true rationale in relating the work of Zenneck and Sommerfeld to the relatively new field of surface plasmons is exposed. A detailed literature study as well as an analytical critique of the field of plasmonics and its relation to Sommerfeld-Zenneck surface waves is presented. Finally, some applications of the new formulation are discussed using numerical simulations.

A STUDY FOR THE PROPAGATION OF
ELECTROMAGNETIC WAVES OVER IMPERFECT GROUND PLANES
BASED ON SCHELKUNOFF INTEGRALS

By

Walid Mohamed Galal Dyab
B.Sc. Alexandria University, 2003
M.Sc. Alexandria University, 2007

DISSERTATION

Submitted in partial fulfillment of the requirements for the
degree of Doctor of Philosophy in Electrical and Computer Engineering
in the Graduate School of Syracuse University

December 2014

Copyright 2014 Walid Mohamed Galal Dyab

All Rights Reserved

Acknowledgment

The author is grateful to the Graduate School of Syracuse University for offering him a three-year fellowship to pursue his graduate studies. The author is also thankful to the EECS department of L. C. Smith College of Engineering and Computer Science for offering him Graduate and Teaching Assistantship during the last few years.

I'd like to thank my advisor, Prof. Tapan Sarkar, for his continuous support and advice. His experience helped me through the years to overcome a lot of difficulties and to keep going through the long path of the PhD study.

Special thanks go to Prof. Jay K. Lee who taught me many electromagnetics courses which significantly increased my knowledge in this field.

The author is thankful to his exam committee members, Dr. Bart Farell, Dr. Jay K. Lee, Dr. Carlos Hartmann, Dr. Tomislav Bujanovic and Dr. Mustafa Gursoy.

The author is grateful to all of his colleagues in the CEM lab. Special thanks go to Mr. Mohammad Abdallah with whom I had a lot of fruitful discussions. I'd like also to thank all of my coauthors who helped me publish my work in scientific journals, especially, Prof. Magdalena Salazar-Palma who always supported me with useful critique and comments.

I'd like to thank Prof. Hassan Elkamchouchi of Alexandria University, Alexandria, Egypt, who advised me during my M.Sc. studies.

Before and after all, the author is thankful to his Lord and creator, ALLAH, to whom we belong and to whom we shall return.

To my parents...

Table of Contents

Abstract	i
Acknowledgment	iv
Table of Contents	v
List of Figures	viii
1 Introduction and Motivation	1
1.1 A Thought Experiment.....	4
1.2 Controversial Sommerfeld Integrals	6
1.3 Dissertation Organization.....	7
2 Schelkunoff Integrals for Vertical Dipoles	10
2.1 Introduction	10
2.2 Schelkunoff Formulation.....	13
2.3 Computational Comparison.....	16
2.4 Green's Function	22
2.5 Conclusion.....	27
3 Schelkunoff Integrals for Horizontal Dipoles.....	29
3.1 Introduction	29
3.2 Schelkunoff Formulation for Horizontal Dipoles	31
3.3 Features of Schelkunoff Integrals and Some Useful Expressions.....	36
3.4 Numerical Examples	38
3.5 Conclusion.....	48
4 A Comparison between Sommerfeld and Schelkunoff Formulations	50

4.1	Introduction	50
4.2	Anatomy of Sommerfeld and Schelkunoff Integrals.....	51
4.3	Formulations for the half-space problem	58
4.4	Numerical Analysis of the Half-Space Problem	68
4.5	Conclusion.....	78
5	Surface Waves versus Surface Plasmons.....	80
5.1	Introduction	81
5.2	Evolution of the word Plasmons	83
5.3	Evolution of the term Sommerfeld-Zenneck Wave	89
5.4	Examining the theoretical basis of the Sommerfeld Pole	92
5.5	Physical visualization of the problem	97
5.6	Conclusion.....	100
6	Applications of Schelkunoff Formulation	101
6.1	Regeneration of Okumura's Data.....	101
6.2	A Distinction between Various Types of Surface Waves.....	105
6.3	Absence of Surface Waves/Plasmons at Terahertz Frequencies.....	111
7	Summary, Conclusion and Future Work	115
7.1	Summary and Conclusion	115
7.2	Future Work	119
	Appendix A: Proof of the Schelkunoff Identity.....	120
	Appendix B: Validation of the Vertical Dipole Formulation	124
	Appendix C: Validation of the Horizontal Dipole Formulation	127

Appendix D: Sommerfeld Formulation for Horizontal Dipoles	133
Appendix E: Derivation of the Boundary Conditions for the Horizontal Dipole Case ..	135
References.....	137
Biography.....	141

List of Figures

Fig. 1.1 Lake View at the city of Chicago, IL, USA, showing the famous Willis tower with its top mounted antennas, and the city lights and their reflections on the surface of Lake Michigan. Picture is available at: http://jessica-joy.deviantart.com/art/Chicago-lights-64177963 . The figure is to visualize the famous Sommerfeld half-space problem .	2
Fig. 2.1 Geometry of the problem of a vertical dipole over imperfect ground plane.	11
Fig. 2.2 Decomposition of Spherical waves into plane waves according to the two different formulations.	15
Fig. 2.3 Comparison of the numerical behavior of the complex integrands of the Schelkunoff and the Sommerfeld formulation for different radial and vertical distances from the source normalized to the wavelength, w	18
Fig. 2.4 Comparison of the numerical integration using Schelkunoff and Sommerfeld formulations in terms of accuracy and time for calculations, for different radial and vertical distances from the source normalized to the wavelength, w	18
Fig. 2.5 Illustration of the suitable regions for Sommerfeld and Schelkunoff formulations.	21
Fig. 2.6 Real and imaginary parts of the Reflection coefficients for Sommerfeld and Schelkunoff formulations.....	25
Fig. 3.1 Geometry of the problem of a horizontal dipole over imperfect ground plane. ...	30
Fig. 3.2 A comparison between the integrands of Schelkunoff and Sommerfeld formulations: (a) The main (bounded) part of the contour: ξ (or λ) $< k_1$, or equivalently	

$\beta' : 0 \rightarrow \pi / 2$, (b) The tail (unbounded) part of the contour ξ (or λ) $> k_1$ or equivalently	
$\beta'' : 0 \rightarrow \infty$	40
Fig. 3.3 A comparison between the integrands on the tail part of the contour for a horizontal separation of 10m : (a) Schelkunoff (b) Sommerfeld.....	41
Fig. 3.4 A comparison between the integrands on the tail part of the contour for a horizontal separation of 100m : (a) Schelkunoff (b) Sommerfeld.....	41
Fig. 3.5 A comparison between the results obtained using Schelkunoff and Sommerfeld integrals for the case of seawater where each of the source and field points is 10 m high from the interface	43
Fig. 3.6 A comparison between the results obtained using Schelkunoff and Sommerfeld integrals for the case of urban ground where each of the source and field points is 5 m high from the interface.....	43
Fig. 3.7 The calculated integral of g_{sH} using both Sommerfeld and Schelkunoff formulations. The horizontal and vertical distances are normalized to the wavelength w	46
Fig. 3.8 Time elapsed to calculate the values of Fig. 3.7 for $(z+h)/w=0.1$. The horizontal and vertical distances are normalized to the wavelength w	46
Fig. 3.9 Time elapsed to calculate the values of Fig. 3.7 for $(z+h) / w = 1$. The horizontal and vertical distances are normalized to the wavelength w	47
Fig. 3.10 Time elapsed to calculate the values of Fig. 3.7 when $(z+h) = 0$	47
Fig. 4.1 Mapping of the real axis of λ in different complex planes : (a) λ - plane , (b) ξ - plane , (c) α - plane , (d) β - plane	54
Fig. 4.2 Mapping of the real axis of ξ in different complex planes : (a) λ - plane , (b) ξ - plane , (c) α - plane , (d) β - plane	55

Fig. 4.3 Representation of the integrands in the complex λ -plane (a) and the complex ξ -plane (b) for the case of $k_1 = 1$. The color bar is in degrees and represents the phase angle of the integrands. The contour lines in black represent the lines of constant magnitudes of the integrands. 56

Fig. 4.4 Representation of the integrands in the complex λ -plane (a) and the complex ξ -plane (b) for the case of $k_1 = 1 - j0.25$. The color bar is in degrees and represents the phase angle of the integrands. The contour lines in black represent the lines of constant magnitudes of the integrands. 56

Fig. 4.5 Application of Cauchy's theorem in the λ -plane (a) and the complex ξ -plane (b). 57

Fig. 4.6 Numerical plot of the reflection coefficient function in: (a) the complex λ -plane, and (b) the complex ξ -plane. 62

Fig. 4.7 Application of the Cauchy's theorem on the integrals that include the reflection coefficient function in: (a) the complex λ -plane, and (b) the complex ξ -plane. 65

Fig. 4.8 Numerical comparison between Schelkunoff and Sommerfeld formulations for a vertical electric dipole over urban ground, $z+h=100$ wavelengths: (a) The secondary part of the vector potential, (b) The total magnitude of the vector potential, (c) time to numerically calculate the integrals, (d) the tail-to-main ratio. 70

Fig. 4.9 Numerical comparison between Schelkunoff and Sommerfeld formulations for a vertical electric dipole over urban ground, $z+h=1$ wavelengths: (a) The secondary part of the vector potential, (b) The total magnitude of the vector potential, (c) time to numerically calculate the integrals, (d) the tail-to-main ratio. 71

- Fig. 4.10 Numerical comparison between Schelkunoff and Sommerfeld formulations for a vertical electric dipole over a very good conductor, $z+h=1$ wavelengths: (a) The secondary part of the vector potential, (b) The total magnitude of the vector potential, (c) time to numerically calculate the integrals, (d) the tail-to-main ratio..... 72
- Fig. 4.11 Numerical comparison between Schelkunoff and Sommerfeld formulations for a vertical electric dipole over a very good conductor, $z+h=0.1$ wavelengths: (a) The secondary part of the vector potential, (b) The total magnitude of the vector potential, (c) time to numerically calculate the integrals, (d) the tail-to-main ratio..... 73
- Fig. 4.12 Numerical comparison between Schelkunoff and Sommerfeld formulations for a vertical electric dipole over a conducting ground, $\sigma = 10^4$ S/m, $z+h=0.1$ wavelengths: (a) The secondary part of the vector potential, (b) The total magnitude of the vector potential, (c) time to numerically calculate the integrals, (d) the tail-to-main ratio. 74
- Fig. 4.13 Absolute value of the error in dB as compared to the absolute value of the result of Schelkunoff formulation. Ground parameters of $\epsilon_r = 4$ and $\sigma = 0.002$ S/m . The vertical and horizontal axes are normalized to the wavelength w 75
- Fig. 4.14 Absolute value of the error in dB as compared to the absolute value of the result of Schelkunoff formulation for the horizontal dipole. Ground parameters of $\epsilon_r = 10$ and $\sigma = 5$ S/m . The vertical and horizontal axes are normalized to the wavelength w 76
- Fig. 4.15 Absolute value of the error in dB as compared to the absolute value of the result of Schelkunoff formulation for the horizontal dipole. Ground parameters of $\epsilon_r = 81$ and $\sigma = 5$ S/m . The vertical and horizontal axes are normalized to the wavelength w 76

Fig. 4.16 Absolute value of the error in dB as compared to the absolute value of the result of Schelkunoff formulation for the vertical dipole. Ground parameters of $\epsilon_r = 10$ and $\sigma = 3 \text{ S/m}$. The vertical and horizontal axes are normalized to the wavelength w	77
Fig. 4.17 Absolute value of the error in dB as compared to the absolute value of the result of Schelkunoff formulation for the vertical dipole. Ground parameters of $\epsilon_r = 81$ and $\sigma = 5 \text{ S/m}$. The vertical and horizontal axes are normalized to the wavelength w	78
Fig. 5.1 The absolute value (height) and phase in degrees (color-bar) of the denominator of the reflection coefficient in the complex ϵ plane. Riemann surface with horizontal branch cuts.	95
Fig. 5.2 The absolute value (height) and phase in degrees (color-bar) of the denominator of the reflection coefficient in the complex ϵ plane. Riemann surface with vertical branch cuts	96
Fig. 5.3 A visualization of the Sommerfeld problem of two-layer reflection. The figure represents the comparison between the two cases of perfect (left) and imperfect (right) reflectivity.	98
Fig. 5.4 A visualization of the Sommerfeld problem of two-layer reflection. The imperfect reflectivity in this case is due to the roughness of the surface	98
Fig. 6.1 Comparison between the experimental (Okumura et al.) and theoretical predictions (Schelkunoff and Somerfeld formulations) computed through a macro model for predicting propagation path loss in an urban environment at: (a) 453 MHz, (b) 922 MHz, (c) 1920 MHz.....	105
Fig. 6.2 Plot of the transverse component of the reflected fields at 100 m from the source.	110

Fig. 6.3 Measurement setup of the work presented in [30] in search of the surface waves at THz frequency.....	112
Fig. 6.4 Plot of the transverse component of the reflected fields as a function of the radial distance from the source.	113
Fig. 6.5 Plot of the transverse component of the reflected fields as a function of the vertical distance from the interface at 0.4 THz.....	114
Fig. 6.6 Plot of the transverse component of the reflected fields as a function of the vertical distance from the interface at 0.3 THz.....	114

1 Introduction and Motivation

No doubt that one of the most important scientific discoveries in the history of mankind is the discovery of the relation between light, electricity and magnetism. The understanding of the fact that light is a visible electromagnetic wave opened the way for the exploitation of the useful benefits of the invisible part of the spectrum, which we call now radio-waves. Based on this fact, when one comes across a very exciting natural phenomenon like the one shown in Fig. 1.1, the following questions should arise:

1. What is the propagation mechanism by which light reaches the viewer's eye generating this colorful images on the surface of the lake?
2. What is the difference between the images seen in Fig. 1.1 and the case one can imagine if the surface of the water is replaced by a perfect mirror?
3. If one is standing on the other side of the lake, where the light sources are located, and looking towards the lake, what would be the view in this case?
4. If radio waves are visible, what would one expect to see from the radiation of the Willis tower (tallest building in Fig. 1.1) antennas which are mostly radiating in the VHF-UHF band?
5. Is there any available software that can simulate this situation to give the expected length and intensity of the elongated images of the light sources and the radio-waves antennas?
6. Is this propagation mechanism fully exploited in telecommunications?



Fig. 1.1 Lake View at the city of Chicago, IL, USA, showing the famous Willis tower with its top mounted antennas, and the city lights and their reflections on the surface of Lake Michigan. Picture is available at: <http://jessica-joy.deviantart.com/art/Chicago-lights-64177963>. The figure is to visualize the famous Sommerfeld half-space problem

To answer all of those questions one should revisit the very famous Sommerfeld problem. In 1909, Sommerfeld published an eloquent paper about the propagation of electromagnetic waves over the earth's surface. That was one of the earliest scientific attempts to explain how electromagnetic waves radiated from a source can reach to a receiver which is beyond the horizon, a situation like what happened in Marconi's first transatlantic transmission. On revisiting this famous problem, one will find the following facts:

1. Sommerfeld's solution of the problem generated one of the most celebrated controversies in the last century.
2. After more than hundred years since Sommerfeld, the debate about his solution has not been settled yet.

3. The most debatable part in the problem is about the existence of what is called Sommerfeld-Zenneck surface wave in the total radiation of elementary sources over ground planes.
4. The so called Sommerfeld-Zenneck wave arises from a debatable singularity of the integrands that appear in Sommerfeld's solution.
5. Despite the discovery of the Kenneli-Heaviside layer (the ionosphere) and its role in the propagation of electromagnetic waves over the horizon, the interest in the Sommerfeld problem and the associated surface waves has never been demolished.

Just to give a glimpse about the Sommerfeld controversy, we mention one example. After about fifty years from the first publication of Sommerfeld [1], Banos wrote a complete book in an attempt to settle the debate once and for all [2]. In his book, Banos reported most of the work on the problem up to the sixties of the twentieth century. He advocated for the existence of *surface waves* in the dipole radiation over imperfect grounds. He also affirmed the famous *sign error* that Sommerfeld did in his initial analysis. Fifty years later (almost a hundred years after Sommerfeld's paper), Collin published a lucid paper supported with rigorous mathematical analysis to prove that the famous *sign error* of Sommerfeld is actually a myth and *surface waves* do not exist in the dipole radiation over imperfect ground planes [3]!

Those facts mentioned above, with no doubt, had negative effects which were represented, for example, as a total avoidance of the problem in the design of vital commercial communication systems like cellular networks.

1.1 A Thought Experiment

Due to the analogy between visible light and radio-waves, used in cellular networks for example, one can carry out the following thought experiment. Consider that the light sources shown in Fig. 1.1 are base station antennas of a cellular system. Imagine that the information to be transmitted by those base stations is whether the transmitter is on or off. Try to compare the two following situations: The situation which is depicted in Fig. 1.1, and the other situation where the lake surface is replaced by a perfect mirror. Note that in the later situation, the image size will be exactly as the source size. Consider the following question: Which of the two situations facilitates the spread of the information about the state of the light source whether it is on or off?

It is quite obvious that the existence of an imperfect surface helps the information to be spread out more than the perfect reflector. This is because the image of a point source on top of a perfectly reflecting ground is of the same size as the source. On the other hand, the image of a point source on top of an imperfectly reflecting ground is a line source of theoretically infinite extent. Although this fact was mentioned explicitly by Van der pol in 1935 [4], very few researches mention this analogy.

In fact, the problem of estimating the path loss exponent related to the electromagnetic wave propagation in different environments is a well-known problem. Due to its great importance to wireless systems design, this problem has been tackled by numerous researchers and explained in many text books as well. Conventionally, in wireless communications text books, such as [5], this problem is tackled first by explaining the two-ray model on a flat perfectly conducting earth. After explaining the two-ray model, empirical models are usually presented, such as the very famous

Okumura-Hata model [6]. Although empirical models have been extensively applied with good results, they suffer from some disadvantages. The main disadvantage is that empirical models provide no physical insight into the mechanism by which propagation occurs. This is besides that they are limited to the environments and parameters used in measurements. So to find more satisfactory models, researchers usually go into one of two paths. Either they go to find more sophisticated physical models which encounter other propagation mechanisms such as diffraction, scattering and ray tracing [6], or they go into statistical modeling [5]. To clarify this more, we quote a very interesting conclusion from [6]:

*“Although the plane earth model has a path loss exponent close to that observed in actual measurements (i.e. path loss exponent of 4), the simple physical situation it describes is rarely applicable in practice. The mobile is always almost operated (at least in macrocells) in situations where it does not have a line-of-sight path to either the base station or to the ground reflection **point**, so the two-ray situation on which the plane earth model relies is hardly ever applicable. To find a more satisfactory physical propagation model, we examine diffraction as a potential mechanism”.*

In our opinion, instead of examining diffraction as a potential mechanism or going to statistical modeling, the situation shown in Fig. 1.1 directly implies that the physical model of propagation in the cellular environment described above should be considered by solving the Sommerfeld problem. This will not only give us a physical insight into how waves propagate in mobile communications, but also it should answer the question of why smart antennas and beamforming are not very successful in cellular communications, despite all of the research efforts done in those fields [7]- [8]. If the real

scenario of propagation is something similar to what we see in Fig. 1.1, then application of ray tracing for channel modeling should really be questioned. In Fig. 1.1, which ray should be traced from any of the light sources to the lens of the camera. There is no one *reflection point* on the water surface to trace the reflected ray, instead there are infinite rays to be traced, though we have only one reflector. This represents a great visualization for the Sommerfeld problem.

Following the line of thoughts mentioned here in this dissertation, initial attempts have been already made to apply the analysis of the Sommerfeld problem in cellular communications [9]- [10]. However, more efforts are still needed to provide the cellular network designer by an electromagnetic simulator that incorporates the propagation mechanism shown in Fig. 1.1. Mainly, what is needed is to find the most efficient, practical and accurate way to calculate the reflected electromagnetic fields based on the Sommerfeld formulation. It is not a trivial task to find this efficient and accurate way due to the vast amount of work reported in the literature and the associated debate mentioned earlier in this chapter.

1.2 Controversial Sommerfeld Integrals

After Sommerfeld showed his formulation given in [1], many researchers have tried to find different other forms for the Sommerfeld integrals. Those different trials generated the celebrated controversy, especially about the singularity that the integrand might have and associating a surface cylindrical wave arising from that singularity. The details of the debate can be found in countless publications which give different explanations from different perspectives such as [2]- [3]. However, the important thing that we want to mention here is that the work of Schelkunoff [11] is rarely mentioned in

any of the work on Sommerfeld problem. For example, in Banos's attempt to settle the Sommerfeld debate [2], he did a collective comparison between all of the approaches done by all researchers on the subject in an attempt to settle down the debate about Sommerfeld's solution. Although, Banos never mentioned the work of Schelkunoff, even though the latter had published his book [11] twenty years earlier. We find the work of Schelkunoff and his different formulation of the same exact problem are quite revealing. For example, Schelkunoff stated explicitly that for the case of a TM (Transverse Magnetic) wave, the integrands of Sommerfeld can never have a singularity. Schelkunoff said: "*For transverse magnetic waves the characteristic wave impedance is either a resistance or negative reactance; hence this equation can have no roots, the integrands can have no poles, and there are no surface waves. This conclusion is contrary to that reached by early writers on the subject.*" [11, p. 430]. The most interesting part of Schelkunoff's work is that his integrals are performed over the vertical component of the propagation vector rather than the horizontal component.

1.3 Dissertation Organization

This dissertation is organized as follows: In chapter 2, the problem of radiation of a vertical electric dipole on top of a planar interface between free space and a medium of arbitrary parameters is studied thoroughly. The original procedure of Sommerfeld is studied and the source of the Sommerfeld integral tails problem is explained from a physical point of view. In the same chapter, an alternative procedure is derived based on the Schelkunoff integrals rather than the Sommerfeld integrals. The potential of having more numerical stability using the new integrals is illustrated with numerical examples. In Chapter 3, the new integrals are used to derive the expressions for the horizontal

electric dipole case. This case is a little more complicated than the case of chapter 2 because the vector potential of the reflected fields is not only oriented in the horizontal direction parallel to the dipole, but also has a vertically oriented component which gives the dominant part of the field in the far field. Detailed expressions with derivations are given in that chapter, supported also with numerical examples.

Due to the unavoidable debatable nature of the problem, it was so important to dedicate a complete chapter for studying the results of the Sommerfeld integrals as compared to the results of the expressions derived in this dissertation based on Schelkunoff integrals. This comparison is done from an analytical point view using complex integration theorems and is given in Chapter 4. In addition, the analytical results are supported with numerical examples. As explained earlier in this introduction, the understanding of the propagation mechanism in cellular networks is one of the most important motivating targets in this dissertation, most of the numerical examples are given for parameters that are practically suitable for cellular networks.

Based on the analysis given in Chapter 4, it is important to have a detailed study of the Sommerfeld pole which is the claimed source of the term “*Sommerfeld-Zenneck surface wave*”. The mathematical origin of this term is explained in Chapter 5. In the light of Schelkunoff integrals given in this dissertation, the truth about the existence/absence of the Sommerfeld pole is exposed based on a new approach. This new approach, which is one of the main contributions of this dissertation, is based on the study of the nature of the Sommerfeld integrands in a complex domain other than the usual domain used in the literature. The analysis given in Chapter 5 also examines the rationale in relating the Sommerfeld pole to the relatively new research field of Surface

Plasmons. The field of Surface Plasmons is an evolving inter-disciplinary area of research in which many researchers relate the physical phenomenon of surface plasmon polaritons to the Sommerfeld pole. Unfortunately, this relation is not based on any scientific evidence and it is becoming more and more elusive because of the already controversial nature of the Sommerfeld problem. Chapter 5 gives an analytical critique of this subject. In chapter 6, the applications in which the new formulation is useful are investigated. Two applications are studied. First, the regeneration of Okumura's experimental data is presented. Second the absence of surface waves/plasmons at terahertz frequencies is proved based on numerical simulations using the new formulation and experimental results published in the literature. Finally the dissertation is summarized and concluded in the last chapter. Five appendixes are given at the end of the dissertation to support some of the mathematical derivations given.

2 Schelkunoff Integrals for Vertical Dipoles

2.1 Introduction

In 1909, Sommerfeld formulated a solution for the radiation from short dipoles over an imperfectly conducting flat earth [1]. His formulation was based on the decomposition of the spherical wave function into an integral of a continuous spectrum of plane waves in the following form:

$$\frac{e^{-jkr}}{r} = \int_0^{\infty} J_0(\lambda\rho) e^{-z\sqrt{\lambda^2 - k^2}} \frac{\lambda}{\sqrt{\lambda^2 - k^2}} d\lambda \quad (2.1)$$

where $r = \sqrt{\rho^2 + z^2}$, ρ and z are the radial and vertical distances, respectively, between the source and the field points. $J_0(x)$ is the zeroth order Bessel function of the first kind. The left-hand side of (2.1) represents the Green's function for a source in a homogeneous medium whose propagation constant is k . The right-hand side of (2.1) represents the continuous spectrum of plane wave decomposition of a spherical wave. From (2.1), it is seen that Sommerfeld characterized each of the plane waves by their horizontal (parallel to the boundary) component of the propagation vector, according to:

$$k^2 = k_{\rho}^2 + k_z^2 = \lambda^2 + k_z^2 \quad (2.2)$$

where λ is the propagation constant in the ρ -direction. It is important to note here that the integration in (2.1) can be decomposed mathematically into two parts: one from 0 to k and the other part from k to infinity. Physically, the main difference between the two parts of the integral is that in the first one, the integrand represents homogeneous waves whose horizontal and vertical components of the propagation vector are both smaller than

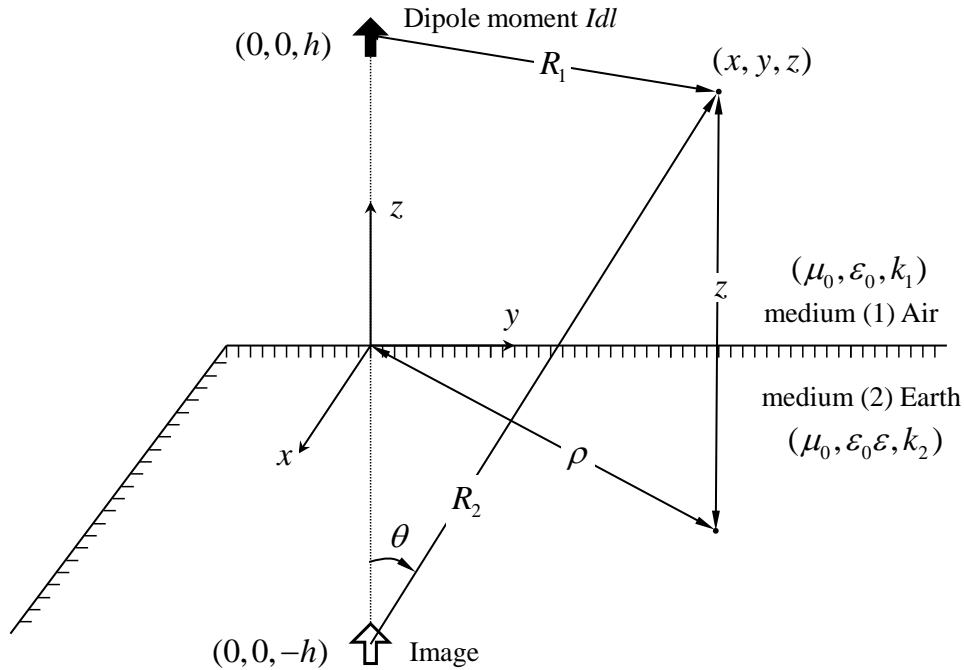


Fig. 2.1 Geometry of the problem of a vertical dipole over imperfect ground plane.

the propagation constant of the medium, k . Whereas in the second part (from k to infinity) the integrand represents slow inhomogeneous plane waves. Those waves have the component k_ρ (or λ) which is larger than the propagation constant of the medium, k . Thus, they are called slow waves, and from (2.2), we note that the vertical component, k_z , of those waves is purely imaginary, thus they are inhomogeneous plane waves [12].

If the source of the waves in (2.1) is placed at a height, h , over a homogenous medium filling the half-space $z < 0$, as shown in Fig. 2.1, each of those plane waves will be reflected by a specific reflection coefficient which depends on its angle of incidence. Thus, one can write the wave function (Π) associated with the reflected part of the fields according to the Sommerfeld formulation as follows:

$$\Pi_{1z}^{ref} = \int_0^\infty R(\lambda) J_0(\lambda \rho) e^{-(z+h)\sqrt{\lambda^2 - k^2}} \frac{\lambda}{\sqrt{\lambda^2 - k^2}} d\lambda, \quad z > 0 \quad (2.3)$$

where $R(\lambda)$ is the reflection coefficient for the plane wave whose horizontal component of its propagation vector is λ . The properties of the function $R(\lambda)$ are discussed in more details later in this chapter.

After Sommerfeld introduced this formulation given in (2.3) in 1909, it provided a mechanism for analysis of propagation of electromagnetic waves over real grounds (e.g. earth and sea). However, in the first part of the 20th century, the integrals in (2.3) had to be solved analytically due to a lack of powerful computing machines at that time. One of the major points of confusion in the past literature using the Sommerfeld formulation was the existence of a pole in the function $R(\lambda)$ which on integration may give rise to surface waves. It turns out that such a pole does not exist in spite of what all the authors have described in the past including Sommerfeld [11, p. 430]. In this dissertation, this century old controversy can be cleared up by simply looking at the new expressions as we shall illustrate later on. In the second half of the 20th century, and with the advent of the field of computational electromagnetics, the numerical calculation of the Sommerfeld integrals became of practical interest. However, the challenge that was faced is the numerical computation of that part of the integral which follows a semi-infinite contour going from k to ∞ . Along this contour, the integrand is a Bessel function, $J_0(x)$, which is an oscillating and slowly-decaying function, hence the problem of the integration associated with the tails of the Sommerfeld integrals. In this dissertation, it is shown that the source of this problem is primarily due to the choice that Sommerfeld made when he chose to carry out the integration over the horizontal rather than the vertical component of the propagation vectors, i.e., over λ instead of k_z in (2.2). Therefore, in this chapter, the main objective is to study the effect of that choice and to resolve the whole problem based on

the selection of a different integration variable. In other words, it is required to observe how the integrals in (2.1) and (2.3) will behave if the integration is carried out in terms of the vertical component of the propagation vectors k_z and then provide a physical explanation for the consequences. A new approach to the classical Sommerfeld problem, thus, is one of the unique features of this dissertation. This chapter is organized as follows: In section 2.2, the Schelkunoff integrals are defined and their relationship to the Sommerfeld integrals is given. In section 2.3, a detailed comparison between the numerical behaviors of both types of integrals is shown along with a numerical example. This will show the potential benefits of using the new formulation in integral equation-based solvers. Section 2.4 aims to derive a new Green's function for vertical dipoles over imperfect ground planes based on the new formulation.

2.2 Schelkunoff Formulation

In 1935, Schelkunoff, introduced what he called the modified Sommerfeld integrals [13]. The purpose of this introduction is to obtain a certain integral expressing the fundamental wave function. In his words, *this integral should be suitable to calculate the radiation resistances of small doublets and small loops placed inside infinite hollow cylinders* [13]. Schelkunoff found that the well-known formulation of Sommerfeld for dipoles over imperfect flat earth was not suitable for satisfying the boundary conditions in the case of cylindrical boundaries.

As indicated in the introduction, Sommerfeld formulated the solution by integrating over the horizontal component of the propagation vector, namely λ (or k_ρ), and he wrote the other component k_z in terms of λ as:

$$k_z = j\sqrt{\lambda^2 - k^2} \quad (2.4)$$

which appears in the exponential term in (2.1) and (2.3). The objective now is to integrate the function in terms of the vertical component of the propagation vector instead. By looking at the modified Sommerfeld integral in [13], it is found that Schelkunoff started from an identity which is very similar to (2.1) but has some important differences:

$$\frac{e^{-jkr}}{r} = \frac{2}{\pi} \int_0^{\infty} K_0\left(\rho\sqrt{\xi^2 - k^2}\right) \cos(\xi z) d\xi \quad (2.5)$$

The integral in (2.5) will be named from now on as the Schelkunoff formulation or the proposed formulation. By comparing (2.1) and (2.5) it is seen that the later involves $K_0(x)$, the modified Bessel function of the second kind, which represents a monotonically decaying function for real $\sqrt{\xi^2 - k^2}$ (i.e. $\xi > k$), whereas $J_0(x)$, in (2.1), represents a highly oscillatory integral and decays extremely slowly as its argument increases, for real values of λ .

It is important to note that the Schelkunoff formulation is also based on decomposing the spherical wave into a continuous spectrum of plane waves, but this time the integration in (2.5) is carried out over the vertical component of the propagation vector k_z (or ξ). Thus this formulation is in fact what we are looking for. Even though (2.1) and (2.5) are mathematically identical, numerically (2.5) is more stable and numerically accurate to compute than (2.1). The function, $J_0(x)$, is a slowly decaying oscillatory function, and many researchers over the years have developed methodologies to obtain a more efficient way to deal with the integration of the tails of the Sommerfeld integrals [14]- [15]- [16]. However, when the radial distance from the transmitter

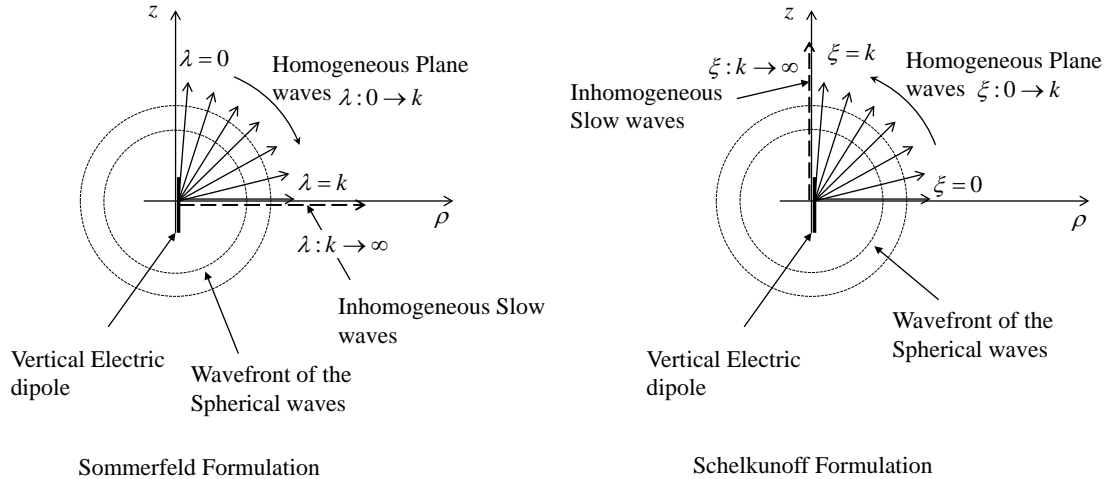


Fig. 2.2 Decomposition of Spherical waves into plane waves according to the two different formulations.

increases by many orders of magnitudes compared to the wavelength, the Sommerfeld integral tails become impossible to evaluate numerically. In this case, the Sommerfeld formulation will generate unstable numerical results [17]. On the other hand, the modified Bessel function, $K_0(x)$, is a very fast-decaying non-oscillatory function, and hence this problem will be nonexistent in the new formulation resulting in a more stable and an accurate characterization of the environment. Thus, it is important now to note the following identity from a mathematical point of view, whereas from a numerical point of view their characterizations are completely different:

$$\frac{2}{\pi} \int_0^{\infty} K_0\left(\rho\sqrt{\xi^2 - k^2}\right) \cos(\xi z) d\xi = \int_0^{\infty} J_0(\lambda\rho) e^{-|z|\sqrt{\lambda^2 - k^2}} \frac{\lambda}{\sqrt{\lambda^2 - k^2}} d\lambda \quad (2.6)$$

A proof of (2.6) is given in Appendix A, which is slightly different than the one given by Schelkunoff in [13].

It is important to note that both of the integrations in (2.6) are carried out along the positive real axis, either for λ or for ξ . The physical interpretation of this mathematical identity is intuitive for the portions of the contour going from 0 to k . However, this is not

the case for the other part of the contour going from k to ∞ ; for the first part, being composed of homogeneous plane waves, while the later part is composed of inhomogeneous plane waves. Hence, the proof given in appendix A is considered to be pertinent.

2.3 Computational Comparison

To illustrate the differences between the two formulations in terms of numerical evaluation, we proceed with an example of a vertical dipole located at the origin in free space. Suppose that we need to calculate the fields for this case numerically.

Assume a small Hertzian dipole oriented along the z -axis and lies at the origin as shown in Fig. 2.2. The Hertz vector potential is given by:

$$\bar{\Pi} = \Pi_z \hat{a}_z \quad (2.7)$$

where Π_z is the solution of:

$$\nabla^2 \Pi + k^2 \Pi = 0 \quad (2.8)$$

That is

$$\bar{\Pi} = P \frac{e^{-jkr}}{r} \hat{a}_z \quad (2.9)$$

where P is a constant that depends on the dipole moment, the frequency of operation, and the medium characteristics. Suppose, it is required to evaluate the function in (2.9) when $z = 0$, i.e., the evaluation of:

$$\frac{e^{-jk\rho}}{\rho} = \int_0^\infty J_0(\lambda\rho) \frac{\lambda}{\sqrt{\lambda^2 - k^2}} d\lambda = \frac{2}{\pi} \int_0^\infty K_0\left(\rho\sqrt{\xi^2 - k^2}\right) d\xi \quad (2.10)$$

First, one should note that the singularities at $\lambda = k$ and $\xi = k$ both represent integrable singularities, which do not introduce any numerical problem. If the numerical

behavior of the integrand is to be studied as a function of the integration variable (λ in case of Sommerfeld and ζ in case of Schelkunoff formulation) for different values of ρ , then one needs to split the contour into two parts: The first part from 0 to k and the second from k to infinity. The differences in the two parts come from the fact that the integration from 0 to k involves the homogeneous waves in the spectrum, whereas the integration from k to infinity involves the slow inhomogeneous plane waves. This implies that in the Sommerfeld formulation, the integration starts over all homogeneous plane waves from those that are propagating in the z -direction ($\lambda = 0$) to those waves which are propagating in the ρ -direction ($\lambda = k$). The other part of the contour (from k to infinity) involves those inhomogeneous waves propagating in the ρ -direction with propagation constants larger than the constant of the medium ($\lambda > k$) and decay exponentially in the z -direction. The same situation holds for Schelkunoff's formulation but with a different orientation. This means that in Schelkunoff's formulation, the integration starts for all homogeneous plane waves from those that are propagating in the ρ -direction ($\zeta = 0$) to those waves which are propagating in the z -direction ($\zeta = k$). The other part of the contour (from k to infinity) involves those inhomogeneous waves propagating in the z -direction with propagation constants larger than the constant of the medium ($\zeta > k$) and decay exponentially in the ρ -direction. This is illustrated pictorially in Fig. 2.2.

The numerical problem now is concentrated only in that part of the integration that is from k to infinity. It is possible to calculate this part of the integration only if the

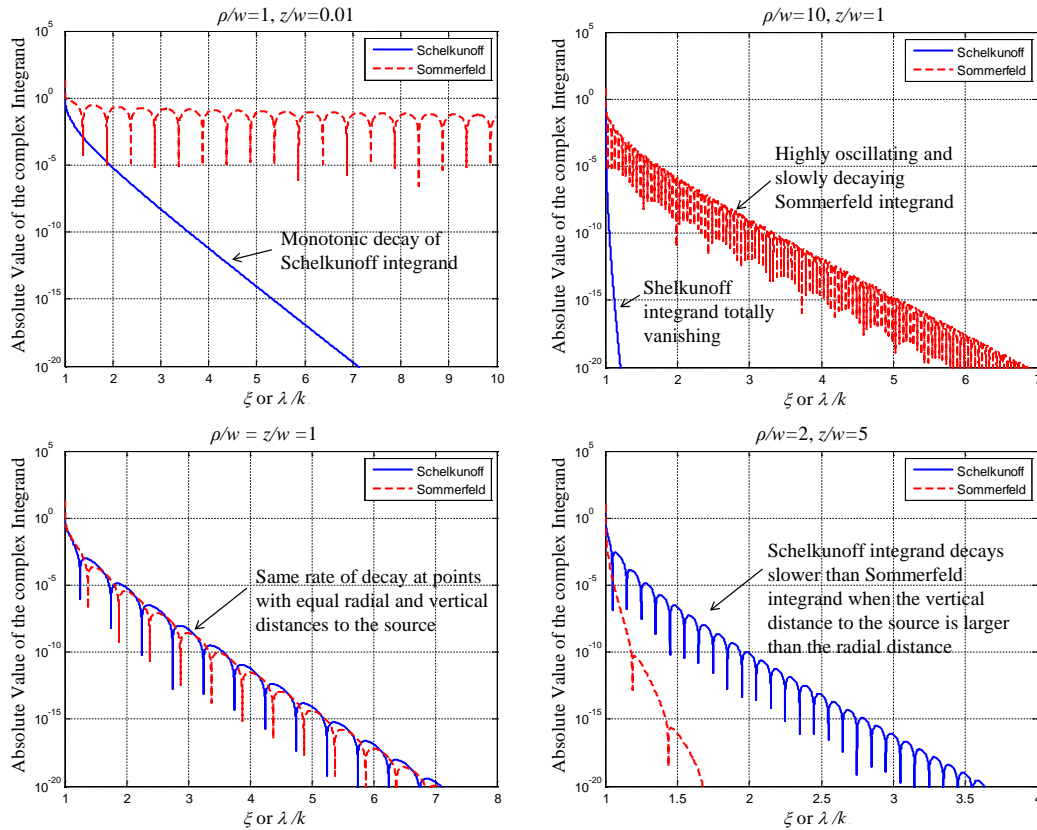


Fig. 2.3 Comparison of the numerical behavior of the complex integrands of the Schelkunoff and the Sommerfeld formulation for different radial and vertical distances from the source normalized to the wavelength, w .

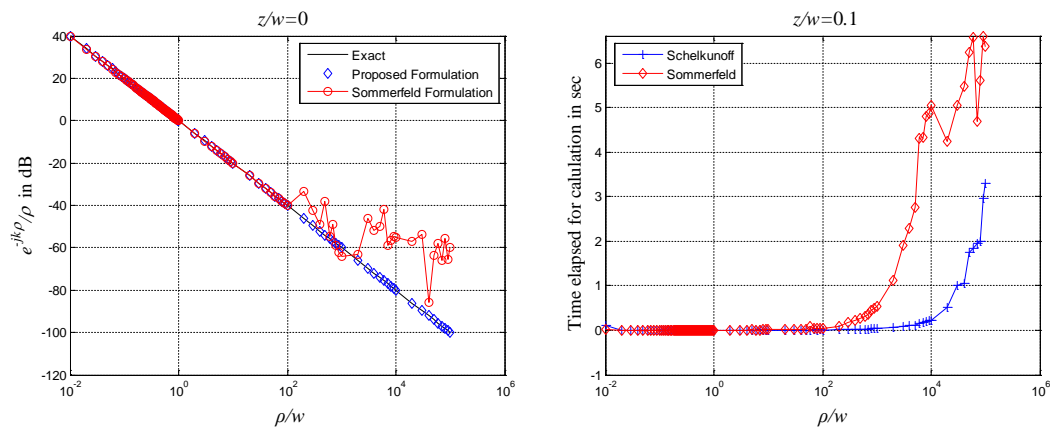


Fig. 2.4 Comparison of the numerical integration using Schelkunoff and Sommerfeld formulations in terms of accuracy and time for calculations, for different radial and vertical distances from the source normalized to the wavelength, w .

integrand decays appropriately as the integration variable tends to infinity. It is well known that the Bessel function, $J_0(x)$, is a slowly-decaying and oscillating function which

makes the integration in the first equality in (2.10) almost impossible to calculate accurately for very large radial distances.

On the other-hand, the integrand in Schelkunoff's formulation, which has to be integrated from k to infinity, is the modified Bessel function, $K_0(x)$, and on the integration path $\xi > k$, it will be of a pure real argument, and so the function $K_0(x)$ will decay exponentially as its argument increases. To illustrate this fact, the absolute value of the integrands in (2.10), or more precisely in (2.6), is plotted in terms of the integration variables and for different values of ρ and z . Fig. 2.3 shows that whenever the radial distance ρ is greater than the vertical distance z , the integrand in the Schelkunoff formulation decays much faster than the integrand in the Sommerfeld formulation and with less oscillation. It also shows that whenever the radial distance is equal to the vertical distance, both integrands decay by the same rate and with the same rate of oscillation. However, the disadvantage of the new Schelkunoff formulation may occur whenever the field point lies at a point whose vertical distance is much larger than the radial distance to the source. If we examine (2.6) once more, we will find that in the Schelkunoff formulation the decay rate depends on the modified Bessel function K_0 only, whereas the frequency of oscillation depends only on the cosine function of argument z . However, in the Sommerfeld formulation the rate of decay depends on both the exponential function in z and the Bessel function in ρ . The same statement applies to the frequency of oscillation; it depends on both the exponential in z and the Bessel function in ρ . Fig. 2.4 shows the accuracy of the calculation using both of the formulations, as well as the time required to perform the numerical integration. Both integrations are computed using the gauss quadrature method of integration [18], and the time shown in Fig. 2.4 is

the time elapsed to calculate the total integral in (2.6). By the total integral we mean both parts going from 0 to k and from k to infinity.

It is interesting to note that on the contour going from 0 to k , both formulations behave identically the same. That part of the integration may take more time for large radial or vertical distances (for both formulations) but since the contour is finite, the accurate calculation of such an integral is always practically possible. In fact, the integrand in the Schelkunoff formulation in this finite part of the contour will be of complex argument, and the K_0 function will be replaced by J_0 and N_0 , the Bessel functions of the first and second kind, respectively. This is shown in Appendix B. The important observation is that on the infinite contour, the integrand in Schelkunoff formulation is always non-oscillatory for small values of z , no matter how large the radial distance is. This characteristic has great potential to facilitate the simulation of electrically large problems including lossy ground planes using integral equation solvers. One example is the calculation of the radar cross section of ships over the surface of the ocean which is very lossy. Such capability is missing in most of the available electromagnetic simulation codes.

The physical explanation for the numerical results that we get from the previous example is actually straightforward. With the aid of Fig. 2.2, and having in mind that the waves which contribute to the tails for the Sommerfeld integrals are the inhomogeneous slow waves in both formulations, we can explain the previous observations as follows:

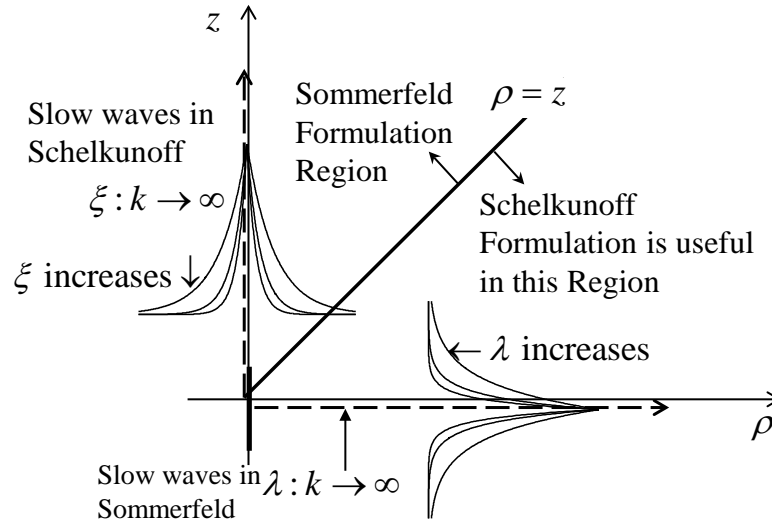


Fig. 2.5 Illustration of the suitable regions for Sommerfeld and Schelkunoff formulations.

2.3.1 Sommerfeld formulation:

As shown in Fig. 2.5, the slow inhomogeneous waves propagate with a phase constant $\lambda > k$ along the ρ -axis, and decay exponentially along the z -axis. So for small values of z those waves have not decayed enough to have their contribution to the total field neglected. For example, at $z=0$, no matter what is the value of λ , those waves would not decay anyway, and we need to take the contribution from all of them into account (till $\lambda=\infty$). On the contrary, as z increases, the field associated with those slow waves decays exponentially depending on z and on the attenuation constant $\sqrt{\lambda^2 - k^2}$, so as λ increases along the contour of integration, those waves decay fast and hence a small portion of the contour is enough to get the total fields accurately.

2.3.2 Schelkunoff formulation:

On the other hand, the slow inhomogeneous waves in the Schelkunoff formulation are waves with propagation constant $\xi > k$ propagating along the z -axis, and decay exponentially along the ρ -axis. So for low values of ρ those waves have not decayed

enough to have their contribution to the total field neglected. While as ρ increases, the field associated with those slow waves decays exponentially along the ρ -direction and depending on the attenuation constant $\sqrt{\xi^2 - k^2}$, so as ξ increases, those waves decay faster and hence a shorter amount of the contour is enough to get the total fields accurately. This is illustrated in Fig. 2.5.

In most practical cases, we are interested in the fields near the surface of the earth. That was the primary reason for which Sommerfeld formulated his solution in the first place. However, as we see from Fig. 2.3, Fig. 2.4 and Fig. 2.5, the Sommerfeld formulation is not suitable for numerical calculations of the fields in regions close to the horizontal axis. It is quite unfortunate that for the last 100 years, we have been using the Sommerfeld formulation in the wrong region. Furthermore, it is not only the value of ρ and z that determines which of the formulations is more suitable than the other; it is also the orientation of the boundary that affects the numerical behavior of the two approaches as explained in the following section.

2.4 Green's Function

As seen in Fig. 2.4, the Schelkunoff formulation has strength for small values of z whereas for large values of z , both formulations will perform equally well. In addition, for small values of ρ , the Sommerfeld formulation is suitable, but for medium and large values of ρ , the Schelkunoff formulation is really desirable. Given the usefulness of the Schelkunoff formulation, it is worthwhile to formulate a new solution for the radiation of Hertzian vertical dipole over an imperfectly-conducting ground plane. This solution should be used in the regions when it is more useful as pointed out earlier.

2.4.1 Vertical Antenna above arbitrary ground:

The new formulation based on Schelkunoff's expansion is now used to analyze antennas over a planar imperfect ground, as we are interested in the nature of the fields far away from the transmitting antenna. In this case, we choose a Hertzian vertical dipole over a planar imperfect ground plane of relative complex permittivity ϵ as shown in Fig. 2.1. The Hertz vector potentials can be formulated as follows:

$$\Pi_{1z} = \Pi_1^{prim} + \Pi_1^{sec} \quad (2.11)$$

$$\& \quad \Pi_{2z} = \Pi_2^{sec} \quad (2.12)$$

where the subscript 1 or 2 represent the media in which the potential is calculated. The legend z characterizes the z - component. The superscript *prim* represents the direct contribution from the source when it is located in free space and the *sec* represents the contribution from the source due to the presence of the ground. A harmonic time variation of the form $\exp(j\omega t)$ is assumed throughout the analysis.

$$\Pi_1^{prim} = \frac{2}{\pi} \int_0^{\infty} K_0 \left(\rho \sqrt{\xi^2 - k_1^2} \right) \cos(\xi(z-h)) d\xi \quad (2.13)$$

$$\Pi_1^{sec} = \frac{2}{\pi} \int_0^{\infty} R(\xi) K_0 \left(\rho \sqrt{\xi^2 - k_1^2} \right) \cos(\xi(z+h)) d\xi \quad (2.14)$$

Now we have to assume a form for the solution in the second medium as

$$\Pi_2^{sec} = \frac{2}{\pi} \int_0^{\infty} T(\xi) K_0 \left(\rho \sqrt{\xi^2 - k_2^2} \right) \cos(\xi_2 z - \xi h) d\xi \quad (2.15)$$

For the form in (2.15) to be correct, it has to satisfy the equation $\nabla^2 \Pi + k_2^2 \Pi = 0$, and satisfy the boundary conditions at $z = 0$, namely

$$\frac{\partial}{\partial z} \Pi_{1z} = \frac{\partial}{\partial z} \Pi_{2z} \quad (2.16)$$

$$\Pi_{1z} = \varepsilon \Pi_{2z} \quad (2.17)$$

Following the procedure shown in Appendix B to solve for the functions $R(\xi)$ and $T(\xi)$, one obtains the total solution as:

$$\Pi_{1z} = \frac{e^{-jk_1 R_1}}{R_1} + \Pi_{1z}^{ref} \quad (2.18)$$

where

$$\begin{aligned} \Pi_{1z}^{ref} = & \frac{2}{\pi} \int_0^{k_1} \frac{\varepsilon \xi - \sqrt{\xi^2 - (1-\varepsilon)k_1^2}}{\varepsilon \xi + \sqrt{\xi^2 - (1-\varepsilon)k_1^2}} K_0 \left(j \rho \sqrt{k_1^2 - \xi^2} \right) \cos(\xi(z+h)) d\xi \\ & + \frac{2}{\pi} \int_{k_1}^{\infty} \frac{\varepsilon \xi - \sqrt{\xi^2 - (1-\varepsilon)k_1^2}}{\varepsilon \xi + \sqrt{\xi^2 - (1-\varepsilon)k_1^2}} K_0 \left(\rho \sqrt{\xi^2 - k_1^2} \right) \cos(\xi(z+h)) d\xi \end{aligned} \quad (2.19)$$

$$\Pi_{2z} = \frac{4}{\pi} \int_0^{\infty} \frac{\xi}{\varepsilon \xi + \sqrt{\xi^2 - (1-\varepsilon)k_1^2}} K_0 \left(\rho \sqrt{\xi^2 - k_1^2} \right) \cos(\xi_2 z - \xi h) d\xi \quad (2.20)$$

where $\xi_2^2 = \xi^2 - k_1^2 + k_2^2$, ε is the relative complex permittivity of the ground, k_1 and k_2 are the propagation constants of medium 1 and 2 respectively. The singularity of the function $K_0(x)$ can easily be eliminated using the transformation:

$$\xi = k_1 \sin \beta = k_1 \sin(\beta' + j\beta'') \quad (2.21)$$

where $\beta = \beta' + j\beta''$ is a dummy complex integration variable. Thus, we can rewrite (2.19) as follows:

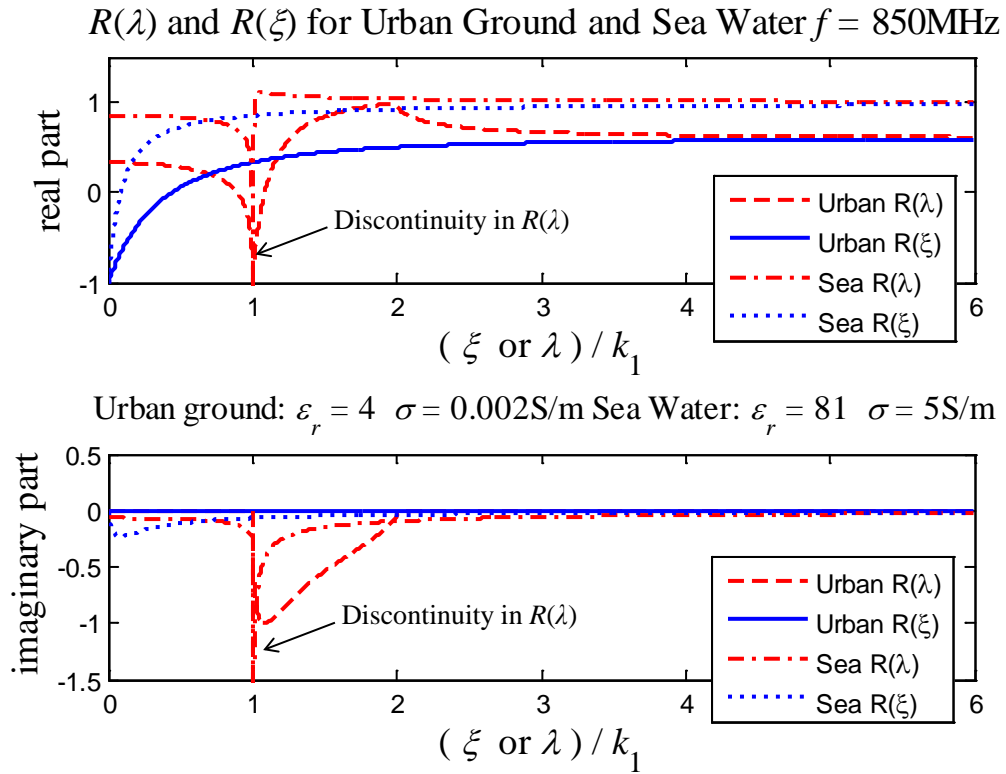


Fig. 2.6 Real and imaginary parts of the Reflection coefficients for Sommerfeld and Schelkunoff formulations.

$$\begin{aligned}
 \Pi_{1z}^{ref} = & \frac{2}{\pi} \int_0^{\pi/2} \frac{\epsilon \sin \beta' - \sqrt{\epsilon - \cos^2 \beta'}}{\epsilon \sin \beta' + \sqrt{\epsilon - \cos^2 \beta'}} \\
 & \left[k_1 \cos \beta' K_0(jk_1 \rho \cos \beta') \right] \cos(k_1(z+h) \sin \beta') d\beta' \\
 & + \frac{2}{\pi} \int_0^{\infty} \frac{\epsilon \cosh \beta'' - \sqrt{\epsilon + \sinh^2 \beta''}}{\epsilon \cosh \beta'' + \sqrt{\epsilon + \sinh^2 \beta''}} \\
 & \left[k_1 \sinh \beta'' K_0(k_1 \rho \sinh \beta'') \right] \cos(k_1(z+h) \cosh \beta'') d\beta''
 \end{aligned} \tag{2.22}$$

The advantage of the new methodology advocated here is illustrated by the second part of the right-hand side of (2.22). This part represents the integration over an infinite contour but, at the same time, the integrand is decaying dramatically as the integration variable increases. Also as ρ increases to be of a few kilometers, which is

more practical, the integrand decays faster and faster. Thus the problem that has plagued the electromagnetic community for decades related to the evaluation of the oscillatory Sommerfeld integrals for large values of ρ is totally eliminated for most of the practical cases.

2.4.2 Features of the new integrands

Comparing the reflection and transmission coefficients of the Sommerfeld and Schelkunoff formulations is quite revealing as will be seen in the following discussion. The comparison is shown in Fig. 2.6.

It is clear from Fig. 2.6 that none of the reflection coefficients (either $R(\zeta)$ or $R(\lambda)$ given in Appendix B) has any poles along the whole integration path. Hence the pole which gives rise to the surface waves and its associated controversies does not exist! What is important to note that this is true for both the Sommerfeld and the Schelkunoff formulation! This is stated by Schelkunoff in his book [11, p. 430]: He categorically states that: *“the denominator of the term inside the brackets in equation (B.18 of this dissertation) can have no roots, the integrals can have no poles, and there are no surface waves. This conclusion is contrary to that reached by early writers on the subject”*. More details about this topic can be found in [9]- [10]. The interesting observation, however, is the discontinuity that $R(\lambda)$ goes through around $\lambda = k_1$, which is non-existent in $R(\zeta)$. This can easily be visualized from Fig. 2.2, since at $\lambda = k$ the angle of incidence of that ray is at the grazing angle, and therefore the value of the reflection coefficient should be -1 regardless of the medium properties. However, in the Schelkunoff formulation resulting in $R(\zeta)$, the slow waves are perpendicular to the boundary, hence this function is very

well behaved as seen in Fig. 2.6. This is another important advantage of the proposed formulation.

2.5 Conclusion

In this chapter, Green's function for the radiation of vertical dipoles over imperfectly-conducting ground planes is derived based on Schelkunoff integrals rather than Sommerfeld integrals. In the new formulation of the Green's function the integrand is a monotonically decaying function rather than the oscillatory and slowly-decaying functions of Sommerfeld formulation. This holds for the regions near the planar boundary (e.g. earth's surface) and for moderate as well as large radial distances from the transmitting antenna. The new formulation totally eliminates the well-known Sommerfeld integral tails problem in the indicated region (see Fig. 2.5).

It was aimed in this chapter to address the Sommerfeld formulation from its very fundamental basics. Most of the recent work start from Sommerfeld integrals and try to find a way to accelerate the numerical computation of those integrals either by changing the integration path or by extrapolating the function to avoid integrating the tails like in [14]- [15]. However, in this chapter we tried to solve the problem from the same point where Sommerfeld started. We chose a different integration variable and checked what does this have to mean physically. Following this path, we found that the Sommerfeld integral tails problem can be totally avoided from a physics point of view instead of having a work around as in [19].

Using the substitution (2.21) and noting the behavior of the reflection coefficients in Fig. 2.6, one gets to the conclusion that the integrands in both formulations have no poles whatsoever neither on the contour of integration nor near to it. Thus, the pole that

gives rise to the surface wave in Sommerfeld solution is actually a myth, at least in the case of vertical electric dipole over a lossy ground. This is consistent with Schelkunoff's conclusion in [11, p. 430]. The extension of this discussion to the case of multilayered media is considered as future work.

The new formulation is more suitable to problems where the planar boundaries are parallel to the horizontal axis; since in this case the reflection coefficient $R(\xi)$ has no discontinuities and is a very well behaved function suitable for integration along the whole contour. The numerical simulation of the well-known experimental data such as Okumara et al.'s experiment [20] is considered as future work to validate the derived formulation. It is aimed in such a simulation to show the capability of the formulas derived in this chapter to enhance the convergence rate of the Green's function. Specially, in electrically large problems such as Okumara's experiment which included the whole city of Tokyo [20].

3 Schelkunoff Integrals for Horizontal Dipoles

3.1 Introduction

Consider an elementary dipole of moment Idl oriented horizontally over a planar infinite ground plane, as shown in Fig. 3.1. The upper medium in which the dipole is located is termed air with the assumption $\epsilon_r = 1$. The dipole is located over a planar imperfect ground plane characterized by a complex relative dielectric constant given by $\epsilon = \epsilon_r - j\sigma / \omega\epsilon_0$, where ϵ_r represents the relative permittivity of the ground, ϵ_0 is the permittivity of vacuum, σ is the conductivity of the ground, ω stands for the angular frequency, and j is the imaginary unit, i.e., $j = \sqrt{-1}$. A time variation of $\exp(j\omega t)$ is assumed throughout the analysis, where t is the time variable. The conventional way to solve for the fields radiated in this case is to formulate a solution in terms of a single Hertzian vector $\vec{\Pi}$ of the electric type, as done by Sommerfeld in [1].

The approach is to find a suitable form for this Hertzian vector. This form has to satisfy the wave equation in both media according to:

$$\nabla^2 \vec{\Pi}_i + k_i^2 \vec{\Pi}_i = \begin{cases} \frac{-Id\vec{l}}{j\omega\epsilon_0} \delta(x)\delta(y)\delta(z-h) & , i = 1 \\ 0 & , i = 2 \end{cases} \quad (3.1)$$

The subscript i stands for the medium, as shown in Fig. 3.1. Then the boundary conditions are applied at the interface to find the unknown parameters in the assumed form of the solution. Consequently the fields can be calculated according to Maxwell equations as:

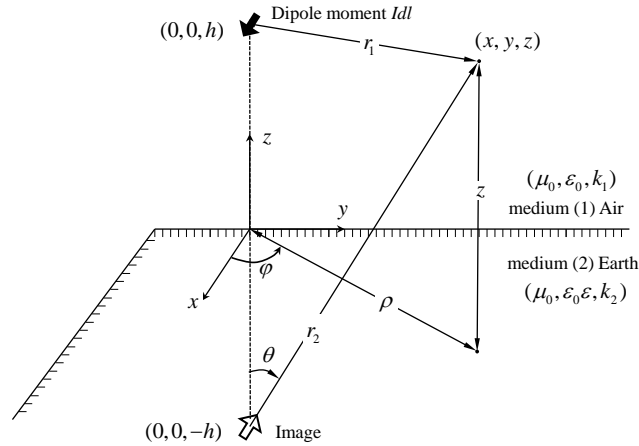


Fig. 3.1 Geometry of the problem of a horizontal dipole over imperfect ground plane.

$$\vec{E}_i = k_i^2 \vec{\Pi}_i + \nabla(\nabla \cdot \vec{\Pi}_i) \quad , i = 1, 2 \quad (3.2)$$

$$\vec{H}_i = j\omega\epsilon_0\epsilon_i \nabla \times \vec{\Pi}_i \quad , i = 1, 2 \quad (3.3)$$

where

$$k_1^2 = \omega^2 \mu_0 \epsilon_0 \quad (3.4)$$

$$k_2^2 = \omega^2 \mu_0 \epsilon_0 \epsilon \quad (3.5)$$

Following this approach, and according to the discussion given in the previous chapter, it is really appealing to extend the utilization of Schelkunoff integrals to derive a new Green's function for the radiation of a horizontal electric dipole over imperfect ground planes. This new Green's function is expected to motivate the development of integral equation-based solvers which are able to incorporate imperfect ground planes without worrying about the convergence problem of the integral tails as in the Sommerfeld case for large values of ρ . The rest of this chapter shows the derivation of the Schelkunoff-based Green's function for the horizontal (parallel to the boundary) dipoles.

3.2 Schelkunoff Formulation for Horizontal Dipoles

In [1], Sommerfeld gave expressions for the case of a horizontal dipole, as given in Appendix B. In this section, we will derive similar expressions but starting from Schelkunoff integrals rather than Sommerfeld integrals. First we need to consider the fact that for the case of an x -oriented dipole over a half space filling the region $z < 0$, shown in Fig. 3.1, the Hertzian vector has to consist of both x and z components [21]:

$$\vec{\Pi}_1 = \Pi_{1x} \hat{a}_x + \Pi_{1z} \hat{a}_z \triangleq (\Pi_{1x}^{prim} + \Pi_{1x}^{sec}) \hat{a}_x + \Pi_{1z}^{sec} \hat{a}_z \quad (3.6)$$

$$\vec{\Pi}_2 = \Pi_{2x} \hat{a}_x + \Pi_{2z} \hat{a}_z \triangleq \Pi_{2x}^{sec} \hat{a}_x + \Pi_{2z}^{sec} \hat{a}_z \quad (3.7)$$

where the superscript *prim* and *sec* denote the direct contribution of the source, and the effect of the presence of the second medium respectively. Using (3.2) and (3.3), and applying the continuity of the tangential components of the electric and magnetic fields, then the boundary conditions at the plane $z = 0$ are given by:

$$\Pi_{1x} = \varepsilon \Pi_{2x} \quad (3.8)$$

$$\frac{\partial}{\partial z} \Pi_{1x} = \varepsilon \frac{\partial}{\partial z} \Pi_{2x} \quad (3.9)$$

$$\Pi_{1z} = \varepsilon \Pi_{2z} \quad (3.10)$$

$$\frac{\partial}{\partial z} \Pi_{1z} - \frac{\partial}{\partial z} \Pi_{2z} = \frac{\partial}{\partial x} \Pi_{2x} - \frac{\partial}{\partial x} \Pi_{1x} \quad (3.11)$$

where $x = \rho \cos \varphi$, $y = \rho \sin \varphi$, $\rho = \sqrt{x^2 + y^2}$,

and
$$\frac{\partial}{\partial x} \equiv \cos \varphi \frac{\partial}{\partial \rho} \quad (3.12)$$

Equations (3.8) and (3.11) follow from the continuity of the x and y components of the electric field, respectively. Equations (3.9) and (3.10) follow from the continuity of the y and x components of the magnetic field, respectively. The angle φ is measured in the x - y plane from the x -axis as shown in Fig. 3.1. The suitable form of the solution can be guessed by inspecting (2.5) and the boundary conditions (3.8)-(3.11). The suitable forms based on Schelkunoff integrals are proposed to be:

$$\Pi_{1x}^{prim} = P \frac{e^{-jk_1 r_1}}{r_1} = P \frac{2}{\pi} \int_0^{\infty} K_0(\rho \sqrt{\xi^2 - k_1^2}) \cos(\xi(z-h)) d\xi \quad (3.13)$$

where

$$P = \frac{Idl}{j\omega 4\pi\epsilon_0}, \quad (3.14)$$

$$\rho = \sqrt{x^2 + y^2}, \quad (3.15)$$

and

$$r_1 = \sqrt{\rho^2 + (z-h)^2} \quad (3.16)$$

For simplicity, we will assume that the value of P in (3.14) is unity. Accordingly, the remaining components of vector potential are given by:

$$\Pi_{1x}^{sec} = \frac{2}{\pi} \int_0^{\infty} R(\xi) K_0(\rho \sqrt{\xi^2 - k_1^2}) \cos(\xi(z+h)) d\xi \quad (3.17)$$

$$\Pi_{2x}^{sec} = \frac{2}{\pi} \int_0^{\infty} T(\xi) K_0(\rho \sqrt{\xi^2 - k_2^2}) \cos(\xi_2 z - \xi h) d\xi \quad (3.18)$$

$$\Pi_{1z}^{sec} = \frac{2}{\pi} \cos \varphi \int_0^{\infty} R_z(\xi) K_1(\rho \sqrt{\xi^2 - k_1^2}) \sin(\xi(z+h)) d\xi \quad (3.19)$$

$$\Pi_{2z}^{sec} = \frac{2}{\pi} \cos \varphi \int_0^{\infty} T_z(\xi) K_1(\rho \sqrt{\xi^2 - k_2^2}) \sin(\xi_2 z - \xi h) d\xi \quad (3.20)$$

where $\xi_2^2 = \xi^2 - k_1^2 + k_2^2$. From the boundary conditions, we can define the functions:

$$R(\xi) = \frac{\xi - \sqrt{\xi^2 - (1-\varepsilon)k_1^2}}{\xi + \sqrt{\xi^2 - (1-\varepsilon)k_1^2}} \quad (3.21)$$

$$T(\xi) = \frac{2}{\varepsilon} \frac{\xi}{\xi + \sqrt{\xi^2 - (1-\varepsilon)k_1^2}} \quad (3.22)$$

$$R_z(\xi) = \frac{-2\xi\sqrt{\xi^2 - k_1^2}}{k_1^2} \frac{\xi - \sqrt{\xi^2 - (1-\varepsilon)k_1^2}}{\varepsilon\xi + \sqrt{\xi^2 - (1-\varepsilon)k_1^2}} \quad (3.23)$$

$$T_z(\xi) = \frac{2\xi\sqrt{\xi^2 - k_1^2}}{k_2^2} \frac{\xi - \sqrt{\xi^2 - (1-\varepsilon)k_1^2}}{\varepsilon\xi + \sqrt{\xi^2 - (1-\varepsilon)k_1^2}} \quad (3.24)$$

The proof that the above solutions satisfy the wave equation, shown in (3.1), is given in Appendix C of this dissertation. The derivation of the expressions (3.21)-(3.24) is given in Appendix E. Consequently, the electric and magnetic fields calculated from (3.2) and (3.3) represent the unique solution of the problem.

Now, the x -component of the Hertz potential in medium (1) is given by:

$$\Pi_{1x} = g_0 - g_1 + g_{sH} \quad (3.25)$$

where g_0 is the contribution of the main source and g_1 is the contribution of a virtual image, shown in Fig. 3.1, which represents the image in the case when the second medium is a perfect conductor. Those contributions are given by:

$$g_0 = \frac{e^{-jk_1 r_1}}{r_1} \quad \text{and} \quad g_1 = \frac{e^{-jk_1 r_2}}{r_2} \quad (3.26)$$

where $r_2 = \sqrt{\rho^2 + (z+h)^2}$. The last term in (3.25), g_{sH} , is the modification due to the imperfect conductivity (and hence imperfect reflectivity) of the ground, and it is given by:

$$g_{sH} = \frac{2}{\pi} \int_0^{\infty} \frac{2\xi}{\xi + \sqrt{\xi^2 - (1-\varepsilon)k_1^2}} K_0(\rho\sqrt{\xi^2 - k_1^2}) \cos(\xi(z+h)) d\xi \quad (3.27)$$

To facilitate the use of the new Green's function in an Integral-Equation based software using the method of moments [22], it is useful to write the z -component of the vector potential in terms of the partial derivative with respect to x as follows:

$$\Pi_{1z} = \Pi_{1z}^{\text{sec}} \triangleq \frac{\partial}{\partial x} g_2, \quad (3.28)$$

where

$$g_2 = \frac{2}{\pi} \int_0^{\infty} \frac{2\xi}{k_1^2} \frac{\xi - \sqrt{\xi^2 - (1-\varepsilon)k_1^2}}{\varepsilon\xi + \sqrt{\xi^2 - (1-\varepsilon)k_1^2}} K_0(\rho\sqrt{\xi^2 - k_1^2}) \sin(\xi(z+h)) d\xi \quad (3.29)$$

The usefulness of this form becomes obvious when the mutual impedance between horizontal dipoles is calculated by integrating the Green's function over the current distribution of the true excitation in the problem, as explained clearly in [22]. The details of applying the method of moments are out of scope of this chapter. What is of importance here is the behavior of the new Green's function as compared to the original Sommerfeld formulation. Since the Hertz vector potential is totally defined in medium (1), therefore the fields can be easily calculated by using (3.2):

$$\vec{E}_1 = k_1^2 \vec{\Pi}_1 + \vec{\nabla} \left(\frac{\partial}{\partial x} \Pi_{1x} + \frac{\partial}{\partial z} \Pi_{1z} \right) \quad (3.30)$$

Substituting for Π_{1x} using (3.25) and for Π_{1z} using (3.28), we get:

$$\frac{\partial}{\partial x} \Pi_{1x} + \frac{\partial}{\partial z} \Pi_{1z} = \frac{\partial}{\partial x} \left(g_0 - g_1 + g_{sH} + \frac{\partial}{\partial z} g_2 \right) \quad (3.31)$$

where the partial derivative operator with respect to x can be taken as a common factor because of (3.28). Furthermore, equation (3.31) can be simplified by substituting for g_{sH} using (3.27) and for g_2 using (3.29):

$$g_3 \triangleq g_{sH} + \frac{\partial}{\partial z} g_2 = \frac{2}{\pi} \int_0^{\infty} \frac{2\xi}{\varepsilon\xi + \sqrt{\xi^2 - (1-\varepsilon)k_1^2}} K_0(\rho\sqrt{\xi^2 - k_1^2}) \cos(\xi(z+h)) d\xi \quad (3.32)$$

Equation (3.30) which represents the electric field in medium (1) can be rewritten now using (3.31) and (3.32) as:

$$\vec{E}_1 = k_1^2 \vec{\Pi}_1 + \vec{\nabla} \left(\frac{\partial}{\partial x} (g_0 - g_1 + g_3) \right) \quad (3.33)$$

Accordingly, the individual components of that electric field in medium (1) become:

$$E_x = k_1^2 (g_0 - g_1 + g_{sH}) + \frac{\partial}{\partial x} \left(\frac{\partial}{\partial x} (g_0 - g_1 + g_3) \right) \quad (3.34)$$

$$E_y = \frac{\partial}{\partial y} \left(\frac{\partial}{\partial x} (g_0 - g_1 + g_3) \right) \quad (3.35)$$

$$E_z = k_1^2 \frac{\partial}{\partial x} g_2 + \frac{\partial}{\partial z} \left(\frac{\partial}{\partial x} (g_0 - g_1 + g_3) \right) \quad (3.36)$$

Note that for an x -oriented Hertzian dipole, the electric field in the y - z plane reduces to the first term of (3.34), $k_1^2 (g_0 - g_1 + g_{sH})$. Thus, in the numerical examples given in this chapter, the scope is limited to the behavior of the term g_{sH} .

3.3 Features of Schelkunoff Integrals and Some Useful Expressions

In the previous section, it was shown that the Green's function for the case of a horizontal dipole can be formulated using Schelkunoff integrals instead of the conventional Sommerfeld integrals. For the sake of comparison, the original Green's function which is based on Sommerfeld integrals is shown in Appendix D of this dissertation. The superiority of the expressions given in (3.27), (3.29) and (3.32) lies in their suitability for numerical calculation over the Sommerfeld expressions given in (D.13), (D.14) and (D.15). The aim of this section is to illustrate this advantage of Schelkunoff integrals.

All of the integrands given in the expressions of g_{sH} , g_2 and g_3 , namely in (3.27), (3.29) and (3.32), can be divided into three parts. The first part is a pure function in the integration variable ξ , the second part is a function in ξ and ρ , the horizontal separation of the source and the observation point. The last part is a function in ξ and $(z+h)$, the vertical separation between the observation and the image points, shown in Fig. 3.1. Therefore, the decaying rate of the whole integrand in the previously mentioned equations is determined by the fastest decaying rate of those three parts. Fortunately, in Schelkunoff formulation derived in the previous section, the fastest decaying rate is that of the modified Bessel function $K_0(x)$, which decays faster than exponential when its argument is real valued, which is the case for $\xi > k_1$. For the integrands shown in (D.13), (D.14) and (D.15) for the Sommerfeld formulation, none of those three parts decays as fast as $K_0(x)$ on the integration contour, specially for small values of $(z+h)$ and large

values of ρ , hence the famous problem of Sommerfeld integral tails which appear when those expressions are to be calculated numerically.

Going back to Schelkunoff formulation, the singularity of the function $K_0(\rho\sqrt{\xi^2 - k_1^2})$ at the point $\rho = 0$ is unavoidable, which limits the use of this formulation on the axis of the dipole, but for $\xi = k_1$, this is an integrable singularity, exactly as the singularity at $\lambda = k_1$ in Sommerfeld integral shown in (2.1). This singularity can be easily eliminated by taking the proper substitution as follows: On the main (bounded) part of the contour where $\xi : 0 \rightarrow k_1$, we use the substitution:

$$\xi = k_1 \sin \beta' \quad \Rightarrow \quad d\xi = k_1 \cos \beta' d\beta', \quad (3.37)$$

$$\sqrt{\xi^2 - k_1^2} = jk_1 \cos \beta', \quad (3.38)$$

$$\& \xi_2 = \sqrt{\xi^2 - (1 - \varepsilon)k_1^2} = k_1 \sqrt{\varepsilon - \cos^2 \beta'} \quad (3.39)$$

While on the remaining (unbounded) part of the contour where $\xi : k_1 \rightarrow \infty$ (which we call the tail of the contour), we use the substitution:

$$\xi = k_1 \sin \left(\frac{\pi}{2} + j\beta'' \right) = k_1 \cosh \beta'' \quad (3.40)$$

$$\Rightarrow \quad d\xi = k_1 \sinh \beta'' d\beta''$$

$$\sqrt{\xi^2 - k_1^2} = k_1 \sinh \beta'', \quad (3.41)$$

$$\& \xi_2 = \sqrt{\xi^2 - (1 - \varepsilon)k_1^2} = k_1 \sqrt{\varepsilon + \sinh^2 \beta''} \quad (3.42)$$

Using the substitutions defined in (3.37)-(3.42), g_{sH} becomes:

$$\begin{aligned}
g_{sH} = & \frac{2}{\pi} \int_0^{\pi/2} \frac{2 \sin \beta'}{\sin \beta' + \sqrt{\varepsilon - \cos^2 \beta'}} K_0(jk_1 \rho \cos \beta') k_1 \cos \beta' \\
& \cos(k_1 \sin \beta' (z+h)) d\beta' \\
& + \frac{2}{\pi} \int_0^{\infty} \frac{2 \cosh \beta''}{\cosh \beta'' + \sqrt{\varepsilon + \sinh^2 \beta''}} K_0(k_1 \rho \sinh \beta'') k_1 \sinh \beta'' \\
& \cos(k_1 \cosh \beta'' (z+h)) d\beta''
\end{aligned} \tag{3.43}$$

Using the same substitutions, g_2 becomes:

$$\begin{aligned}
g_2 = & \frac{2}{\pi} \int_0^{\pi/2} \frac{2 \sin \beta'}{k_1} \frac{\sin \beta' - \sqrt{\varepsilon - \cos^2 \beta'}}{\varepsilon \sin \beta' + \sqrt{\varepsilon - \cos^2 \beta'}} K_0(jk_1 \rho \cos \beta') k_1 \cos \beta' \\
& \sin(k_1 \sin \beta' (z+h)) d\beta' \\
& + \frac{2}{\pi} \int_0^{\infty} \frac{2 \cosh \beta''}{k_1} \frac{\cosh \beta'' - \sqrt{\varepsilon + \sinh^2 \beta''}}{\varepsilon \cosh \beta'' + \sqrt{\varepsilon + \sinh^2 \beta''}} K_0(k_1 \rho \sinh \beta'') k_1 \sinh \beta'' \\
& \sin(k_1 \cosh \beta'' (z+h)) d\beta''
\end{aligned} \tag{3.44}$$

Finally, g_3 can be rewritten, as:

$$\begin{aligned}
g_3 = & \frac{2}{\pi} \int_0^{\pi/2} \frac{2 \sin \beta'}{\varepsilon \sin \beta' + \sqrt{\varepsilon - \cos^2 \beta'}} K_0(jk_1 \rho \cos \beta') k_1 \cos \beta' \\
& \cos(k_1 \sin \beta' (z+h)) d\beta' \\
& + \frac{2}{\pi} \int_0^{\infty} \frac{2 \cosh \beta''}{\varepsilon \cosh \beta'' + \sqrt{\varepsilon + \sinh^2 \beta''}} K_0(k_1 \rho \sinh \beta'') k_1 \sinh \beta'' \\
& \cos(k_1 \cosh \beta'' (z+h)) d\beta''
\end{aligned} \tag{3.45}$$

3.4 Numerical Examples

In this section, some numerical examples are given to illustrate the usefulness of the new formulation which is based on Schelkunoff integrals. First, the numerical behavior of the complex integrands in the new formulation is compared to those in Sommerfeld formulation. As discussed earlier, those integrands can be divided into three

parts. To be specific, take g_{sH} as an example. The integrand in (3.27) can be divided into three parts, the first part is a pure function of ξ . Let's define it as $f(\xi, \varepsilon)$, where

$$f(\xi, \varepsilon) = \frac{2\xi}{\xi + \sqrt{\xi^2 - (1-\varepsilon)k_1^2}} \quad (3.46)$$

which is related only to the reflection coefficient at the boundary. The remaining two parts can be combined in one term. Let's define this term as $K(\xi, \rho, z)$, where

$$K(\xi, \rho, z) = K_0(\rho\sqrt{\xi^2 - k_1^2}) \cos(\xi(z+h)) \quad (3.47)$$

In Sommerfeld formulation, given in (D.13), the integrands of g_{sH}^{Som} can also be divided in a similar way, where the reflection coefficient-related part is defined as:

$$f^{Som}(\lambda, \varepsilon) = \frac{2\sqrt{\lambda^2 - k_1^2}}{\sqrt{\lambda^2 - k_1^2} + \sqrt{\lambda^2 - k_2^2}} \quad (3.48)$$

and the remaining two parts can be combined in another term, let's define it as $J(\lambda, \rho, z)$, where:

$$J(\lambda, \rho, z) = J_0(\lambda\rho)e^{-(z+h)\sqrt{\lambda^2 - k_1^2}} \frac{\lambda}{\sqrt{\lambda^2 - k_1^2}} \quad (3.49)$$

In both cases, those integrands have to be carried out on semi-infinite contour from 0 to ∞ . The behavior of both formulations turns out to be the same on the bounded part of the contour where ξ (or λ) $< k_1$. This is obvious because on that part of the contour, the argument of the modified Bessel function in (3.47) becomes imaginary and hence the whole function becomes oscillatory as the Bessel function in (3.49) [23].

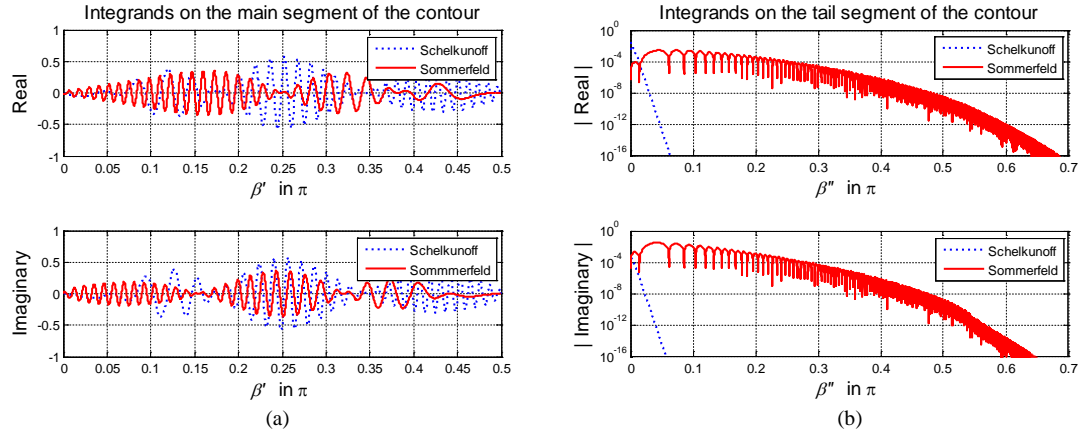


Fig. 3.2 A comparison between the integrands of Schelkunoff and Sommerfeld formulations: (a) The main (bounded) part of the contour: ξ (or λ) $< k_1$, or equivalently $\beta' : 0 \rightarrow \pi/2$, (b) The tail (unbounded) part of the contour ξ (or λ) $> k_1$ or equivalently $\beta'' : 0 \rightarrow \infty$

Despite this fact, the integrals can be evaluated without convergence problem because this part of the contour is limited from 0 to k_1 . Consider the problem illustrated in Fig. 3.1. Assume the frequency is 850 MHz, $\epsilon_r = 4$, $\sigma = 0.02$, and $(z + h) = 0.5\text{m}$. Suppose that the fields are to be calculated at a horizontal distance $\rho = 10\text{m}$ from the source. Using the substitution defined in (3.37)-(3.42), one can show the behavior of the complex integrand in both formulations, as shown in Fig. 3.2. In this figure, the dotted curve (blue) represents the product of (3.46) and (3.47), while the solid curve (red) shows the product of (3.48) and (3.49). From Fig. 3.2a, we see the behavior of the integrands on the bounded part of the contour is almost the same for both formulations. However, on the other part of the contour, in Fig. 3.2b, where ξ (or λ) $> k_1$, the behaviors of both integrands become totally different; because the argument of the modified Bessel function in (3.47) becomes real, hence the whole function decays monotonically as its argument increases. This is the difference which is required to be illustrated here.

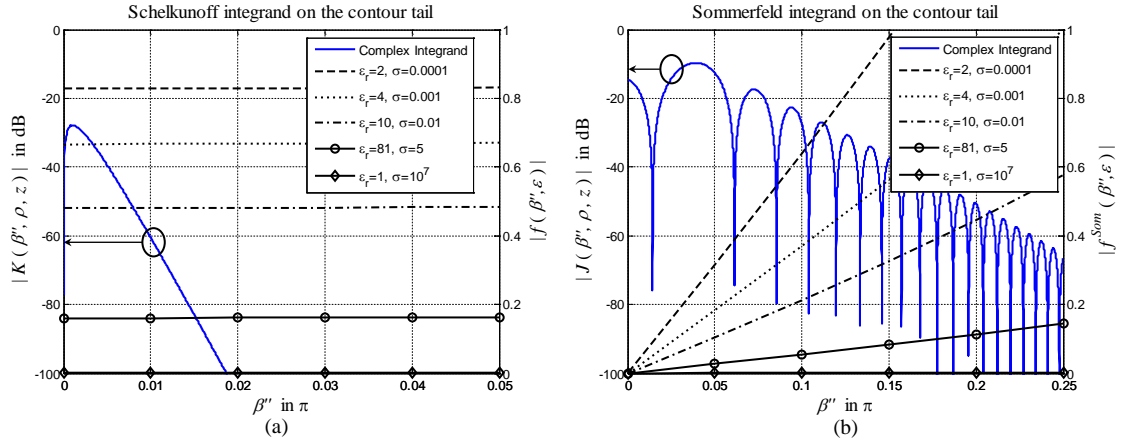


Fig. 3.3 A comparison between the integrands on the tail part of the contour for a horizontal separation of 10m : (a) Schelkunoff (b) Sommerfeld

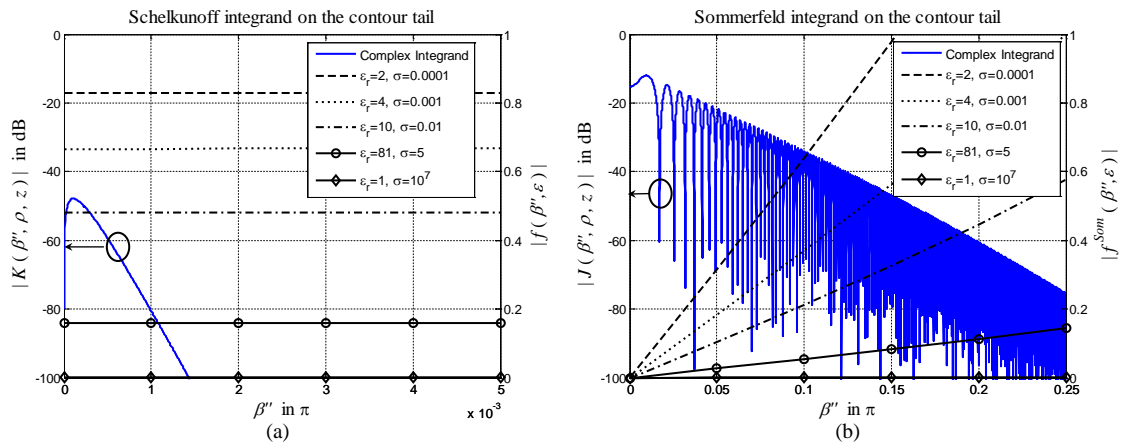


Fig. 3.4 A comparison between the integrands on the tail part of the contour for a horizontal separation of 100m : (a) Schelkunoff (b) Sommerfeld

For further illustration for the different behaviors of the integrands, one can rewrite equations (3.46) and (3.47) as in (3.50) and (3.51), respectively, using the substitution defined in (3.40)-(3.42). This is shown below:

$$f(\beta'', \varepsilon) = \frac{2 \cosh \beta''}{\cosh \beta'' + \sqrt{\varepsilon + \sinh^2 \beta''}} \quad (3.50)$$

$$K(\beta'', \rho, z) = K_0(k_1 \rho \sinh \beta'') k_1 \sinh \beta'' \cos(k_1 \cosh \beta'' (z + h)) \quad (3.51)$$

Using the same substitution, equations (3.48) and (3.49) become equivalent to (3.52) and (3.53) respectively, as shown below:

$$f^{Som}(\beta'', \varepsilon) = \frac{2 \sinh \beta''}{\sinh \beta'' + \sqrt{\cosh^2 \beta'' - \varepsilon}} \quad (3.52)$$

$$J(\beta'', \rho, z) = J_0(k_1 \rho \cosh \beta'') k_1 \rho \cosh \beta'' e^{-(z+h)k_1 \sinh \beta''} \quad (3.53)$$

Assume the same simulation parameters discussed earlier, and considering the tail of the contour $\beta'' : 0 \rightarrow \infty$. The absolute values of (3.50) and (3.51), which represent Schelkunoff formulation, are plotted versus β'' , as shown in Fig. 3.3a. The left vertical axis in Fig. 3.3a shows the absolute value of (3.51), while the right vertical axis shows the absolute value of (3.50) for different ground parameters. Remember that the function shown in Fig. 3.2b is the product of the two vertical axes of Fig. 3.3. For Sommerfeld formulation, the absolute values of (3.52) and (3.53) are plotted versus β'' in Fig. 3.3b. If the horizontal separation between the source and observation points is increased to be of 100 m instead of 10 m, Fig. 3.3a and Fig. 3.3b will correspond then to Fig. 3.4a and Fig. 3.4b respectively. The results shown in those figures make the advantage of the new formulation quite obvious. Observe in Fig. 3.3b. and Fig. 3.4b how the integrands in Sommerfeld formulation are oscillatory and slowly decaying. On the other hand, Fig. 3.3a and Fig. 3.4a show that the integrands in Schelkunoff formulation decay monotonically due to the behavior of the modified Bessel function $K_0(x)$. If one observes the horizontal scale of Fig. 3.3 and Fig. 3.4, it would be quite obvious that the length of the tail of the integration contour in Schelkunoff formulation is much smaller than in Sommerfeld formulation.

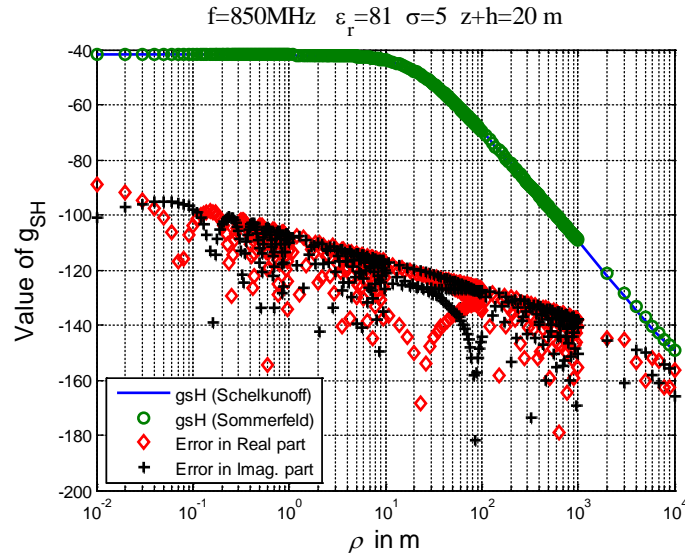


Fig. 3.5 A comparison between the results obtained using Schelkunoff and Sommerfeld integrals for the case of seawater where each of the source and field points is 10 m high from the interface

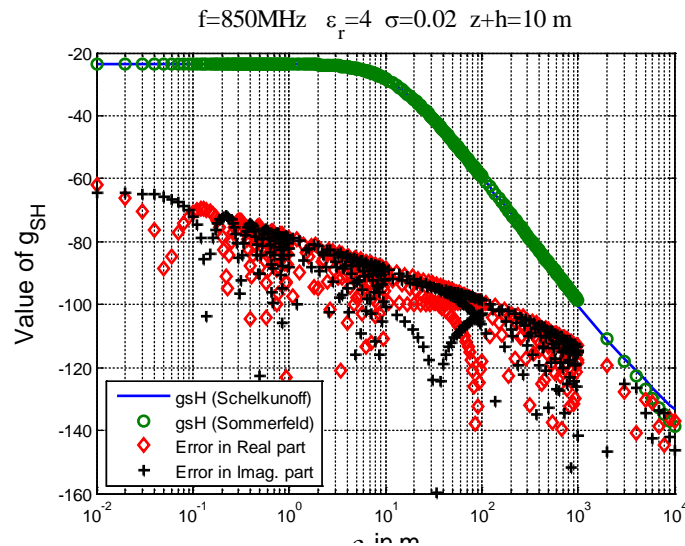


Fig. 3.6 A comparison between the results obtained using Schelkunoff and Sommerfeld integrals for the case of urban ground where each of the source and field points is 5 m high from the interface.

For example, if the horizontal separation between the source and observation points is 10 m, Fig. 3.3b. shows that for the absolute value of the integrand to go below

10^{-4} (-80 dB), the integration variable on the tail of the contour has to go to $\beta'' \approx \pi / 4$. While Fig. 3.3a shows that for the same conditions the integration variable has to go just to $\beta'' \approx 0.015\pi$. When the horizontal separation increases to 100m, Fig. 3.4b shows that the oscillations in Sommerfeld integrals increases while their decaying rate remains the same as in Fig. 3.3b. On the other hand, in Schelkunoff integrals, as shown in Fig. 3.4a the decaying rate becomes faster when the horizontal distance increases (Note that there is one order of magnitude less in the horizontal axis of Fig. 3.4a as compared to Fig. 3.3a).

One more advantage that can be seen from Fig. 3.3 and Fig. 3.4 is the distinction made by the ground parameters which is consistent over the whole path of integration. While in Sommerfeld formulation, the ground parameters do not have that much distinction. This is because of the fact that the starting point on the lower-left corner of Fig. 3.3 and Fig. 3.4 represent grazing incidence in the case of Sommerfeld formulation, while it represents normal incidence in the case of Schelkunoff's. This is explained in details in the previous chapter. This effect appears only for large horizontal separations between the source and the field points.

After discussing the behavior of the integrands, it is important to check the numerical results of integration for both formulations. A comparison between the integration results is shown in Fig. 3.5 and Fig. 3.6 for two different cases. Fig. 3.5 shows the case of $z + h = 20\text{m}$ over sea water ($\epsilon_r = 81$, $\sigma = 5$), while Fig. 3.6 shows the case of $z + h = 10\text{m}$ over urban ground ($\epsilon_r = 4$, $\sigma = 0.02$). The value of g_{sH} is plotted versus the horizontal distance ρ . On the same curves, the difference between the integration results is plotted in dB for both the real and imaginary parts. As seen from both figures, both

formulations are equivalent. For both the real and imaginary parts of the integration results, the error is about 60 dB less than the value of the function itself for most of the horizontal separations. The difference between the two formulations increases for large horizontal separations. This is exactly what was expected because, as shown in Fig. 3.2- Fig. 3.4, the convergence of Sommerfeld integrals becomes more problematic as the value of ρ increases.

Finally, the superiority of Schelkunoff formulation, discussed above, should correspond directly to the time elapsed to calculate the integrals in the Green's function. This is illustrated in Fig. 3.7 and Fig. 3.8. In Fig. 3.7, the value of the computed integral for g_{sH} is shown for a large dynamic range of horizontal distances and for $(z+h) = 0.1w$, where w is the wavelength assumed in the simulation. In this example, the parameters of the ground are the same as medium (1). In this case, where there is no reflection, equation (3.25) dictates that the value of g_{sH} should be exactly equal to g_1 , so that the only contribution in the potential will be that of the original source. Therefore, in this case, we know the exact value of g_{sH} which is $g_{sH} = g_1 = e^{-jk_1 r_2} / r_2$. Fig. 3.7 shows that both Sommerfeld and Schelkunoff formulation give correct values. However, Fig. 3.8 shows that to get to the same accuracy from both formulations, the time elapsed to calculate Schelkunoff integrals is an order of magnitude less than that of Sommerfeld integrals, which becomes very critical when the horizontal separations between the source and observation points increases. In Fig. 3.9 and Fig. 3.10, the time elapsed for the same simulation is shown for a vertical distance $(z+h) = 1w$ and $(z+h) = 0$ respectively.

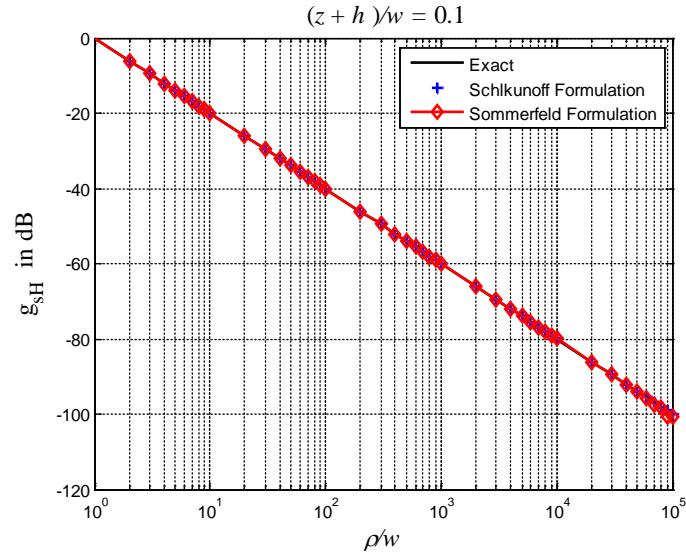


Fig. 3.7 The calculated integral of g_{SH} using both Sommerfeld and Schelkunoff formulations. The horizontal and vertical distances are normalized to the wavelength w

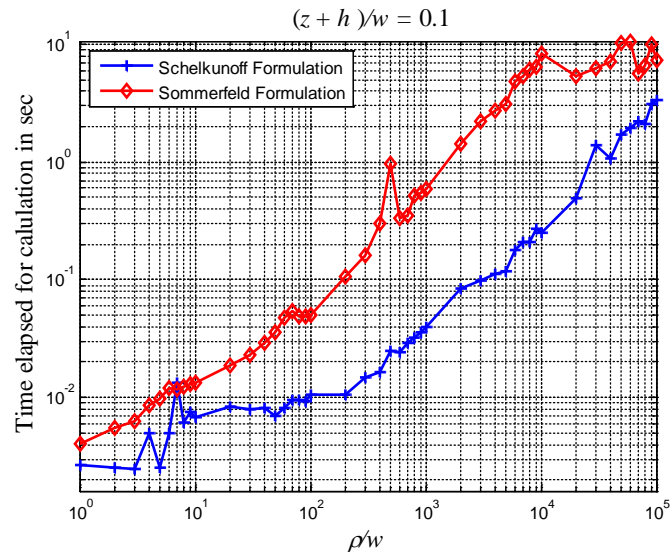


Fig. 3.8 Time elapsed to calculate the values of Fig. 3.7 for $(z+h)/w=0.1$. The horizontal and vertical distances are normalized to the wavelength w

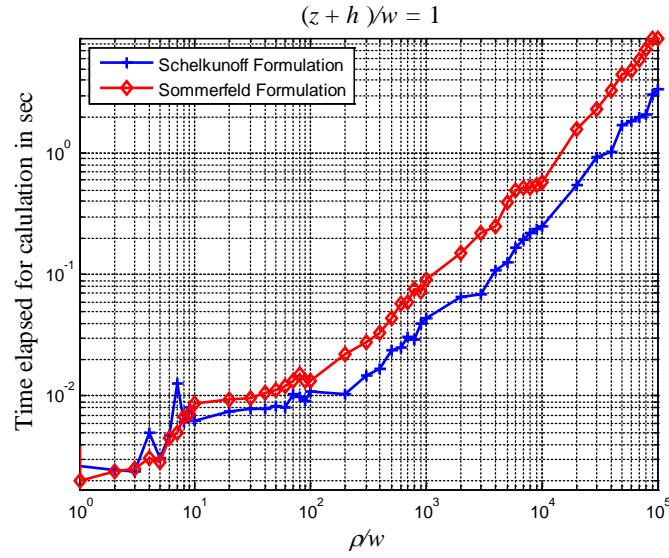


Fig. 3.9 Time elapsed to calculate the values of Fig. 3.7 for $(z+h)/w = 1$. The horizontal and vertical distances are normalized to the wavelength w

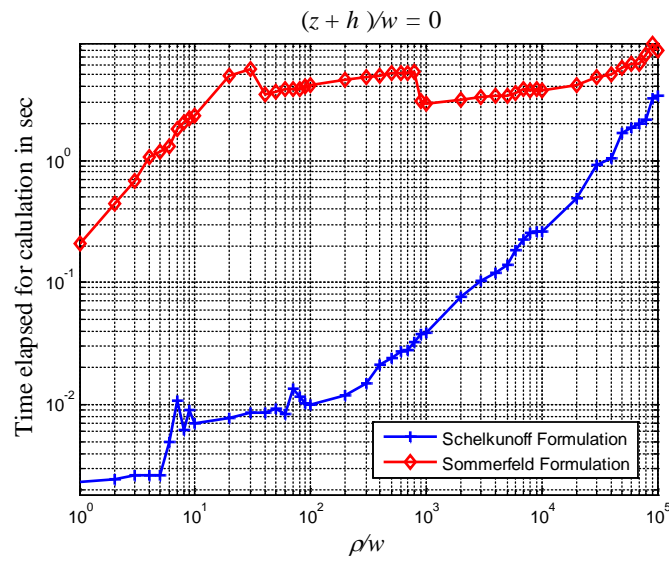


Fig. 3.10 Time elapsed to calculate the values of Fig. 3.7 when $(z+h) = 0$.

The results in Fig. 3.9 show that the convergence of Sommerfeld integrals is better than that of Fig. 3.8. This is because the exponential function on the right hand side of (3.53) enhances the decay rate of Sommerfeld integrals when $(z+h)$ increases.

However, even in this case, Schelkunoff integrals have faster convergence rate as shown in Fig. 3.9. As the vertical distance $(z+h)$ approaches zero, Sommerfeld integrals totally fail to converge as shown in Fig. 3.10. This represents the main advantage of the new formulation. That is, a numerical solution is now applicable for the case where the source and the field points are directly on the interface, without suffering from the integral tails problem which is inherent in the Sommerfeld formulation.

3.5 Conclusion

In this chapter, a new formulation for the Green's function of a horizontal dipole over an imperfect ground plane is derived based on Schelkunoff integrals. This chapter extends the derivation of the vertical dipole, given in Chapter 2, for the case of the horizontal electric dipole. The performance of the new formulation is compared to the conventional Sommerfeld formulation in terms of the numerical behavior and the suitability for numerical integration. The given examples show the superiority of the new formulation over Sommerfeld's in terms of the time needed to get the same accuracy. This superiority is achieved when the field point is at large horizontal distance from the source and for small vertical distances. This gives potential to reduce the time elapsed for a single calculation of the Green's function by at least one order of magnitude, and hence abolishing the well-known problem of Sommerfeld integral tails. This advantage becomes critical when trying to solve electrically large problems in the presence of real

grounds like the earth or the sea, especially when the source and field points are very close to the interface.

4 A Comparison between Sommerfeld and Schelkunoff

Formulations

4.1 Introduction

The problem of dipole radiation over an infinite half-space is more than a hundred years old. Throughout this whole century, tremendous amount of work was done and published to address the same problem which is known as the *Sommerfeld problem*, or sometimes *Sommerfeld half-space problem*. The original work of Sommerfeld can be divided into two main stages. First, finding a suitable formulation (expressions) for the components of the Hertz potential, and then the second stage is to carry out the integrals which appear in his expressions to find a closed form solution for the radiated fields. In the previous two chapters of this dissertation, we addressed only the first stage, where analogous expressions were given based on the modified Sommerfeld integrals, which we call Schelkunoff integrals. We did not address the second stage which is the analytical solution given by Sommerfeld. Instead, numerical solutions were given using the state of the art desktop computers which were not available at the time of Sommerfeld.

However, due to the debatable nature of the problem at hand, it is not avoidable to have some questions arise about the relation between the new formulation presented here and the original Sommerfeld formulation. To answer those questions, we need to have a closer look at the relation between the two formulations and whether they should yield the same results or not from a theoretical point of view. This chapter is dedicated solely for this purpose.

4.2 Anatomy of Sommerfeld and Schelkunoff Integrals

Starting from the homogeneous space Green's function, one can write:

$$\begin{aligned} \frac{e^{-jk_1 R}}{R} &= \int_0^{\infty} J_0(\lambda \rho) e^{-(z+h)\sqrt{\lambda^2 - k_1^2}} \frac{\lambda}{\sqrt{\lambda^2 - k_1^2}} d\lambda \\ &= \frac{1}{2} \int_{-\infty}^{\infty} H_0^{(2)}(\lambda \rho) e^{-(z+h)\sqrt{\lambda^2 - k_1^2}} \frac{\lambda}{\sqrt{\lambda^2 - k_1^2}} d\lambda \end{aligned} \quad (4.1)$$

where $R^2 = \rho^2 + (z+h)^2$ and the second line has been written using the following identities [23]:

$$J_0(\lambda \rho) = \frac{1}{2} [H_0^{(1)}(\lambda \rho) + H_0^{(2)}(\lambda \rho)] \quad (4.2)$$

$$H_0^{(1)}(-x) = -H_0^{(2)}(x) \quad (4.3)$$

Also, one can write:

$$\begin{aligned} \frac{e^{-jk_1 R}}{R} &= \frac{2}{\pi} \int_0^{\infty} K_0(\rho \sqrt{\xi^2 - k_1^2}) \cos(\xi(z+h)) d\xi \\ &= \frac{1}{\pi} \int_{-\infty}^{\infty} K_0(\rho \sqrt{\xi^2 - k_1^2}) e^{-j\xi(z+h)} d\xi \end{aligned} \quad (4.4)$$

Accordingly one can conclude that:

$$\frac{1}{2} \int_{\Gamma} H_0^{(2)}(\lambda \rho) e^{-(z+h)\sqrt{\lambda^2 - k_1^2}} \frac{\lambda}{\sqrt{\lambda^2 - k_1^2}} d\lambda = \frac{1}{\pi} \int_C K_0(\rho \sqrt{\xi^2 - k_1^2}) e^{-j\xi(z+h)} d\xi \quad (4.5)$$

where the integration contours Γ and C are shown in Fig. 4.1. The proof of (4.5) for $z+h=0$ is given in Appendix A. The generalization of the proof of Appendix A to the case where $z+h \neq 0$ is quite cumbersome because of the multiplication by the complex

exponential function. However, an alternative approach to prove (4.5) using complex analysis is quite straight forward. Consider the following substitution:

$$\lambda^2 + \xi^2 = k_1^2 \quad \Rightarrow \quad \lambda = \pm j\sqrt{\xi^2 - k_1^2} \quad \Rightarrow \quad \xi = \pm j\sqrt{\lambda^2 - k_1^2} \quad (4.6)$$

where $\lambda d\lambda = -\xi d\xi$. Since one can write the following relation from the properties of the Bessel functions [23]:

$$K_0(x) = -j \frac{\pi}{2} H_0^{(2)}(jx), \quad \frac{\pi}{2} < \arg(x) \leq 2\pi \quad (4.7)$$

where $\arg(x)$ is the phase angle of the complex number x . Therefore, the integrand on the left-hand side of (4.5) can be written as:

$$\begin{aligned} \frac{1}{2} H_0^{(2)}(\lambda\rho) e^{-(z+h)\sqrt{\lambda^2 - k_1^2}} \frac{\lambda d\lambda}{\sqrt{\lambda^2 - k_1^2}} &= \frac{1}{2} H_0^{(2)}(j\sqrt{\xi^2 - k_1^2}\rho) e^{-j\xi(z+h)} \frac{-\xi d\xi}{-j\xi} \\ &= \frac{1}{\pi} K_0(\sqrt{\xi^2 - k_1^2}\rho) e^{-j\xi(z+h)} d\xi \\ \Rightarrow \quad G(\lambda)d\lambda &= \quad F(\xi)d\xi \end{aligned} \quad (4.8)$$

This means that the integrands on both sides of (4.5) are identical based on the substitution given in (4.6). The trick however is in the contours of integration. To understand this trick very clearly, one should consider the mapping of the integration contours from the complex λ -plane to the complex ξ -plane and vice versa. In words, one can see from (4.6) that as λ goes from $-\infty$ to $-k_1$, ξ goes from $-j\infty$ to 0, and as λ goes from $-k_1$ to 0, ξ goes from 0 to k_1 . Then as λ increases on the positive real axis, ξ goes back from k_1 to 0 and then from 0 to $-j\infty$. This means that the λ -plane contour, Γ in Fig. 4.1-(a), is mapped to the ξ -plane contour C_{BC_1} in Fig. 4.1-(b). Note that

because of the quadratic relation between ξ and λ , namely $\xi = \pm j\sqrt{\lambda^2 - k_1^2}$, the ξ – plane contour C_{BC_1} is not the unique representation of the contour Γ . Another possible contour in the ξ – plane is the one that goes from $-k_1$ to $+j\infty$, which is not drawn in Fig. 4.1-(b) just for the sake of simplicity. For more illustration, the contour Γ is mapped into two additional planes, namely the α – plane and the β – plane, where α and β are the physical angles shown in the right angle triangle of Fig. 4.1.

It is important now to see how the ξ – plane contour C on the right-hand side of (4.5) is mapped into the other planes. This is shown in Fig. 4.2, where we can see that contour C is represented by the contour Γ_{BC_1} in the λ plane. The subscript “ BC_1 ” in C_{BC_1} and Γ_{BC_1} stands for the branch cut emanating from the point k_1 in either of the planes.

This comes from the fact that the expressions on both sides of (4.5) are double valued.

This results from the presence of the square root functions: $\sqrt{\lambda^2 - k_1^2}$ and $\sqrt{\xi^2 - k_1^2}$. To visualize the effect of those branch cuts, a numerical example is shown where we plot the expressions of (4.5) for the case $z + h = 0$. The branch cuts shown in Fig. 4.3 and Fig. 4.4 can be identified by the sharp transitions in color (phase). Those branch cuts represent the lines on which the square roots in the integrands have zero real part. This is easily calculated using Matlab which always yields the square root with a positive real part.

Those branch cuts are shown in Fig. 4.1-(b) and Fig. 4.2-(a) as C_{BC_1} and Γ_{BC_1} respectively.

With the aid of Fig. 4.1-(a), Fig. 4.1-(b) and equation (4.8), one can write:

$$\int_{\Gamma} G(\lambda)d\lambda = \int_{C_{BC_1}} F(\xi)d\xi \quad (4.9)$$

Similarly,
$$\int_{\Gamma_{BC_1}} G(\lambda)d\lambda = \int_C F(\xi)d\xi \tag{4.10}$$

Note that the original contours of integration in (4.5) are along the real axes in either the λ – plane or the ξ – plane . Thus, the remaining task is to prove that the left-hand side of (4.9) is equal to the left-hand side of (4.10) and also to prove the same for the right-hand sides. One can easily do so by applying Cauchy’s theorem.

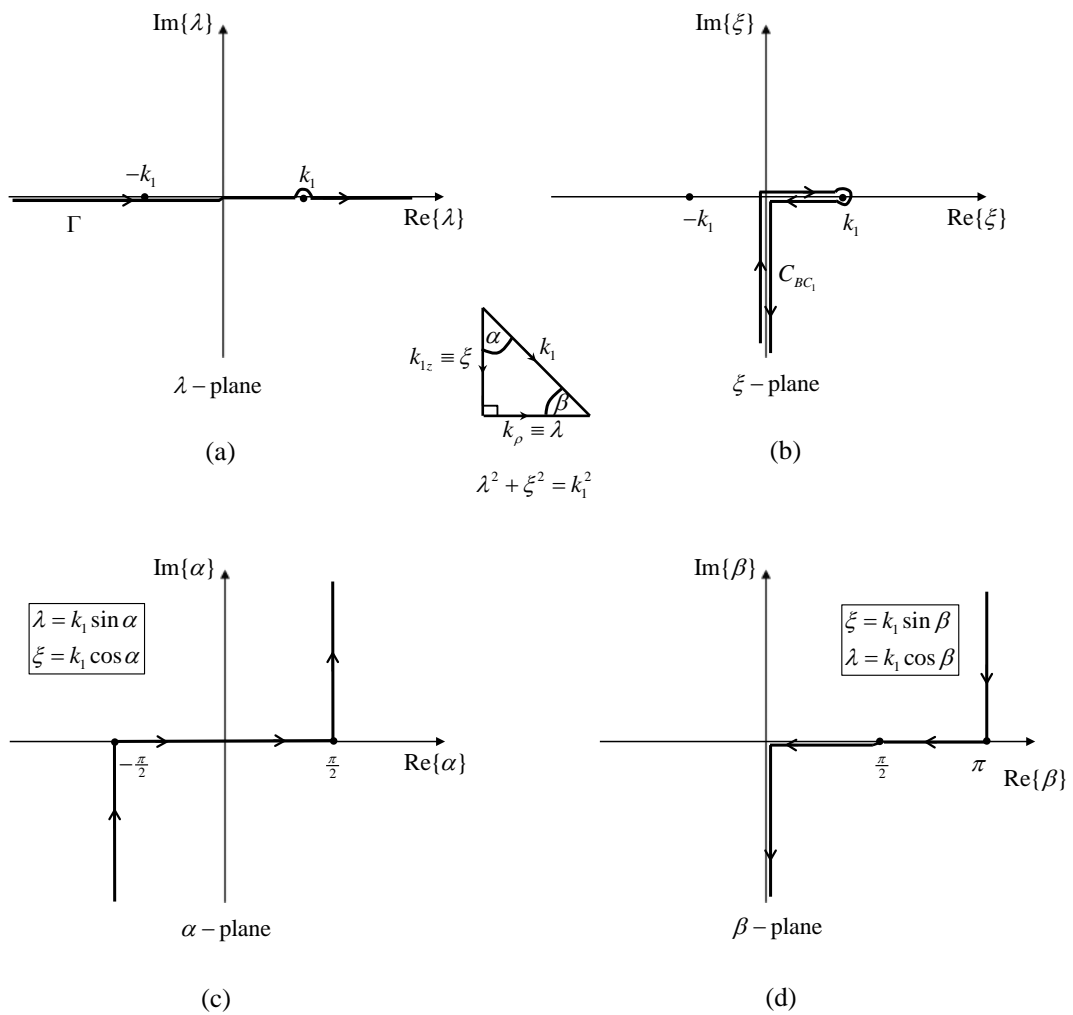


Fig. 4.1 Mapping of the real axis of λ in different complex planes : (a) λ – plane , (b) ξ – plane , (c) α – plane , (d) β – plane

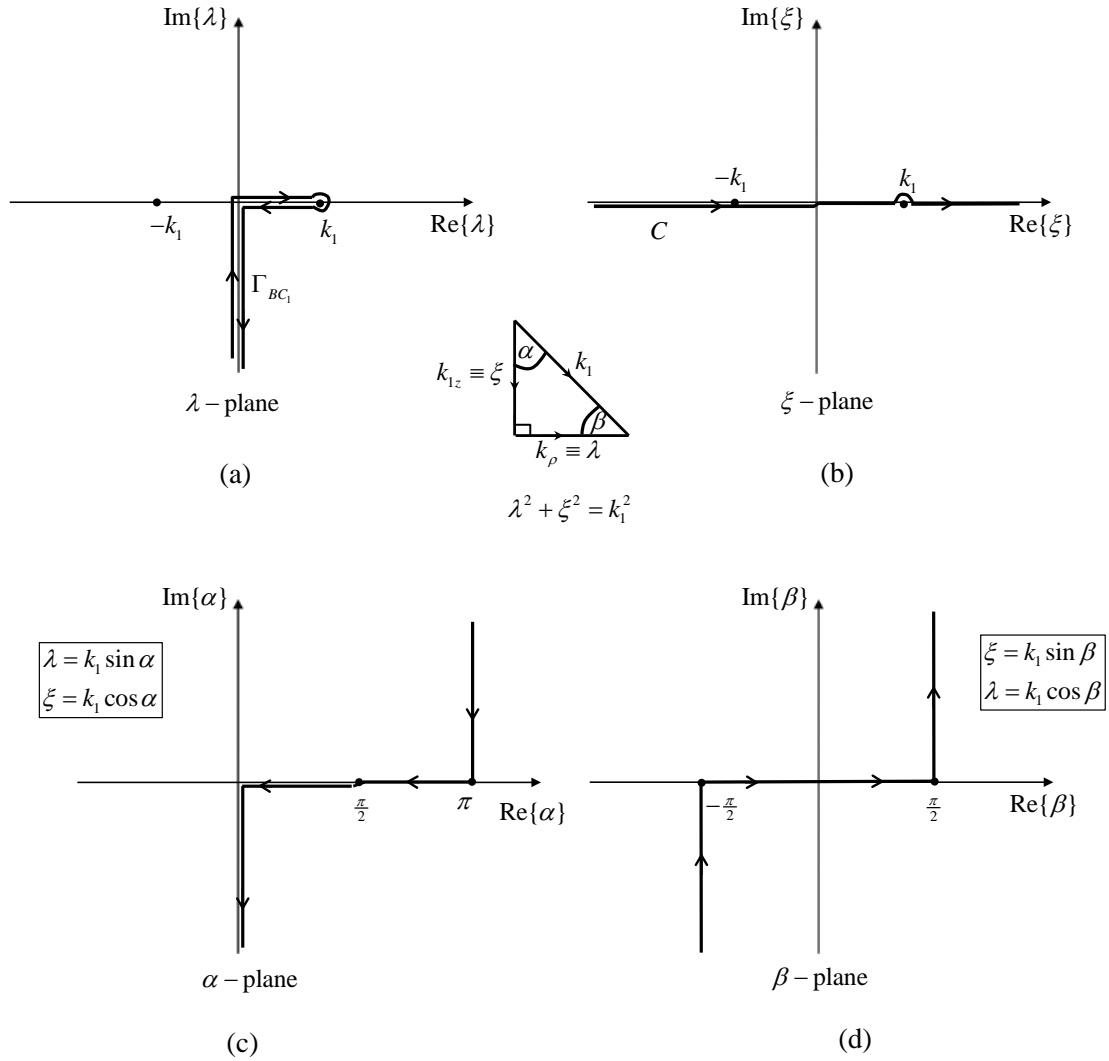


Fig. 4.2 Mapping of the real axis of ξ in different complex planes : (a) λ -plane , (b) ξ -plane , (c) α -plane , (d) β -plane

To calculate the integral on the left-hand side of (4.9), consider the picture shown in Fig. 4.5-(a). Applying Cauchy's theorem, since the integrands have no singularity except the branch point singularity at $\lambda = k_1$, therefore

$$\int_{\Gamma} G(\lambda)d\lambda + \int_{\Gamma_{\infty}} G(\lambda)d\lambda + \int_{-\Gamma_{Bc1}} G(\lambda)d\lambda = 0 \tag{4.11}$$

Since the integrand vanishes at ∞ in the third and fourth quadrants, therefore the integral along Γ_∞ has no contribution, accordingly:

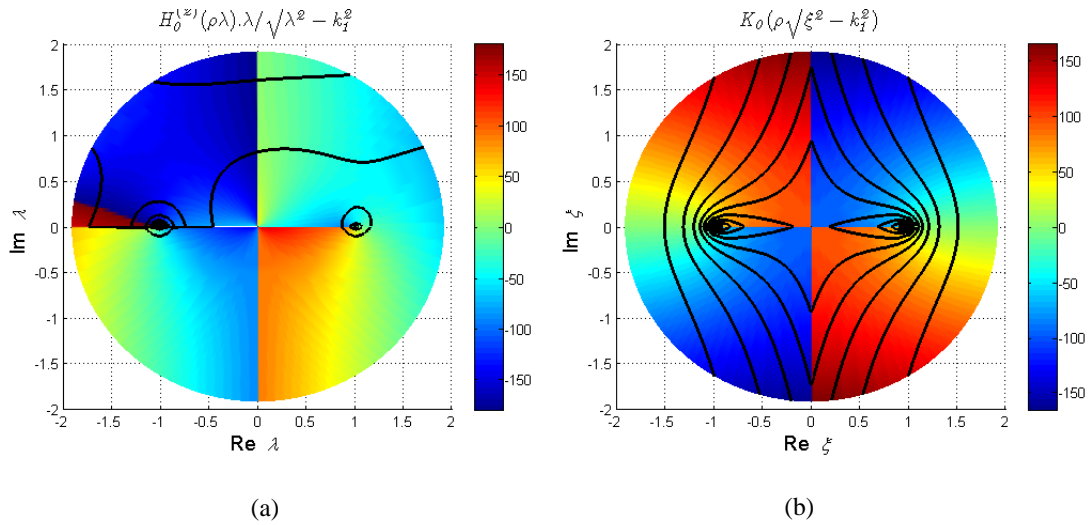


Fig. 4.3 Representation of the integrands in the complex λ – plane (a) and the complex ξ – plane (b) for the case of $k_1 = 1$. The color bar is in degrees and represents the phase angle of the integrands. The contour lines in black represent the lines of constant magnitudes of the integrands.

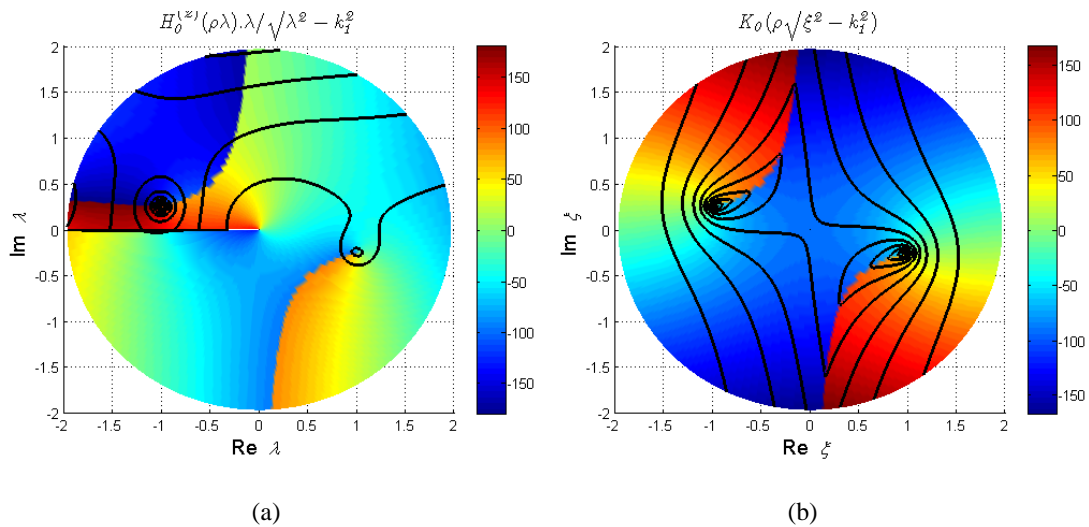


Fig. 4.4 Representation of the integrands in the complex λ – plane (a) and the complex ξ – plane (b) for the case of $k_1 = 1 - j0.25$. The color bar is in degrees and represents the phase angle of the integrands. The contour lines in black represent the lines of constant magnitudes of the integrands.

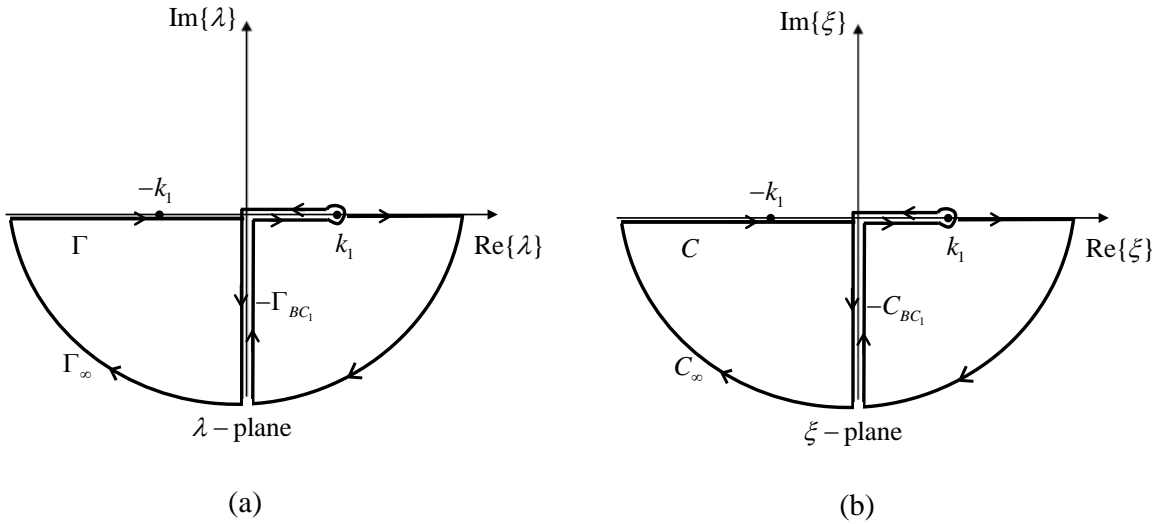


Fig. 4.5 Application of Cauchy's theorem in the λ -plane (a) and the complex ξ -plane (b).

$$\int_{\Gamma} G(\lambda) d\lambda = - \int_{-\Gamma_{BC_1}} G(\lambda) d\lambda = \int_{\Gamma_{BC_1}} G(\lambda) d\lambda \quad (4.12)$$

Similarly, from Fig. 4.5-(b), one can prove that the integrals on the right-hand side of (4.9) and (4.10) are identical by applying Cauchy's theorem:

$$\int_C F(\xi) d\xi + \int_{C_\infty} F(\xi) d\xi + \int_{-C_{BC_1}} F(\xi) d\xi = 0 \quad (4.13)$$

$$\Rightarrow \int_C F(\xi) d\xi = \int_{C_{BC_1}} F(\xi) d\xi \quad (4.14)$$

Where the integral along C_∞ vanishes because of the integrand in this case also vanishes at ∞ in the third and fourth quadrants. Substituting (4.9) in (4.14) or (4.10) in (4.12), we get:

$$\int_{\Gamma} G(\lambda) d\lambda = \int_C F(\xi) d\xi \quad (4.15)$$

4.3 Formulations for the half-space problem

To summarize the forms given in Chapter 2 and compare it to the original Sommerfeld problem, we present the solution of the vertical electric dipole over an infinite half-space in a very compact form as follows:

$$\vec{\Pi}_1 = \Pi_{1z} \hat{a}_z = (\Pi_{1z}^{prim} + \Pi_{1z}^{sec}) \hat{a}_z \quad (4.16)$$

$$\vec{\Pi}_2 = \Pi_{2z} \hat{a}_z = \Pi_{2z}^{sec} \hat{a}_z \quad (4.17)$$

The boundary conditions at $z = 0$ are given by:

$$\Pi_{1z} = \varepsilon \Pi_{2z} \quad \& \quad \frac{\partial}{\partial z} \Pi_{1z} = \varepsilon \frac{\partial}{\partial z} \Pi_{2z} \quad (4.18)$$

4.3.1 Sommerfeld Formulation for vertical electric dipole:

The suitable form of solutions are given by:

$$\Pi_{1z}^{prim} = \frac{1}{2} \int_{-\infty}^{\infty} H_0^{(2)}(\lambda \rho) \exp(\sqrt{\lambda^2 - k_1^2} (z - h)) \frac{\lambda}{\sqrt{\lambda^2 - k_1^2}} d\lambda, \quad 0 < z < h \quad (4.19)$$

$$\Pi_{1z}^{sec} = \frac{1}{2} \int_{-\infty}^{\infty} R(\lambda) H_0^{(2)}(\lambda \rho) \exp(-\sqrt{\lambda^2 - k_1^2} (z + h)) \frac{\lambda}{\sqrt{\lambda^2 - k_1^2}} d\lambda, \quad z > 0 \quad (4.20)$$

$$\Pi_{2z}^{sec} = \frac{1}{2} \int_{-\infty}^{\infty} T(\lambda) H_0^2(\lambda \rho) \exp(\sqrt{\lambda^2 - k_2^2} z - \sqrt{\lambda^2 - k_1^2} h) \frac{\lambda}{\sqrt{\lambda^2 - k_1^2}} d\lambda, \quad z < 0 \quad (4.21)$$

The conditions for convergence of the above integrals are enforced by the radiation condition as follows:

1. $\text{Im}\{\lambda\} < 0$
2. $\text{Re}\{\sqrt{\lambda^2 - k_1^2}\} > 0$

$$3. \operatorname{Re}\left\{\sqrt{\lambda^2 - k_2^2}\right\} > 0$$

From the boundary conditions, we get:

$$R(\lambda) = \frac{\varepsilon\sqrt{\lambda^2 - k_1^2} - \sqrt{\lambda^2 - k_2^2}}{\varepsilon\sqrt{\lambda^2 - k_1^2} + \sqrt{\lambda^2 - k_2^2}} \quad (4.22)$$

$$T(\lambda) = \frac{2\sqrt{\lambda^2 - k_1^2}}{\varepsilon\sqrt{\lambda^2 - k_1^2} + \sqrt{\lambda^2 - k_2^2}} \quad (4.23)$$

4.3.2 Schelkunoff Formulation for vertical electric dipole:

The suitable form of solutions are given by:

$$\Pi_{1z}^{prim} = \frac{1}{\pi} \int_{-\infty}^{\infty} K_0(\rho\sqrt{\xi^2 - k_1^2}) \exp(j\xi(z-h)) d\xi, \quad 0 < z < h \quad (4.24)$$

$$\Pi_{1z}^{sec} = \frac{1}{\pi} \int_{-\infty}^{\infty} R(\xi) K_0(\rho\sqrt{\xi^2 - k_1^2}) \exp(-j\xi(z+h)) d\xi, \quad z > 0 \quad (4.25)$$

$$\Pi_{2z}^{sec} = \frac{1}{\pi} \int_{-\infty}^{\infty} T(\xi) K_0(\rho\sqrt{\xi_2^2 - k_2^2}) \exp(j\xi_2 z - j\xi h) d\xi, \quad z < 0 \quad (4.26)$$

The conditions for convergence are given by:

$$1. \operatorname{Re}\left\{\sqrt{\xi^2 - k_1^2}\right\} > 0$$

$$2. \operatorname{Re}\{j\xi\} > 0 \Rightarrow \operatorname{Im}\{\xi\} < 0$$

$$3. \operatorname{Re}\{j\xi_2\} > 0 \Rightarrow \operatorname{Im}\{\xi_2\} < 0$$

$$\operatorname{Re}\left\{j\sqrt{\xi^2 + (\varepsilon - 1)k_1^2}\right\} > 0 \Rightarrow \operatorname{Im}\left\{\sqrt{\xi^2 + (\varepsilon - 1)k_1^2}\right\} < 0$$

From the boundary conditions, we get:

$$R(\xi) = \frac{j\varepsilon\xi - j\xi_2}{j\varepsilon\xi + j\xi_2} = \frac{j\varepsilon\xi - j\sqrt{\xi^2 + (\varepsilon - 1)k_1^2}}{j\varepsilon\xi + j\sqrt{\xi^2 + (\varepsilon - 1)k_1^2}} \quad (4.27)$$

$$T(\xi) = \frac{2j\xi}{j\varepsilon\xi + j\sqrt{\xi^2 + (\varepsilon - 1)k_1^2}} \quad (4.28)$$

$$\sqrt{\xi^2 - k_1^2} = \sqrt{\xi_2^2 - k_2^2} \quad (4.29)$$

In the previous section, we have proved that (4.19) is identical to (4.24). The main goal now is to examine whether (4.20) and (4.21) are identical to (4.25) and (4.26) respectively or not. To answer this question, we take the following steps:

Substitute for λ by (4.6) in (4.20), and using (4.22) and (4.27), we get:

$$\begin{aligned} \Pi_{1z}^{\text{sec}} &= \frac{1}{2} \int_{\Gamma} R(\lambda) H_0^{(2)}(\lambda\rho) \exp(-\sqrt{\lambda^2 - k_1^2}(z+h)) \frac{\lambda}{\sqrt{\lambda^2 - k_1^2}} d\lambda, \quad z > 0 \\ &= \frac{1}{\pi} \int_{C_{BC_1}} R(\xi) K_0(\rho\sqrt{\xi^2 - k_1^2}) \exp(-j\xi(z+h)) d\xi, \quad z > 0 \end{aligned} \quad (4.30)$$

subject to the conditions: $\text{Re}\{\sqrt{\lambda^2 - k_1^2}\} > 0$, $\text{Re}\{\sqrt{\lambda^2 - k_1^2}\} > 0$, $\text{Im}\{\xi\} < 0$ and

$\text{Im}\{\sqrt{\xi^2 + (\varepsilon - 1)k_1^2}\} < 0$, and the contours Γ and C_{BC_1} are shown in Fig. 4.1-(a) and

Fig. 4.1-(b) respectively.

Similarly, and under the same conditions, if one substitute for ξ by (4.6) in (4.25) and using (4.22) and (4.27), we get:

$$\begin{aligned} \Pi_{1z}^{\text{sec}} &= \frac{1}{\pi} \int_C R(\xi) K_0(\rho\sqrt{\xi^2 - k_1^2}) \exp(-j\xi(z+h)) d\xi, \quad z > 0 \\ &= \frac{1}{2} \int_{\Gamma_{BC_1}} R(\lambda) H_0^{(2)}(\lambda\rho) \exp(-\sqrt{\lambda^2 - k_1^2}(z+h)) \frac{\lambda}{\sqrt{\lambda^2 - k_1^2}} d\lambda, \quad z > 0 \end{aligned} \quad (4.31)$$

where the contours C and Γ_{BC_1} are shown in Fig. 4.2-(b) and Fig. 4.2-(a) respectively.

Therefore, the two formulations are identical **if and only if**:

$$\int_C R(\xi)F(\xi)d\xi = \int_{C_{BC_1}} R(\xi)F(\xi)d\xi \quad (4.32)$$

or equivalently,

$$\int_{\Gamma} R(\lambda)G(\lambda)d\lambda = \int_{\Gamma_{BC_1}} R(\lambda)G(\lambda)d\lambda \quad (4.33)$$

An identical analysis can be done for the forms of medium 2 which are given in (4.21) and (4.26). The problem now is that the deformation of the contours in either the λ – plane or in the ξ – plane becomes tricky and not as straight forward as in the previous section. This is because the integrands in (4.32) and (4.33) contain the functions $R(\xi)$ and $R(\lambda)$ which add more singularities in the complex planes. What type of singularities are added and what are the effect of those singularities; those questions are addressed in the rest of this chapter.

4.3.3 Properties of the reflection coefficient in the complex planes

The case of a vertical dipole represent a TM case where the magnetic field is perpendicular to the plane of incidence for all the elementary waves under the integration sign. The reflection coefficients in this case are given by (4.22) and (4.27), which are identical because of the relation given in (4.6). Remember that those expressions are derived from the continuity of the tangential electric and magnetic fields as shown in (4.18).

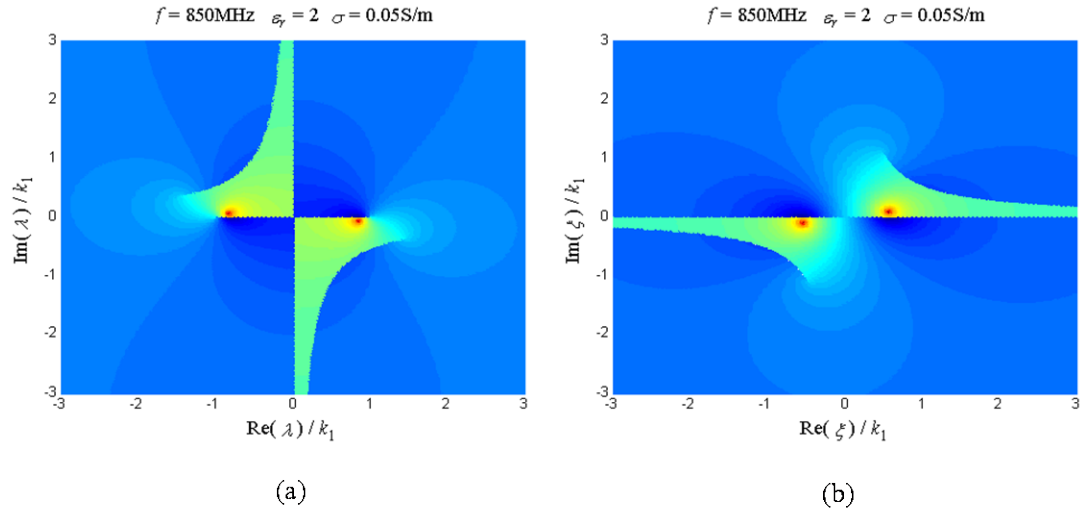


Fig. 4.6 Numerical plot of the reflection coefficient function in: (a) the complex λ -**plane**, and (b) the complex ξ -**plane**.

Fig. 4.6 shows a numerical plot for equations (4.22) and (4.27) for the second medium parameters of $\epsilon_r = 2$ and $\sigma = 0.05$. It is clear in the Fig. 4.6, that the reflection coefficient function adds one more branch point singularity in either domains in addition to the already existing branch point singularity at k_1 shown in Fig. 4.5. Therefore, the integrands would have two branch cuts and accordingly four different Riemann sheets. To be more specific, let's consider each plane separately.

4.3.3.1 Properties of $R(\lambda)$ in the λ -**plane**:

The function given in (4.22) has two branch point singularities at $\lambda = \pm k_1$ and at $\lambda = \pm k_2$. The branch cuts associated with those branch points are illustrated clearly in Fig. 4.6-(a). Only the two branch cuts in the lower half-plane are of interest to us. Those two branch points divide the complex λ -**plane** into four different Riemann sheets as follows:

Sheet 1: $\text{Real}(\sqrt{\lambda^2 - k_1^2}) > 0$ and $\text{Real}(\sqrt{\lambda^2 - k_2^2}) > 0$

Sheet 2: $\text{Real}(\sqrt{\lambda^2 - k_1^2}) < 0$ and $\text{Real}(\sqrt{\lambda^2 - k_2^2}) > 0$

Sheet 3: $\text{Real}(\sqrt{\lambda^2 - k_1^2}) > 0$ and $\text{Real}(\sqrt{\lambda^2 - k_2^2}) < 0$

Sheet 4: $\text{Real}(\sqrt{\lambda^2 - k_1^2}) < 0$ and $\text{Real}(\sqrt{\lambda^2 - k_2^2}) < 0$

Along the branch cuts emanating from the point $\lambda = k_1$ the real part of $\sqrt{\lambda^2 - k_1^2}$ is equal to zero, while along the branch cut emanating from the point $\lambda = k_2$ the real part of $\sqrt{\lambda^2 - k_2^2}$ is equal to zero. Sommerfeld originally chose the only permissible Riemann sheet to be Sheet 1 on which the radiation condition is satisfied. In addition to the branch point singularity there is a pole/zero singularity at the point:

$$\lambda_s = \pm \frac{k_1 k_2}{\sqrt{k_1^2 + k_2^2}} = \pm \sqrt{\frac{\varepsilon}{\varepsilon + 1}} k_1 \quad (4.34)$$

where ε is the complex relative permittivity of medium 2. Depending on the value of ε , the point $\lambda = \lambda_s$ represents a zero of the function $R(\lambda)$ on two Riemann sheets and at the same time it represents a pole of the function on the other two sheets.

4.3.3.2 Properties of $R(\xi)$ in the ξ - plane :

While the analysis given in the previous subsection can be found in a vast amount of sources in the literature, the analysis given here in this subsection can hardly be found. The function given in (4.27) has two branch point singularities at $\xi = 0$ and at $\xi = \pm\sqrt{-(\varepsilon - 1)}k_1$. The first branch point has two associated branch cuts aligned with the real axis as shown in Fig. 4.6-(b). The other branch points lie in the first and third

quadrants and their associated branch cuts are as shown in Fig. 4.6-(b). Only the branch cuts in the third quadrant are of interest due to the enforced condition, $\text{Im}\{\xi\} \leq 0$, mentioned in the previous section, which guarantees the convergence of the fields at infinity. Those two considered branch cuts result in four different Riemann sheets. In addition to the branch point singularities, there is a pole/zero singularity at the point:

$$\xi_s = \pm \sqrt{\frac{1}{\varepsilon + 1}} k_1 \quad (4.35)$$

where ε is the complex relative permittivity of medium 2. Depending on the value of ε , the point $\xi = \xi_s$ represents a zero of the function $R(\xi)$ on two Riemann sheets and at the same time it represents a pole of the function on the other two sheets. It is very important to note the effect of the value of ε on determining whether the singularity in (4.35) is a pole or a zero of the function. A detailed analysis of this effect is left for the next chapter of this dissertation, as it also represents one of the unique contributions of this dissertation. While in the rest of this chapter, the common aspects about the previously mentioned singularities which are widely accepted in the literature are discussed. We address those widely accepted concepts because they are likely to give rise to some controversies about the new formulation, given in this dissertation, as compared to the conventional Sommerfeld formulation.

4.3.4 Cauchy's theorem applied in the complex planes

A straight forward application of the Cauchy's theorem in the λ – plane to calculate the left-hand side of (4.33) yields an equation very similar to (4.11) but with additional two terms as follows:

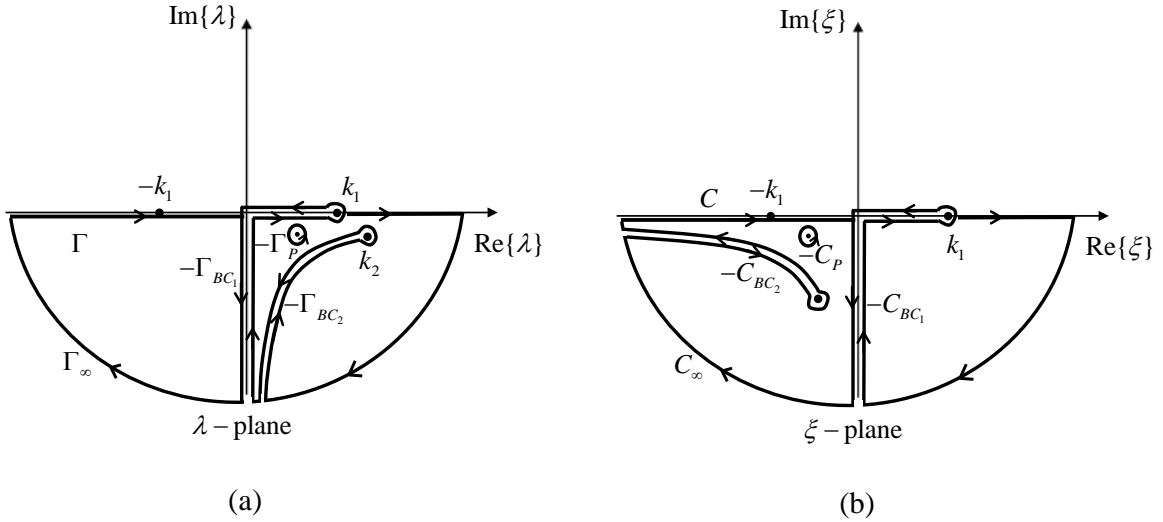


Fig. 4.7 Application of the Cauchy's theorem on the integrals that include the reflection coefficient function in: (a) the complex λ - plane , and (b) the complex ξ - plane .

$$\left\{ \int_{\Gamma} \cdot + \int_{\Gamma_{\infty}} \cdot + \int_{-\Gamma_{BC_1}} \cdot + \int_{-\Gamma_{BC_2}} \cdot + \int_{-\Gamma_P} \cdot \right\} R(\lambda)G(\lambda)d\lambda = 0 \quad (4.36)$$

where Γ_{BC_2} is the contour along the branch cut emanating from the branch point $\lambda = k_2$,

and Γ_P is the contour around the pole location as shown in Fig. 4.7-(a). Accordingly,

Sommerfeld decomposed his original integral into three different terms as follows:

$$\int_{\Gamma} R(\lambda)G(\lambda)d\lambda = \left\{ \int_{\Gamma_{BC_1}} \cdot + \int_{\Gamma_{BC_2}} \cdot + \int_{\Gamma_P} \cdot \right\} R(\lambda)G(\lambda)d\lambda \quad (4.37)$$

Then, Sommerfeld called the branch cut contributions “*the space waves*” and he called the pole contribution “*the surface wave*”. Remember that our target is to prove that the integral along Γ is equivalent to the integral along Γ_{BC_1} only, so that we can say based on

(4.30) and (4.31) that Sommerfeld and the new formulations are identical. In other words, we need to prove that the term $\left\{ \int_{\Gamma_{BC_2}} \cdot + \int_{\Gamma_P} \cdot \right\} R(\lambda)G(\lambda)d\lambda$ can be neglected.

The proof of this fact can be easily found in the literature. For example, in the year 1950 in the proceedings of IRE, a paper by Kahan and Eckart states explicitly in the introduction: “*The integral taken over the branch cut of k_2 may be neglected. The integral of k_1 is developed asymptotically and yields the part of the solution which Sommerfeld calls the “space wave,” and which as we shall see, represents by itself the correct solution” [24].*

Regarding the pole contribution, it is very important to note that the location of the pole in the λ -plane shown in figure-28 of Sommerfeld’s book [21, p. 251] is wrong. This becomes quite obvious if one recalls the formula of the location of the pole in the λ – plane , given by (4.34) which directly implies two important facts:

- 1- The pole should lie inside a circle of radius $|k_1|$ whose center is the origin of the λ – plane . Thus, the location shown in Sommerfeld’s book is wrong.
- 2- As the magnitude of ε increases, the pole comes to a closer proximity of the point k_1 which becomes the saddle point for calculating the field along the surface [24] [3, p. 67]

The first fact indicates that the branch cuts if taken vertically downwards, the pole will automatically go off the proper Riemann sheet implied from the convergence conditions specified earlier by Sommerfeld. A very rigorous analysis which proves this fact is given by Jin A. Kong in [25]. The second fact indicates that if the branch cuts are taken in such a way that the pole is on the proper Riemann sheet, there must be a saddle

point very close to the pole such that their contributions cancel out. More than one proof of this fact is given in [24] and [3, p. 70].

After all, it is well known that the residue of the pole, P , has the form of “Zenneck Surface Wave”, which have been proven experimentally not to exist in the radiation of a dipole over a half-space medium [26] and hence should not appear in the final solution.

Regarding the integral along the branch cut emanating from the branch point $\lambda = k_2$ in the λ – plane, as mentioned earlier, this contribution is always neglected by many authors who wrote on the subject. For example:

In 1967, James R. Wait states that: *“The branch line integration associated with k_2 is carried out in a manner similar to that for k_0 but now the contribution is proportional to $\rho^{-2} \exp(-ik_2\rho)$ which is heavily damped since k_2 has an appreciable imaginary part when the lower medium is finitely conducting. Therefore, in what follows, we assume that this contribution to the integral F is negligible.”* [27]

Another example is what R. E. Collin says: *“The integral around the branch cut running from the point k_2 can be neglected, since the contributions from this part of the integral will have an attenuation at least as great as that of $\exp(ik_2r)$, which is very large for even modest values of r ”* [3, p. 67].

Furthermore, in the rigorous analysis given by Jin A. Kong in [25], it is concluded that the path of the branch cut emanating from k_2 in the λ – plane does not even affect whether the pole exists on the proper Riemann sheet or not. It is only the path of the branch cut of k_1 that is important.

According to the contemporary solutions given in the current literature, one can conclude that the pole contribution cannot stand independently in the final solution. After

all, the function $R(\lambda)$ represents physically the reflection coefficient as a function of the angle of incidence. For a two-media problem, this reflection coefficient can have no poles. There is no meaning to have a reflected field without an incident one. More explanations about this issue are discussed in details in the following chapter.

Now, let's consider applying the Cauchy's theorem in the ξ – plane , an equation similar to (4.37) should occur:

$$\int_C R(\xi)F(\xi)d\xi = \left\{ \int_{C_{BC_1}} \cdot + \int_{C_{BC_2}} \cdot + \int_{C_P} \cdot \right\} R(\xi)F(\xi)d\xi \quad (4.38)$$

where the contours are shown in Fig. 4.7-(b). Again, the target is to prove that the integral along C is equivalent to the integral along C_{BC_1} only. In other words we need to prove

that the term $\left\{ \int_{C_{BC_2}} \cdot + \int_{C_P} \cdot \right\} R(\xi)F(\xi)d\xi$ can be neglected in order to say that the formulation

of Sommerfeld and the new formulation are identical. Regarding the pole contribution, the following chapter of this dissertation is dedicated for a detailed explanation of this pole and whether it should affect the result or not. In the following chapter, it is proved that this pole should not be captured while solving the two-media problem. The remaining term now is the contribution of the integral along the second branch cut C_{BC_2} .

The contribution of this term can always be neglected in almost all practical cases. A numerical study on this issue is given next in this chapter.

4.4 Numerical Analysis of the Half-Space Problem

The philosophy in the numerical analysis given in this section is the same as what was used to get Fig. 3.5 and Fig. 3.6. For a vertical electric dipole, the vector potential of

(2.22), which is identical to the first line of (4.31), is calculated numerically using adaptive gauss quadrature routine of integration. Then, the results are compared to those of the first line of (4.30) calculated using the same routine of integration with the same relative tolerance and number of iterations.

Assume a vertical electric dipole located at a height h from the interface between air and a medium of $(\epsilon_r, \mu_r = 1, \sigma)$. The observation point is at a height z from the interface. The results of numerical integration are calculated and plotted versus the horizontal separation ρ between the source and field points. The plot is repeated for different heights and different ground parameters. All distances in the plots are then normalized to the free space wavelength w .

The results shown in Fig. 4.8 show a comparison between the performance of the two formulations. The frequency is 850 MHz, the height of the source is 20 wavelengths and the height of the field point is 80 wavelengths. The ground parameters are chosen as the urban ground parameters where $\epsilon_r = 10$ and $\sigma = 0.2$ S/m. Fig. 4.8-(a) shows the numerical integration results along with the relative error in the real and imaginary parts. The absolute value of the error between the two formulations, in both the real and the imaginary parts, is more than 40 dB lower than absolute value of the numerical result itself. This indicates that for the given parameters, both formulations give identical results. In Fig. 4.8-(b) The total Green's function, which is the sum of the primary and the secondary stimulations, is plotted as a function of the horizontal separation between the field and source points, ρ . The plot show that both formulations give identical results. The time for calculating each of the integrals for each ρ is shown in Fig. 4.8-(c).

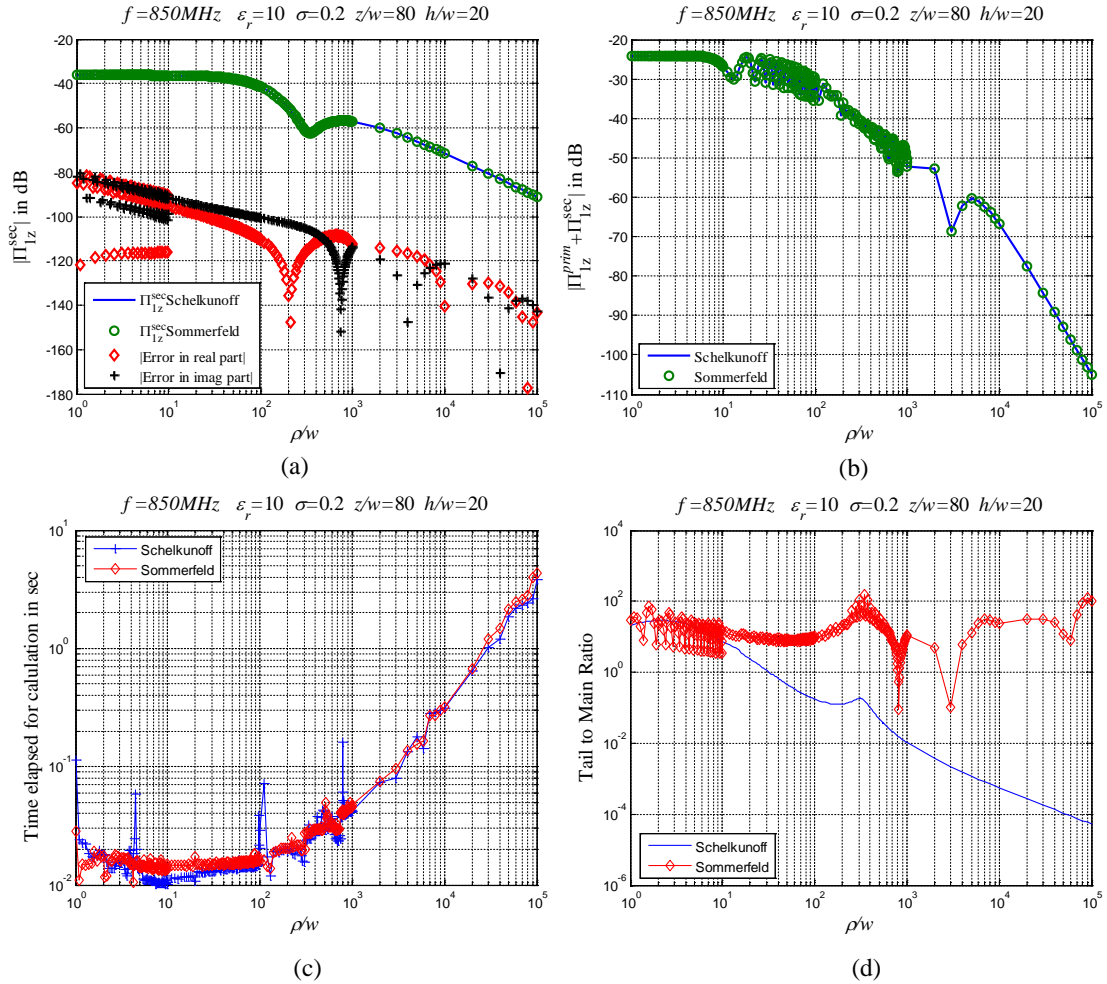


Fig. 4.8 Numerical comparison between Schelkunoff and Sommerfeld formulations for a vertical electric dipole over urban ground, $z+h=100$ wavelengths: (a) The secondary part of the vector potential, (b) The total magnitude of the vector potential, (c) time to numerically calculate the integrals, (d) the tail-to-main ratio.

The Tail-to-Main ratio is shown in Fig. 4.8-(d). This ratio represents the ratio of the second term to the first term of (2.19). Fig. 4.8-(d) show that Schelkunoff formulation does not suffer from the integral tails problem. However, Fig. 4.8-(c) show that the time to calculating the value of the integral on the tail part of the contour does not affect the total time because of the presence of the exponential function in the Sommerfeld formulation as explained in Chapter 2.

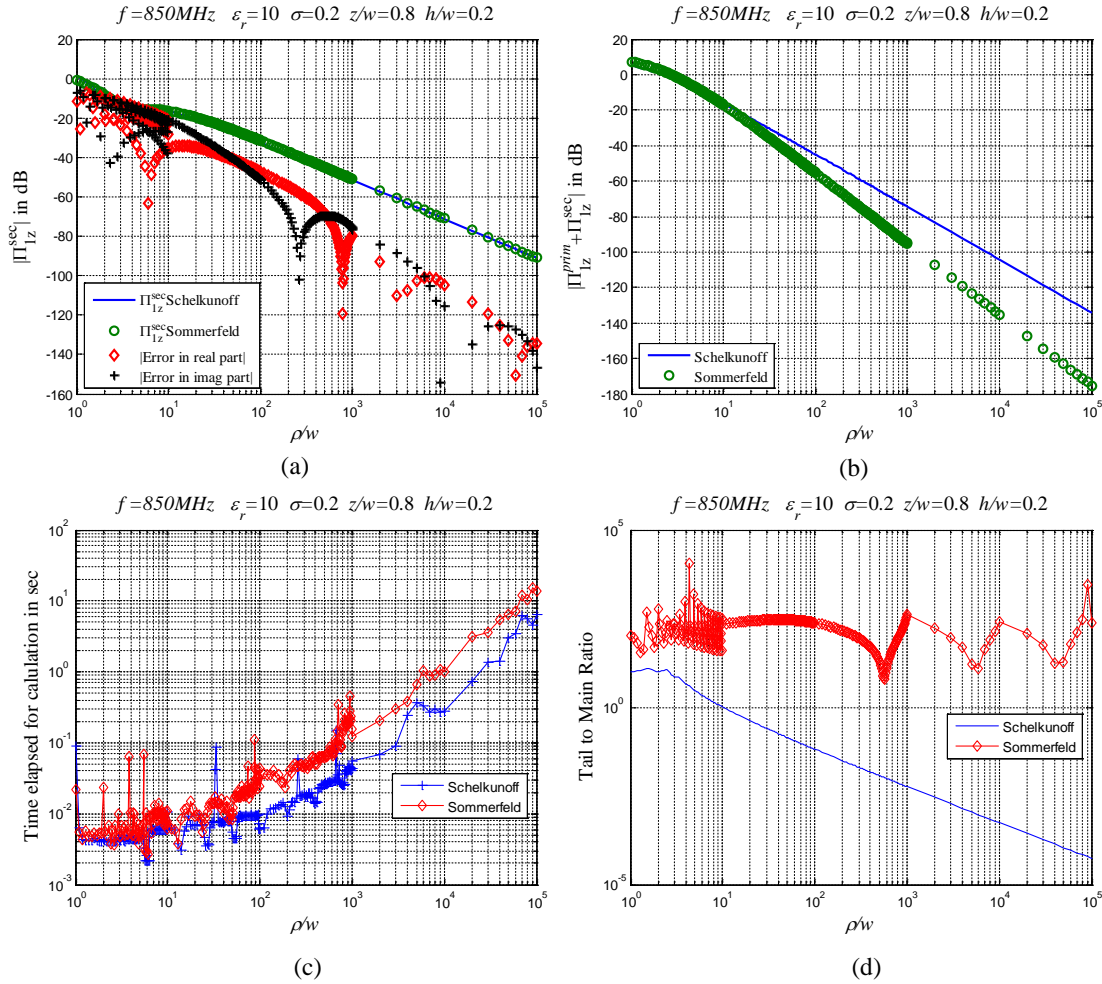


Fig. 4.9 Numerical comparison between Schelkunoff and Sommerfeld formulations for a vertical electric dipole over urban ground, $z+h=1$ wavelengths: (a) The secondary part of the vector potential, (b) The total magnitude of the vector potential, (c) time to numerically calculate the integrals, (d) the tail-to-main ratio.

The previous example show that Schelkunoff formulation and Sommerfeld formulation give exactly identical results which supports the validity of the new formulation. However, in this example the superiority of the new formulation is not very clear since both formulation need approximately the same time for calculation. As the source and field points go closer to the interface, the integral tails in Sommerfeld formulation become more problematic. This is illustrated in the following example where $z+h=1$ wavelength.

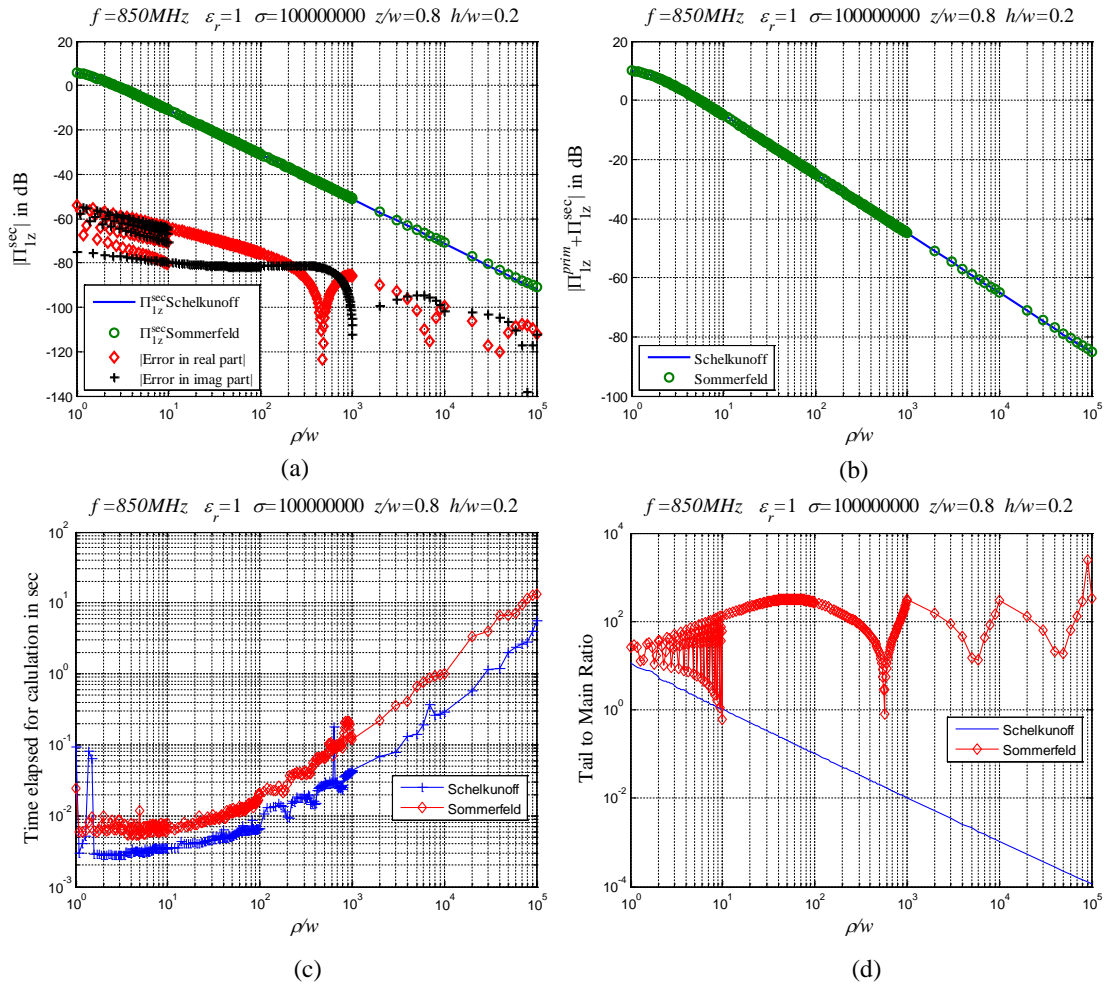


Fig. 4.10 Numerical comparison between Schelkunoff and Sommerfeld formulations for a vertical electric dipole over a very good conductor, $z+h=1$ wavelengths: (a) The secondary part of the vector potential, (b) The total magnitude of the vector potential, (c) time to numerically calculate the integrals, (d) the tail-to-main ratio.

The results shown in Fig. 4.9 show a comparison between the performance of the two formulations when the height of the source is 0.2 wavelengths and the height of the field point is 0.8 wavelengths. The ground parameters are chosen as the urban ground parameters where $\epsilon_r = 10$ and $\sigma = 0.2$ S/m. Fig. 4.9-(a) show that the error between the secondary potential in the two formulations is significant for small values of ρ and the error decreases as ρ increases.

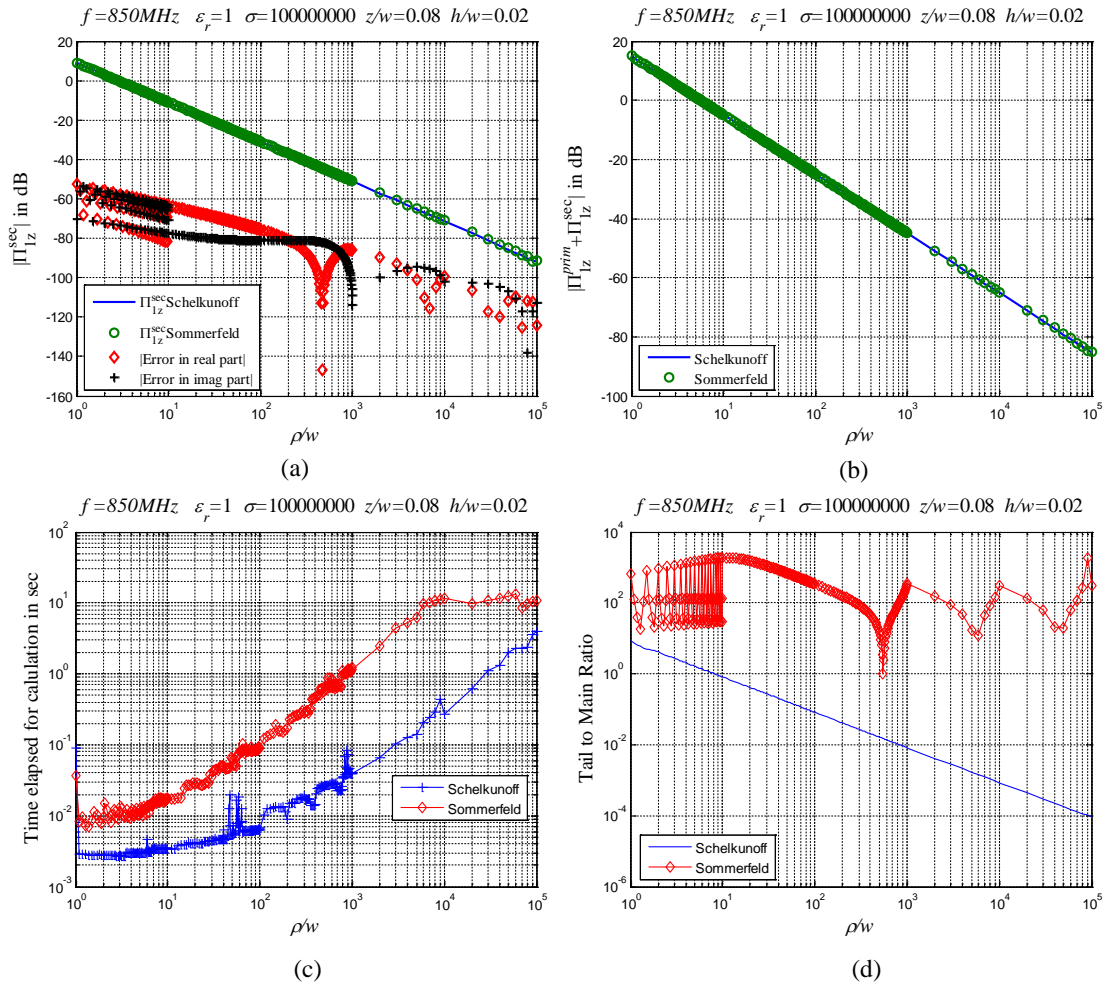


Fig. 4.11 Numerical comparison between Schelkunoff and Sommerfeld formulations for a vertical electric dipole over a very good conductor, $z+h=0.1$ wavelengths: (a) The secondary part of the vector potential, (b) The total magnitude of the vector potential, (c) time to numerically calculate the integrals, (d) the tail-to-main ratio.

However, after adding the secondary part of the potential to the primary (direct) stimulation, the result look different for both formulations, especially for large values of ρ . This could be caused by the instability of the integrands in the Sommerfeld formulation when $z+h$ is small compared to the wavelength. This claim is supported by Fig. 4.9-(c) where it is clear that the time needed to calculate Sommerfeld integrals increased as compared to the Schelkunoff formulation.

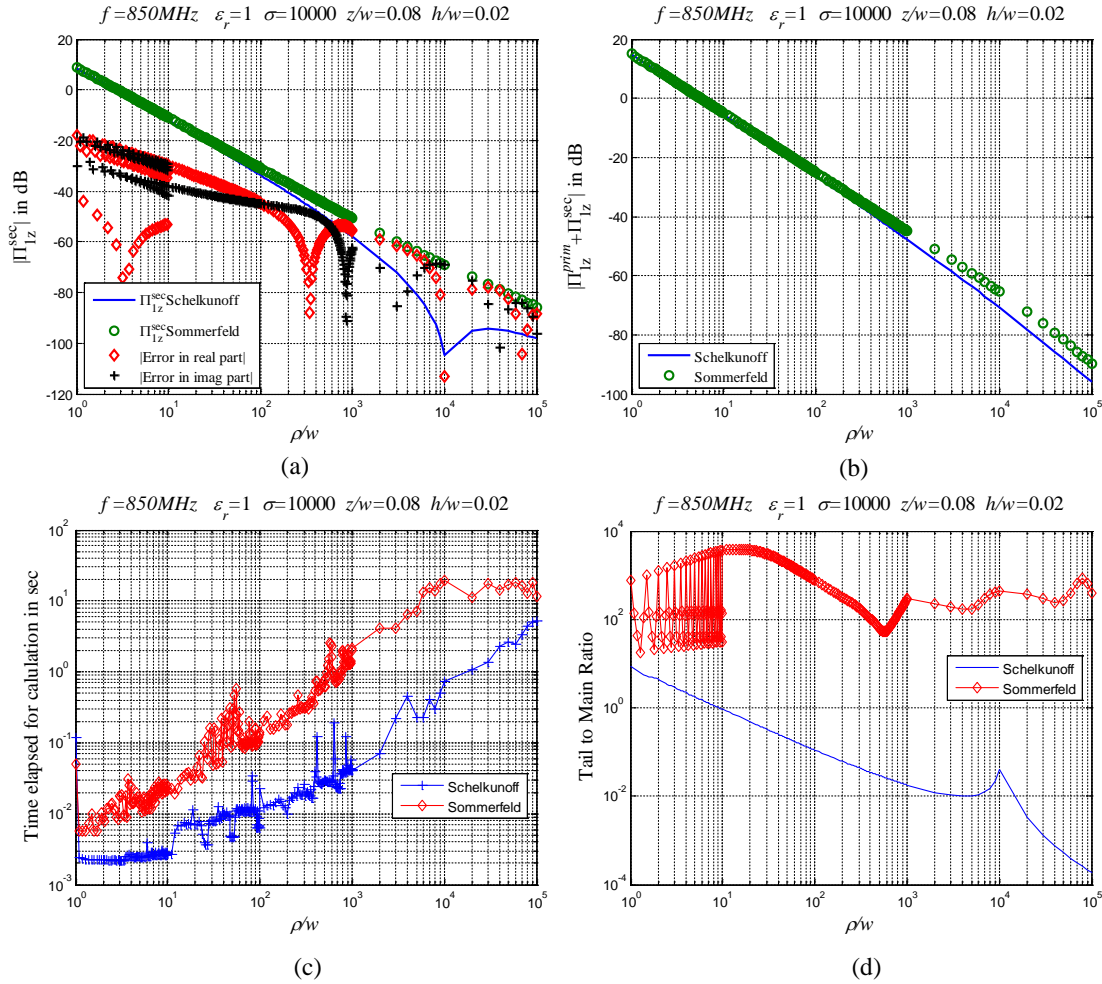


Fig. 4.12 Numerical comparison between Schelkunoff and Sommerfeld formulations for a vertical electric dipole over a conducting ground, $\sigma = 10^4$ S/m, $z+h=0.1$ wavelengths: (a) The secondary part of the vector potential, (b) The total magnitude of the vector potential, (c) time to numerically calculate the integrals, (d) the tail-to-main ratio.

In Fig. 4.10, the same results are shown but for a much higher conductivity of the ground where $\sigma = 10^8$ S/m. Again both formulations give identical results. Even if we check for much smaller heights where $z+h=0.1$ wavelengths and $\sigma = 10^8$ S/m, still both formulations give identical results but with a much smaller calculation time for the Schelkunoff formulation as compared to the Sommerfeld formulation as shown in

Fig. 4.11. If we keep all parameters the same except decreasing the conductivity of the ground to be $\sigma = 10^4 \text{ S/m}$, the results in this case would be as shown in Fig. 4.12.

To give a more detailed picture for the numerical difference between the results of Schelkunoff and Sommerfeld formulations, a two dimensional map for the absolute value of the error is shown in Fig. 4.13 for ground parameters of $\epsilon_r = 4$ and $\sigma = 0.002 \text{ S/m}$. In this case, an x -oriented horizontal dipole is considered and the values are to be calculated along the y -axis. Thus, the value of interest will be that of \mathbf{g}_{sH} given in (3.43), and the error shown is given by:

$$\text{Error in dB} = 20 \log_{10} \left| \frac{\mathbf{g}_{sH} - \mathbf{g}_{sH}^{som}}{|\mathbf{g}_{sH}|} \right| \quad (4.39)$$

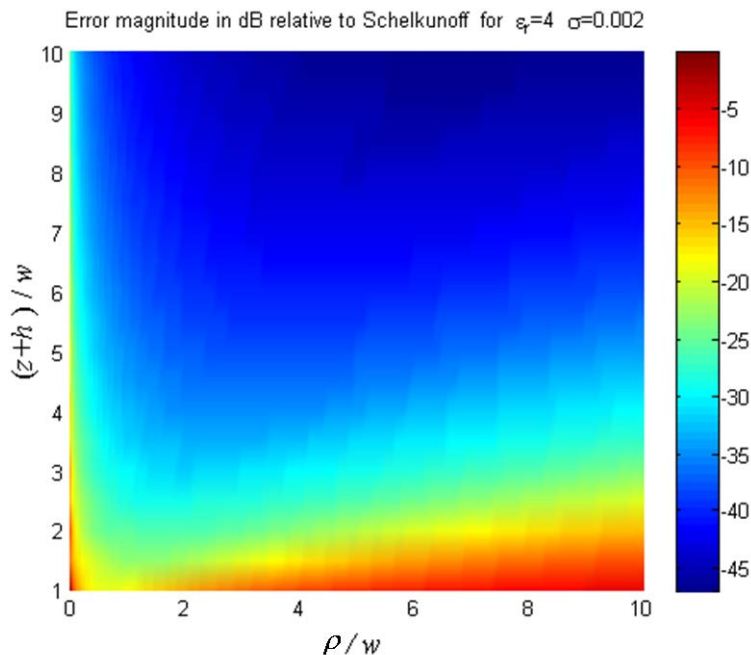


Fig. 4.13 Absolute value of the error in dB as compared to the absolute value of the result of Schelkunoff formulation. Ground parameters of $\epsilon_r = 4$ and $\sigma = 0.002 \text{ S/m}$. The vertical and horizontal axes are normalized to the wavelength w .

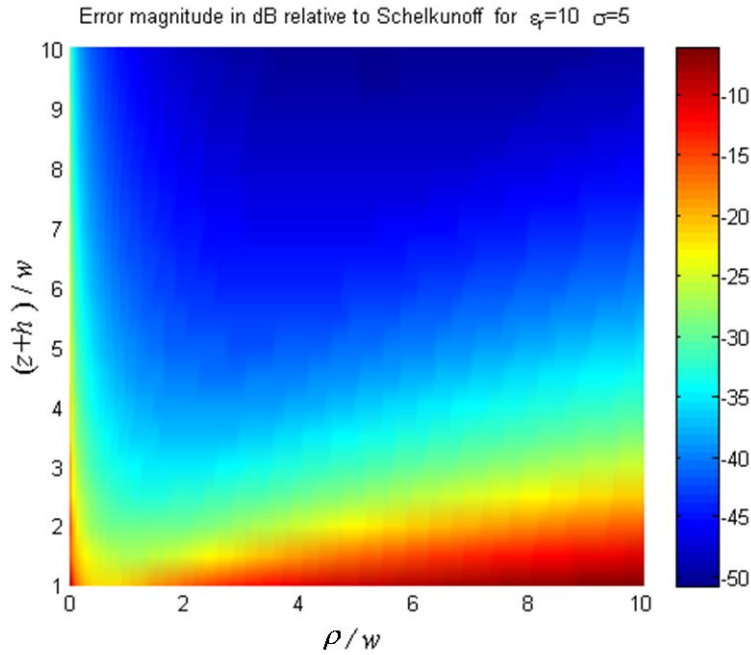


Fig. 4.14 Absolute value of the error in dB as compared to the absolute value of the result of Schelkunoff formulation for the horizontal dipole. Ground parameters of $\epsilon_r = 10$ and $\sigma = 5 \text{ S/m}$. The vertical and horizontal axes are normalized to the wavelength w .

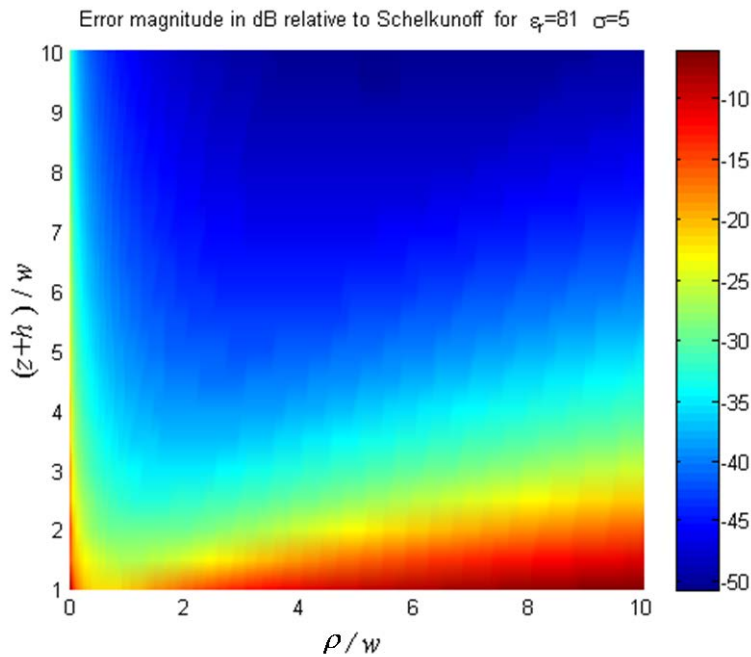


Fig. 4.15 Absolute value of the error in dB as compared to the absolute value of the result of Schelkunoff formulation for the horizontal dipole. Ground parameters of $\epsilon_r = 81$ and $\sigma = 5 \text{ S/m}$. The vertical and horizontal axes are normalized to the wavelength w .

Note that in Fig. 4.13, a value of -20 dB corresponds to 10% relative error whereas a value of -40 dB corresponds to 1% relative error. Observe that the regions where the two formulations do not give identical results are those regions where one of the two formulations has poor convergence behavior. One can easily relate those regions in Fig. 4.13 to the regions indicated in Fig. 2.5. The same comparison is shown for different ground parameters in Fig. 4.14 and Fig. 4.15 below.

For the sake of completeness, another two dimensional map for the complete Green's function of the vertical dipole case, Π_{1z} , is given below for different ground parameters. The error plotted in this case is given by:

$$\text{Error in dB} = 20 \log_{10} \left| \frac{\Pi_{1z} - \Pi_{1z}^{som}}{|\Pi_{1z}|} \right| \quad (4.40)$$

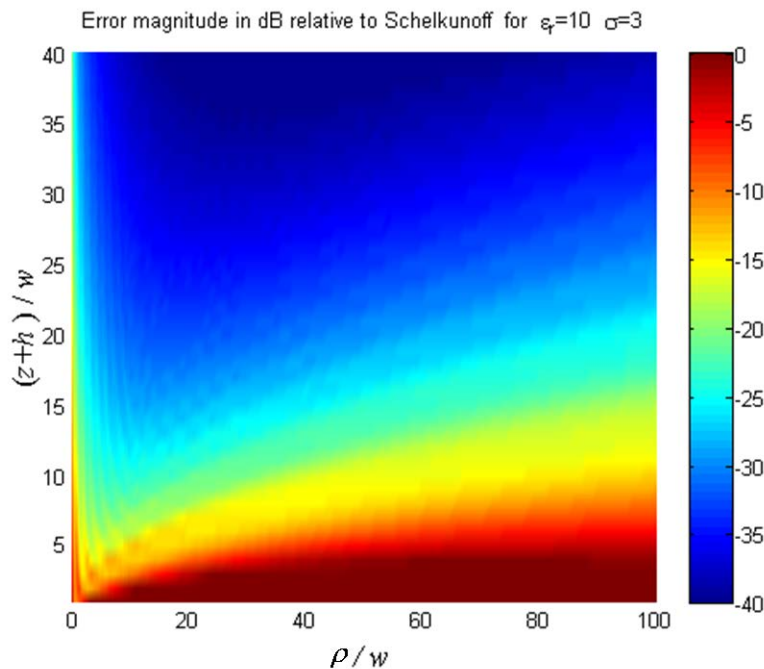


Fig. 4.16 Absolute value of the error in dB as compared to the absolute value of the result of Schelkunoff formulation for the vertical dipole. Ground parameters of $\epsilon_r = 10$ and $\sigma = 3 \text{ S/m}$. The vertical and horizontal axes are normalized to the wavelength w .

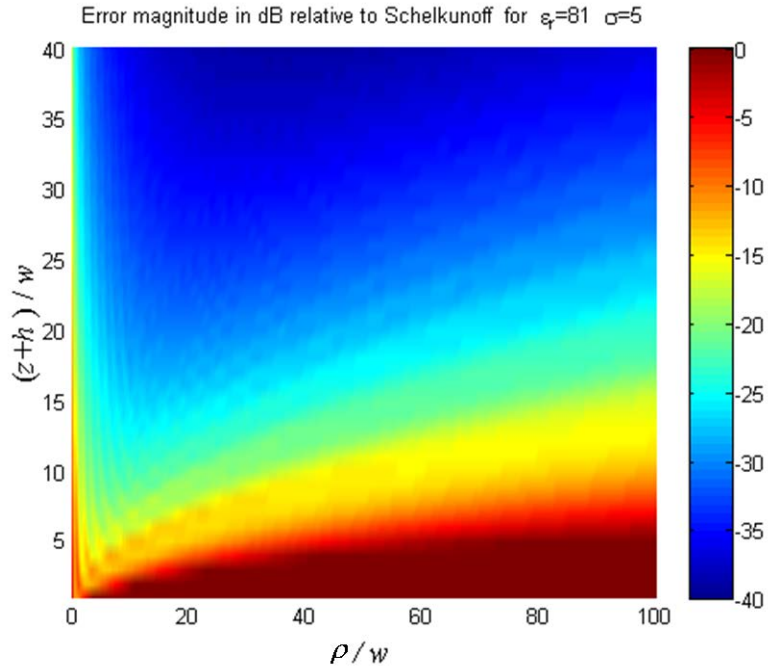


Fig. 4.17 Absolute value of the error in dB as compared to the absolute value of the result of Schelkunoff formulation for the vertical dipole. Ground parameters of $\epsilon_r = 81$ and $\sigma = 5 \text{ S/m}$. The vertical and horizontal axes are normalized to the wavelength w .

4.5 Conclusion

In this chapter, it is shown that from a mathematical point view, the two formulations are identical when calculated in one homogeneous medium. Whereas, in a two-media problem the Sommerfeld and Schelkunoff formulations differ possibly by the pole and branch cut contributions associated with the reflection coefficient function added inside the integration sign. Numerically, both formulations give identical results when the field and source points are at relatively high elevations as compared to the operating wavelength. When both the field and source points are at an electrically small distance from the interface, both formulations give different results except for very high conductivity of the ground. In the following chapter, based on physical and mathematical

explanations, it will be shown that this difference between the two formulations cannot be due to the pole of the reflection coefficient function; as this pole has to be excluded when solving the two-media problem. Thus, the difference will be shown to be only due to the second branch cut associated with the second medium. However, this contribution has no effect when the source and/or the field points are at a vertical distance from the interface that is large compared to the wavelength. Furthermore, the second branch cut contribution has no effect when the conductivity of the ground is large even if the source and field point are very close to the interface.

5 Surface Waves versus Surface Plasmons

The main goal in this chapter is to explain the physics related to the Sommerfeld pole of the reflection coefficient function. The claim found in the literature is that this pole is what gives rise to “*Surface Waves*”. Recently, an inter-disciplinary research area has been emerged related to what is called “*Surface Plasmons*”. It is interesting, and also somewhat confusing, to see in the literature that Surface plasmons are claimed to be the same phenomenon as surface waves but at a different frequency, and the mathematical explanation of both is the Sommerfeld pole. This claim is theoretically examined in this chapter.

The term “Surface Plasmons” was first coined in the middle of the twentieth century to study the response of thin metal foils in response to fast electron bombardment. In the literature, Surface Plasmons are frequently related to Electromagnetic Surface Waves, which were first studied by Zenneck and independently by Sommerfeld in the early 1900’s. However, Zenneck and Sommerfeld surface waves are rarely examined thoroughly in the current literature on Surface Plasmons. Looking for a good technical understanding of the relation between Surface Plasmons and Electromagnetic Surface Waves, it was necessary to carry out a detailed literature review on the two subjects. In the light of this literature review, an attempt to explain the true relation between the two phenomena is presented in this chapter. This is in direct contact with the discussion given in the previous chapter since the claimed mathematical explanation of the two phenomena is usually taken as the pole of the reflection coefficient

function. Hence, in the discussion given in this chapter, the uncertainty about the pole contribution is going to be clarified.

5.1 Introduction

In 1959, Sergei A. Schelkunoff from Bell Labs wrote on the “Anatomy of Surface Waves” [28]. He recognized eleven types of different electromagnetic phenomena, all of which are called “surface waves”. He concluded: *“The loose use of the term surface wave is unfortunate and causes a great deal of unnecessary confusion. If it is continued, the best that one could hope for is that the term will become entirely devoid of meaning. This writer (Schelkunoff) hopes however, that the classical definition of the term (Lord Rayleigh’s) will be restored. Sommerfeld and Zenneck adhered to it, although they have made an unfortunate slip in their analysis which subsequently confused the issue”*.

In the opinion of the author of this dissertation, Schelkunoff’s interpretation about the term was true, and one of the hardest tasks nowadays is to define exactly what an electromagnetic surface wave is, and the task is more complicated to find the true relation between what is known now as Surface Plasmons, and Electromagnetic Surface Waves.

According to [29], Ritchie was the first, in 1957, to use the term “surface plasmons” to study the response of thin metal foils to fast electron bombardment. Since then the surface plasmons found a variety of applications in different areas of science. Frequently, one can find the surface plasmons related to Zenneck and Sommerfeld waves such as in [30]- [31]. It is interesting to see in the title in [30] that the word “*Surface plasmon*” was put between brackets as a substitute to the Zenneck wave as follows: “*THz Zenneck surface wave (THz surface plasmon) propagation on a metal sheet*”. That’s where confusion might arise. At least the question is: Do we really mean the Zenneck

type of surface waves? Or which type from the 11 types mentioned by Schelkunoff in [28]. Another example is in [31] where the term “*Sommerfeld wave*” was used to represent the propagation of THz pulses on a single metal wire. One more example is in [32] where the experimental study was entitled: “*Surface plasmons and Sommerfeld-Zenneck waves on corrugated surfaces*”.

In this chapter, and up to this point only, the reader might have the following questions in mind. What is the standard definition of the word “plasmon”? “surface plasmon”? “is there a volume plasmon”? What is meant by “surface plasmon polaritons”? What is the standard definition of “surface waves” in general and “Sommerfeld waves” and “Zenneck waves” in specific? Then the important question comes: what is the true physical relation between all of those terminologies?

As a matter of fact, the task of answering those questions is not trivial. The main purpose of this chapter is to attempt to give a satisfying answer for those issues. Hence, one could reach a satisfying conclusion about the physical and mathematical aspects related to the surface waves in general and the Sommerfeld pole in specific. The chapter is organized as follows: A detailed literature review on the terms related to plasmons is given in section 5.2, where we tried to search the literature for the points where surface plasmons were related to surface electromagnetic waves and try to explain the rationale in relating the two phenomena. In section 5.3, on the other hand, different definitions of surface electromagnetic waves are given. Specifically, the work of Sommerfeld on relating the pole of the reflection coefficient function to the phenomena of surface waves is examined. The slip in the analysis of Sommerfeld mentioned earlier by Schelkunoff is highlighted from an unconventional point of view. This explanation is given in section

5.4. In the last section, a physical visualization of some of the discussed electromagnetic phenomena is given.

5.2 Evolution of the word Plasmons

The starting point in our literature review was chosen to be the paper by Ritchie on Plasma losses by fast electron in thin films, published in 1957 [33]. That was one of the earliest paper in which the term “surface plasmon, SP” was found. Ritchie was studying the angle-energy distribution of a fast electron bombarding a metal foil and losing its energy to plasma oscillations in the sea of the conduction electrons in the metal. Ritchie called the plasma oscillations of the conduction electrons “plasmons”. He then used the term “surface plasmon” trying to differentiate between the plasma oscillations that appear on the surface of the metal from those which appear in the volume of a thick metal foil. In fact, “volume plasmons” were studied by the Nobel laureate, Dennis Gabor. He first criticized Ritchie’s work and negated the existence of “surface plasmons”. Then Ritchie showed in [33] that Gabor was studying only volume plasmon modes in bounded media. This made Gabor enforce the electric field to be zero at the surface of the metal, which does not apply in the case of very thin metal films. By the year 1985, Ritchie’s paper had been already cited in more than 435 scientific publications [34]. The reason for citing his paper so frequently was, as Ritchie said, the rapid development in surface science. It was also because surface plasmons were a prominent feature in electron energy loss experiments, electron spectroscopy, optical response of solids, low energy electron diffraction, etc. Also surface plasmons were a stimulus to the development of the many-body theory of the bounded electron gas [34]. In 1961, Ritchie wrote another paper on the optical radiation of foils irradiated by charged particles [35]. In that paper, he

made a detailed prediction of the energy and angle distribution of the photons emitted from the excited surface plasmon in the foil. Twelve years later, in 1973, Ritchie wrote a review of what he called “surface plasmon physics” [36]. That was due to the significant progress made toward the systematic use of surface plasmons as a diagnostic tool to characterize the state of matter at the surface and in the bulk of solids. By that time, the effects of surface plasmons which he also called “surface collective modes in solids” were found to be related to energy loss spectra of fast electrons passing through thin solid films and tunneling of electrons through thin insulating layers, etc [36]. The very important point that needs to be noticed is that in [33]- [36], electromagnetic surface waves were never related to the research work done on surface plasmons. Ritchie never mentioned Sommerfeld or Zenneck in the papers he wrote over the period of more than two decades, except in his latest paper, [36], where he wrote only three lines in a twenty-page paper! He said: “*Note that the analogous case of very long wavelength surface waves in radio transmission over a plane air-earth or air-water interface has been much discussed in the theoretical literature [37]. These are termed Sommerfeld-Zenneck waves*”. He directed his reader to the book by Stratton on electromagnetics [37], which is a very classical book on electromagnetic theory. Ritchie’s view was that surface plasmons were related to very short wavelength phenomena in the optical regime, whereas “Sommerfeld-Zenneck waves” are related to very long wavelength transmission on top of planar boundaries. There is nothing else that can be inferred about the analogy which he mentioned in those three lines.

In 1968, another paper was published by Otto on the optical excitation of plasma oscillations in silver by the method of *frustrated total reflection* [38]. In that paper, Otto

showed a method to excite electron oscillations in metal films (the surface plasmons of Ritchie) but using optical excitation rather than fast charged particles. Otto introduced the term “surface plasma waves”, which he defined as: “*transverse magnetic waves travelling along interfaces of two different media*”. Then he defined the “surface plasmons” as the *quanta* of the “surface plasma waves” [38]. The only time Otto referred to Sommerfeld in that paper was in only one line where he wrote: “*Nonradiative surface plasma waves are known as solutions of Maxwell’s equations since Sommerfeld [1]-[21]*”. Note that Otto never used the term “Sommerfeld-Zenneck wave”. He just tried to justify that his “surface plasma waves” are indeed a valid solution of Maxwell’s equation. Otto concluded in the paper that nonradiative surface plasma waves can be coupled to light waves by the method of *frustrated total reflection*. This coupling is usually referred to as “surface plasmon polariton”. Unfortunately, in later work by different authors, this coupling between surface plasmons and electromagnetic waves is claimed at different frequency bands and without even the use of Otto’s method of frustrated total reflection. This will be shown later in this section.

In 1988, a book by Raether was published on the basic physics of surface plasmons on smooth and rough surfaces [39]. In the preface of the book, Raether defined surface plasmons as: “*SPs represent electromagnetic surface waves that have their intensity maximum **in** the surface and exponentially decaying fields perpendicular to it*”. Then in his text, Raether mentioned electromagnetic surface waves only once more. He said that at low frequencies or large permittivity the field of the surface plasmon resembles a guided photon field. He added between brackets the term “Zenneck-Sommerfeld wave” [39, p. 7]. This is very similar to what Ritchie did in [36].

In 1998, experimental results were published on an observed extraordinary optical transmission through sub-wavelength hole-arrays [40]. The interest in surface plasmons was renewed because the phenomenon reported in [40] was explained by surface plasmons. A surface plasmon-based theory for that extraordinary optical transmission through sub-wavelength hole-arrays in metal films was reported in [41]. Then the theory in [41] was questioned because similar optical transmission enhancement occurred in nonmetallic systems that do not support surface plasmons. A different theory was developed based on what is called “diffracted evanescent wave” and was reported in [42]. A comparison between the two theories was given in [43]. As will be shown in the rest of this literature review, the research work reported in [40]- [42] has a great influence on the later work in which surface plasmons are put in a clueless relation to electromagnetic surface waves. However, the authors in [40]- [43] never referred to electromagnetic surface waves, and never mentioned Sommerfeld or Zenneck waves.

However, in the same year, 1998, a paper was published in Surface Science about the application of surface plasmons to high- T_c superconductors [32]. It was reported in [32] that: *“Another feature we found in our experiment, as $\varepsilon_i(\omega)$ becomes larger than $|\varepsilon_r(\omega)|$ in the relevant frequency regime for $T > T_c$ is that the surface plasmon resonances change into Sommerfeld-Zenneck waves [44]”* The only reference which was given to that statement was Zenneck’s paper in 1907!

In the first decade of the 21st century, various research efforts were directed to the field of terahertz science. Interest was there to apply the plasmonics research in the terahertz regime since this could enable near field imaging and bio-sensing with unprecedented sensitivity [45]. The problem faced was that surface plasmons give their

interesting features only close to the plasma frequency of the conductors which for most metals is near the visible and the ultraviolet part of the spectrum [45]. Then the authors in [45] wrote: “*At terahertz frequencies, on the other hand, metals resemble in many ways a perfect conductor, and the negligible penetration of the electromagnetic fields leads to highly delocalized surface plasmon polaritons akin to grazing-incidence light fields. In this frequency range, surface plasmon polaritons are also known as Sommerfeld-Zenneck waves* [46].” Reference [46] is Goubou’s work which is well known to be related to surface waves only and not to surface plasmons. Then in many papers to follow, specifically in the terahertz research, the terms “surface waves” and “surface plasmons” were used interchangeably, such as in [30], [31], [47]- [48]- [49]. In the same time, however, in one of the earliest papers on the experimental results of terahertz surface plasmon polaritons, one can find no mention of Sommerfeld-Zenneck waves at all [50]. This is also totally missing from one of the latest collective works on the physics and applications of surface plasmon polaritons [51]. How this could be possible, unless there is no real connection between the two phenomena.

In 2004, in a paper in the field of metamaterials, the existence of microwave surface plasmons was reported at the interface between right-handed and left-handed media [52]. In that paper, a definition for the relation between Zenneck waves and surface plasmons was given explicitly as: “*The main physical difference between Zenneck waves and surface plasmons is that in the latter case the real (propagating) part of the normal component of the wave number in the metal region has generally (but not always) the same (instead of opposite) sign as that in the positive permittivity region, as pointed out in [53]. Thus a surface plasmon is the same physical entity as a Zenneck wave*”. The

work of [52] gives the idea that the problem of the existence of a surface plasmon (which is defined by the authors in [52] to be the same exact entity as a Zenneck wave) lies in the value of the permittivity of metals at microwave frequencies. They proposed to overcome this problem by using left handed media so as to be able to excite a surface plasmon at microwave frequencies. Then one finds in [54], an experimental study of microwave transmission through a single sub-wavelength slit. This work represents a replica of the work reported in [40] but in the microwave rather than the optical regime. The transmission reported in [54] is also explained by the surface-wave assistance, exactly as what was done in [40] which was then proved to be not strictly true as shown in [42]. Moreover, the surface-wave assistance reported in [54] is claimed to exist in the microwave regime without facing the same problem of the permittivity of metals and without the need of left-handed media which is reported in [52].

It is clear now that indeed, in the literature, surface plasmons are frequently defined as Sommerfeld-Zenneck waves, sometimes it's related to Zenneck Waves and some other times it's related to Sommerfeld waves. However, in the early times, when surface plasmon were first discovered in the 1950's, this relation was never mentioned, and the phenomena were never shown to be related. However, it is amazing to note that with time and misuse of these terms mentioned above, surface plasmons were related to surface waves, which is not true as shown in the detailed literature survey given in this chapter. It is exactly as Schelkunoff wrote in 1959: *“For obvious reasons the same word conveys different meanings to different individuals. Hence, some “noise” in communication between us is unavoidable. As long as the noise level is relatively low, we manage to understand each other reasonably well. When the noise level becomes high, serious*

misunderstandings are inevitable, and needless as well as wasteful controversies may arise. Such a situation has arisen in microwave theory in connection with the so called Surface waves" [28]. If that was the case at the time before even the discovery of surface plasmons, then what would one expect if the surface plasmons, at some point, were defined as any of the types of surface waves. It is clear from the given literature review that the definition of the true and physical relation between surface plasmons and any type of surface waves needs first a standard definition of the terms used. Since the term used by Ritchie, one of the earliest authors on the topic, was the Sommerfeld-Zenneck wave. Therefore, the rest of the chapter is dedicated to the clarification of the physical fundamentals of that term.

5.3 Evolution of the term Sommerfeld-Zenneck Wave

It should be clear to the reader from the previous section that most of the surface wave terminologies are loosely used and are not defined from a scientific point of view. There are often offhand remarks connecting the various phenomena without providing any scientific details. It is not avoidable, however, to use some of the terms in our discussion. Thus, it is of great importance to note that no strict meaning should be connected to any of the surface wave terms unless it is explicitly mentioned.

In this section, the term Sommerfeld-Zenneck wave is of main concern. This term is composed of two parts. One is the Zenneck wave, which was the topic of a seminal paper by Zenneck in 1907 [44]. The other part is Sommerfeld wave. Let's start by Zenneck waves.

The main contribution of Zenneck was the exposure of a specific type of solution of Maxwell's equations in a three dimensional space. This solution is an inhomogeneous

type of plane waves, whose field components can be derived as follows: In the three dimensional rectangular coordinates, consider that the plane $z=0$ is the boundary between medium 1, free space, and medium 2 which is of arbitrary parameters (ϵ, μ, σ) . Zenneck showed that there exists a solution for Maxwell's equation in this two-layer problem. This solution represents a wave that has progressive phase propagation in the x -direction, while at the same time decays exponentially in the positive and negative z -directions. This wave has to be a TM wave with respect to the x - z plane. The field components for such a wave in medium 1 are given by:

$$E_{1x} = E_1 \exp(-jk_x x - k_{1z} z) \quad , z > 0 \quad (5.1)$$

$$H_{1y} = H_1 \exp(-jk_x x - k_{1z} z) \quad , z > 0 \quad (5.2)$$

where a harmonic time variation of frequency ω is assumed. The corresponding forms in medium 2 are given by:

$$E_{2x} = E_2 \exp(-jk_x x + k_{2z} z) \quad , z < 0 \quad (5.3)$$

$$H_{2y} = H_2 \exp(-jk_x x + k_{2z} z) \quad , z < 0 \quad (5.4)$$

where E_1, E_2, H_1 and H_2 are constant values representing the amplitude of the field components. k_x is the magnitude of the propagation vector component in the direction tangential to the boundary. k_{1z} and k_{2z} represent the propagation constants in the positive and negative z -directions respectively. According to Zenneck, the real parts of k_{1z} and k_{2z} should be positive. Thus the wave given in (5.1)-(5.4) decays exponentially away from the boundary which lies at the plane $z = 0$. The dispersion relation relating the propagation vector components is determined by the value of the frequency ω and the

medium parameters (ϵ, μ, σ) . An attempt to bridge the gap between plasmonics and Zenneck waves was given in [55]. The explanation given in [55] depends mainly on checking the relation between k_x , k_{1z} and k_{2z} for different frequencies and different values of (ϵ, μ, σ) . The conclusion in [55] was: “*The analysis in the present article has shown how the field and wave solutions of the Zenneck wave carry over to the epsilon near-zero and plasmonic regimes, as long as the square roots and proper character of the wave vectors are correctly accounted for... As was shown in the numerical examples, the character of the Zenneck wave changes drastically, even if continuously, when entering the plasmonic region*”. There are two things to be noted here. First, there is in fact a need to understand the true relation between plasmonics and Zenneck waves. This is primarily the motivation of this chapter. Second, the analysis done in [55] depends on the field components given in (5.1)-(5.4) which represent plane wave solutions. It is well known that in a realistic situation, plane waves do not exist.

If we assume temporarily that plasmons are indeed a Zenneck wave, then the question is how to excite such a wave in a realistic situation. Thus, the bottom line is: If a Zenneck wave cannot be excited in a two-layer problem (discussed earlier), then surface plasmons cannot be excited either, regardless the frequency or the medium parameters. Nonetheless, if it is argued that surface plasmons can indeed be excited in metal foils of special thickness and in response to charged particle bombardment, as Ritchie showed in [33], then surface plasmons should not be related to Zenneck waves and the exciting conditions should be strictly defined. Unfortunately, this is missing, for example, in most of the recent work on terahertz surface plasmons as discussed in the previous section.

Sommerfeld, in 1909, tried to address the question of whether a Zenneck wave can be excited by a practical source in a two-layer problem or not. Unfortunately, Sommerfeld concluded that a Zenneck wave can be excited in a two-layer problem. Hence, the term ‘‘Sommerfeld-Zenneck wave’’ was originated in 1909. In contrary to what Sommerfeld concluded, it was shown later by experiments that such kind of wave does not exist and cannot be excited in a two-layer problem. See for example the experimental results collected on top of Seneca Lake by Burrows in [26]. At this point, it is not intended in this chapter to raise a controversy about Sommerfeld’s work; since the debate is already there for almost a century. As an alternative, the approach taken in this chapter is to expose a mathematical problem that Sommerfeld might have missed in his solution.

5.4 Examining the theoretical basis of the Sommerfeld Pole

As explained in details in the previous chapters, Sommerfeld formulation was based on the decomposition of the spherical wave function into an integral of a continuous spectrum of plane waves. Then, to find the reflected fields represented by a vector potential, a specular reflection function is multiplied under the integration sign as shown in (2.3) for example. The reflection coefficient $R(\lambda)$ for the case of a vertical dipole is rewritten here for clarity:

$$R(\lambda) = \frac{k_2^2 \sqrt{\lambda^2 - k_1^2} - k_1^2 \sqrt{\lambda^2 - k_2^2}}{k_2^2 \sqrt{\lambda^2 - k_1^2} + k_1^2 \sqrt{\lambda^2 - k_2^2}} \quad (5.5)$$

where k_2 is the propagation constant in the imperfect ground plane whose complex relative permittivity is ε , filling the half-space $z < 0$. i.e. $k_2^2 = \varepsilon k_1^2$. If the ground plane is

metallic perfect conductor with $R(\lambda) = 1$, then the reflected vector potential represents a spherical wave emanating from the perfect image location. If the ground plane does not have perfect reflectivity, then $R(\lambda)$ represents a complex function that has four branch points at $\pm k_1$ and $\pm k_2$. This divides the complex λ plane into four different Riemann sheets. Sommerfeld chose the proper Riemann sheet according to what he called the *radiation condition*, which is the physical constraint that requires the fields at infinity to be zero. Namely, the sheet that has $\text{Re}\{\sqrt{\lambda^2 - k_{1,2}^2}\} > 0$. On this Riemann sheet, there is a pole for the function $R(\lambda)$. This pole is always thought of as what gives rise to *Sommerfeld-Zenneck* wave. Moreover, recently this pole is presented as the source of the phenomenon of SP. In fact, both statements are far from being true.

The main goal in this chapter is to show the reasons for which this cannot be the proper analysis of SP. Those reasons are given below:

First, Sommerfeld associated the presence of a surface wave (*Sommerfeld-zenneck* wave) in his final solution to the contribution of the pole; because this contribution has the form of the Hankel function, $H_0^{(2)}(\lambda_p \rho)$, where λ_p is the location at which the pole appears in the complex λ plane. Sommerfeld was proven wrong in this point by experiment [26] and extensive theoretical analysis [3]. It is important to stress here that the error is much more serious than the famous sign error which is actually a myth [3]. Collin in [3] showed that the pole contribution must be cancelled out by a part of the contribution from the branch-cut emanating from $\lambda = k_1$.

Second, when the first reason mentioned above is made clear, the claim that usually arises is the following: “The pole does not give rise to a *Sommerfeld-Zenneck*

wave until there is a change in sign in the real part of the permittivity (i.e. ε has a negative real part), and in this case the wave is called SP^{''}. Our aim here is to bring awareness to the confusion that such a statement adds to the already controversial issues of surface waves.

To clarify our point, we present a very important conceptual question about the pole of $R(\lambda)$. This pole appears when the denominator in (2) vanishes, i.e.

$$\varepsilon\sqrt{\lambda^2 - k_1^2} + \sqrt{\lambda^2 - \varepsilon k_1^2} = 0 \quad \text{at} \quad \lambda = \lambda_p = \pm\sqrt{\frac{\varepsilon}{\varepsilon+1}}k_1 \quad (5.6)$$

If one substitute back by λ_p in (5.5), we get:

$$R(\lambda_p, \varepsilon) = \frac{\varepsilon\sqrt{-1/(\varepsilon+1)} - \sqrt{-\varepsilon^2/(\varepsilon+1)}}{\varepsilon\sqrt{-1/(\varepsilon+1)} + \sqrt{-\varepsilon^2/(\varepsilon+1)}} \quad (5.7)$$

which is a complex valued function in the complex variable ε . In the complex ε plane, this function has one branch cut emanating from the point $\varepsilon = 0$. This branch cut separates two distinct Riemann surfaces. The question now is which Riemann surface of the complex ε plane is supposed to be the proper Riemann surface. Remember that Sommerfeld chose the proper Riemann surface in the complex λ plane according to the physical constraint of the radiation condition. Similarly, one should intuitively expect that there must be a physical constraint governing the choice of the proper Riemann surface in the complex ε plane. Unfortunately, the reflection coefficient in (5.5) has never been studied as a complex function of two complex variables. Its behavior has been always studied only in the complex λ plane. In this section, the behavior of the reflection coefficient at $\lambda = \lambda_p$ is studied in the complex ε plane. Fig. 5.1 shows the value of the

denominator of (5.7) as a function of the complex permittivity ϵ . This is done by calculating the value of the denominator using Matlab where the square root function of a complex variable always yields the solution that has a positive real part. The plot shown in Fig. 5.1 confirms that on the positive real axis of ϵ , the denominator of (5.7) does not vanish, i.e. there is no pole, whereas in the rest of the plane the denominator is zero. This implies that no matter how small the imaginary part of ϵ is, as long as it is not exactly zero, there is a pole and the function in (5.5) blows up. This behavior cannot be accepted if we associate with the presence of the pole the presence of a certain guided mode in the propagating fields. This is because, as Collin mentioned in [3], a solution to a physical problem must vary continuously with the physical parameters. Moreover, Fig. 5.1 shows that there is no transition in the nature of the pole when we go from the left half-plane to the right half-plane. In other words, the pole does not depend on the sign of the real part of ϵ .

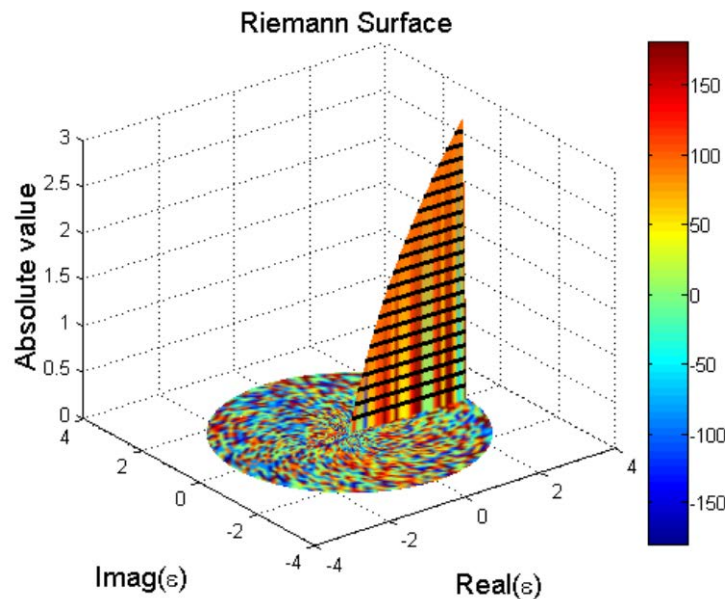


Fig. 5.1 The absolute value (height) and phase in degrees (color-bar) of the denominator of the reflection coefficient in the complex ϵ plane. Riemann surface with horizontal branch cuts.

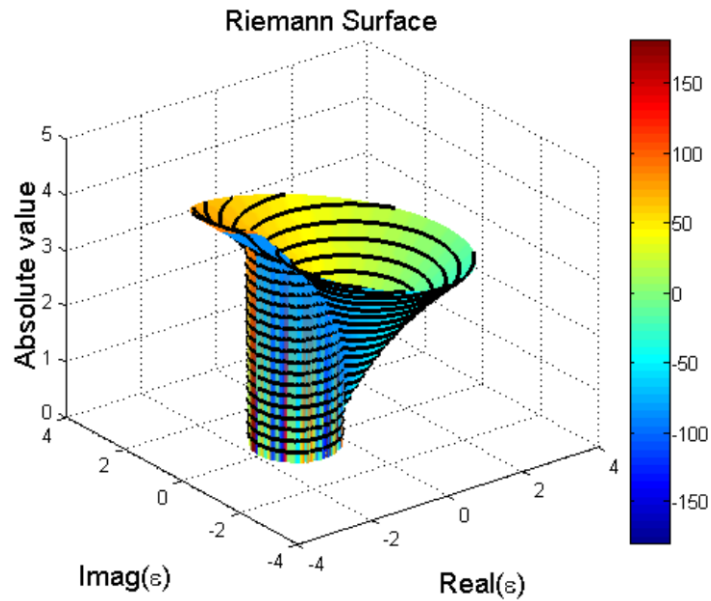


Fig. 5.2 The absolute value (height) and phase in degrees (color-bar) of the denominator of the reflection coefficient in the complex ε plane. Riemann surface with vertical branch cuts

Furthermore, a different choice of the branch cut yields a totally different picture. For example, by taking the minus sign under the square root as a common factor from (5.7), the plot will be as shown in Fig. 5.2. In this case, the denominator does not vanish in the ε plane except inside the circle whose center is -1 and radius is 1.

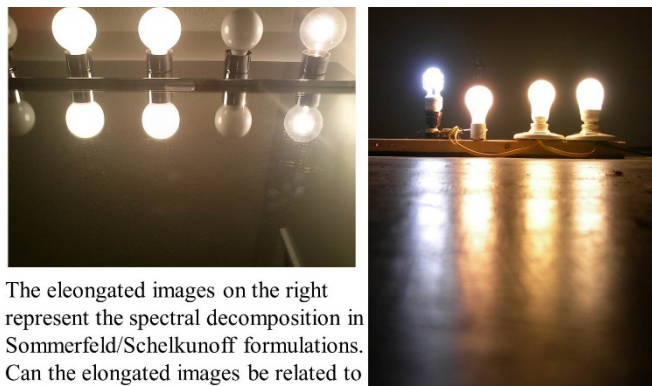
The third reason for the unsuitability of Sommerfeld's analysis is that it deals purely with linear interactions between the incident source and the planar interface. SP involve nonlinear effects like Raman scattering [56], in which the scattered field has a frequency which is different from the incident one. Those effects can never be studied using the type of analysis shown here because it neither takes any microscopic nonlinear effects into account nor it requires any special type of excitation like that described by Otto [38]. Instead one needs to use the Maxwell-Bloch equations to study the SP as they

are due to the inelastic Raman scattering rather than the elastic Rayleigh scattering which is guided by Maxwell equations.

5.5 Physical visualization of the problem

We have seen now that the formulation of Sommerfeld solution depends on the decomposition of the spherical wave into cylindrical waves. Those cylindrical waves are represented by the integrand in (2.3) in terms of the horizontal propagation constant, λ . The integration limits however go from 0 to infinity. For that part of the integration contour where λ is less than k_1 , the integrand represents a normal homogeneous cylindrical wave. However, for the rest (tail) of the contour, going from k_1 to infinity, the integrand represents inhomogeneous waves which are propagating in the ρ direction tangential to the boundary, and exponentially decaying in the z -direction perpendicular to the boundary. The form of the latter waves resembles the form of Zenneck waves given in (5.1)-(5.4). However, this does not necessarily imply that the result of integration contains the same form of Zenneck waves, or that those waves are guided by the boundary. This might be clear if one examines the other formulation. In Schelkunoff formulation, the integration contour can be decomposed in the same manner. However, the inhomogeneous Zenneck-like waves are propagating in the z -direction perpendicular to the boundary while they decay exponentially in the direction tangential to the surface. The integration result in the two formulations in free space, however, is proved mathematically to be identical, as shown in Appendix A.

What physically happens in a two-layer problem can be visualized by inspecting the path of each of the waves represented by the integrands in (2.3), for example, especially, those waves represented by the main part of the contour going from 0 to k_1 .



The elongated images on the right represent the spectral decomposition in Sommerfeld/Schelkunoff formulations. Can the elongated images be related to surface plasmons?

Fig. 5.3 A visualization of the Sommerfeld problem of two-layer reflection. The figure represents the comparison between the two cases of perfect (left) and imperfect (right) reflectivity.

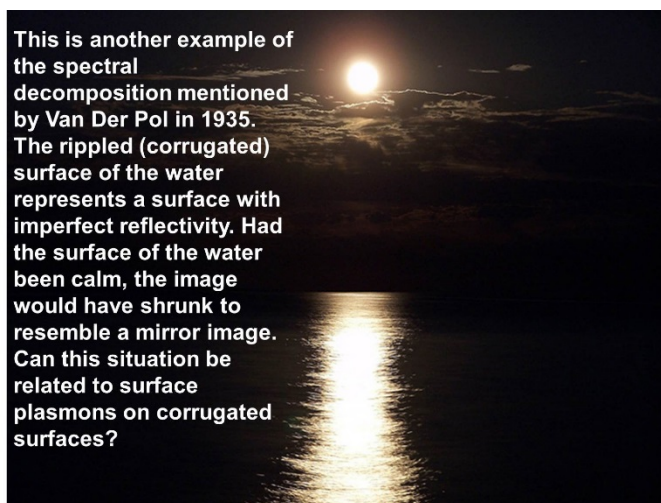


Fig. 5.4 A visualization of the Sommerfeld problem of two-layer reflection. The imperfect reflectivity in this case is due to the roughness of the surface

Those waves when they hit the ground, which is imperfectly conducting, they suffer from different reflection coefficients which depend on their different angles of incidence. On reflection, the rays diverge forming a semi-infinite image. The rays will never converge to form a perfect image of the same size as the source except in case that the second medium is perfectly conducting and perfectly smooth. This fact was predicted in 1935 by Van der Pol [4] which explains the elongated image of the moon on a wavy lake. This can be visualized in the pictures shown in Fig. 5.3 and Fig. 5.4.

Note that the visualized examples given here are for the light frequencies and not for radio frequencies. Yet, the concept of both Sommerfeld and Schelkunoff formulations along with Van Der Pol's interpretation still apply. Note that the earliest hint on the analogy between surface plasmons and Sommerfeld-Zenneck waves, given by Ritchie, relied only on the frequency separation between the two phenomena. The pictures shown in Fig. 5.3 and Fig. 5.4 show that the Sommerfeld problem can be visualized and interpreted in the optical regime without relying on any surface wave concept. It is just the decomposition of a bundle of rays originating from a spherical wave source.

At terahertz frequencies, if one considers the experimental work presented in [3], one could find a great similarity in concept as what is shown in Fig. 5.3. The only difference is the frequency scaling and the high permittivity of the ground plane used in [3] ($\epsilon = -33000 - j1.6e6$). This frequency scaling between what is shown in Fig. 5.3 and the terahertz experiment in [3] does not necessarily imply that the concepts of surface plasmons should be invoked. In our theory, the high magnitude of the permittivity will make the fields reduce to the form of a spherical wave and the fields would decay as $1/R$, which is exactly the conclusion in [3]. Note that a field that decays as $1/R$ can never represent a surface wave, at least in Sommerfeld's terminology. This is because a surface wave is a two-dimensional wave. It is known that for a wave propagating in three dimensions, its field decays as $1/R$ where R is the distance from the source to the field point. This is because its energy is distributed over the surface of a sphere. Accordingly the field of a two-dimensional surface wave should decay as $R^{-1/2}$. Those facts however cannot be inferred from the forms of Zenneck wave given in (5.1)-(5.4) because those forms are addressing only the case of plane waves, not for cylindrical waves. This is also

something that is always missing in the analogy of plasmons and Zenneck waves such as in [29]. A detailed analysis of the decay rate of “*surface waves*” is given in [40-41].

5.6 Conclusion

Finally, based on the critical analysis given in this chapter, one can conclude: The claim which says surface plasmons are one form of the Sommerfeld-Zenneck wave arising from the pole of Sommerfeld integrands is not legitimate. The pioneers of the field of surface plasmons, such as Ritchie, did not attempt in the first place to relate the two phenomena. This kind of relation was done after more than twenty years of the discovery of surface plasmons. However, this relation was not based on any scientific analysis. The claimed pole of Sommerfeld integrands did not give rise to the Sommerfeld-Zenneck wave in the first place. This directly implies that relating the pole of Sommerfeld to surface plasmons is nothing but a demonstration of the worries of Schelkunoff about the misuse of the term “*surface waves*”. It is recommended by the author of this dissertation to avoid any attempt to relate the Sommerfeld-Zenneck wave to the electron oscillations of surface plasmons. The latter being a microscopic phenomenon which might give rise to a certain mode of radiation. This mode, of course, must satisfy Maxwell’s equations and might take a similar form like the Zenneck wave, however, any attempt to relate that mode to the solution of Sommerfeld of a two-media problem will confuse the issue more than clarify it.

6 Applications of Schelkunoff Formulation

6.1 Regeneration of Okumura's Data

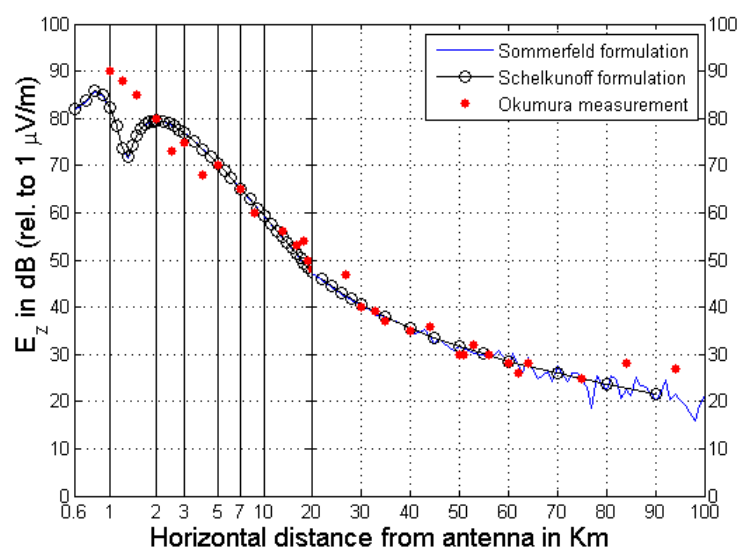
The analysis presented in the previous chapters is now used for the analysis of the propagation data measured by Okumura et al. [20] in their classic propagation measurements in the city of Tokyo. Okumura placed a transmitting antenna with different heights in Tokyo, Japan, we will choose the height of 140 m. The signal is received by another vertically polarized antenna located on top of a van 3 m above the ground. The receiving antenna had a gain of 1.5 dB. The transmitting antenna was a 5 element Yagi having a gain of approximately 11 dB and radiating 150 W of power. The van was then driven in the city of Tokyo from 1 km to 100 km from the transmitting antenna. Here we consider the measurements done at 453 MHz. Since, the 5-element Yagi was an antenna composed of wires, in our simulations we used an optimized 5-element Yagi antenna array which had a gain of 11 dB. In our analysis, the Yagi antenna was synthesized and was used in the computations.

First the integral equation using the Schelkunoff formulation for the Green's function was used to solve for the current distribution on the transmitting antenna and then these currents were used to compute the radiating fields. The way we solve for the fields is by replacing the new Green's function instead of the Sommerfeld Green's function in a code that has been already developed for the analysis of radiation over imperfect ground planes based on Sommerfeld integrals. An example for such a code is AWAS [57]. The parameters for the urban ground were: relative permittivity of $\epsilon_r = 4$, and $\sigma = 2 \times 10^{-4}$ mhos/m [6]. However, since we did not know how Okumura et al.

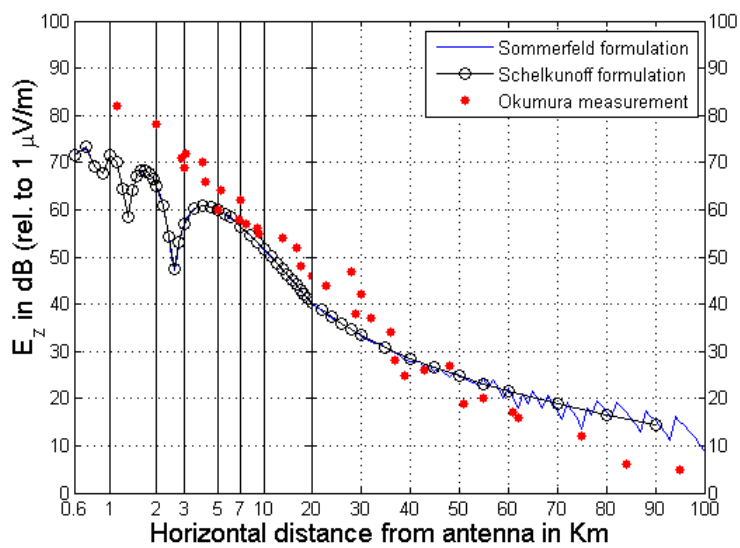
matched their antennas and how it was exactly fed, we used a simple 1 V as an excitation for the Yagi. Then we shifted all of our computations by a constant value in decibels (98 dB), so that the two plots matched at 7 km as shown in Fig. 6.1-(a). We then overlaid the two plots, theoretical predictions by the Schelkunoff formulation and Okumura et al.'s experimental data. The two plots show remarkable similarity. It is interesting to note that the simulation using the Schelkunoff Green's function provided a good qualitative plot of the field from 1 km to 100 km from the base station antenna. The results here are numerically much more stable than the results provided by the code AWAS which used the Sommerfeld formulation [57]. This is also shown in Fig. 6.1 Comparison between the experimental (Okumura et al.) and theoretical predictions (Schelkunoff and Sommerfeld formulations) computed through a macro model for predicting propagation path loss in an urban environment at: (a) 453 MHz, (b) 922 MHz, (c) 1920 MHz. In AWAS, the results for the fields became somewhat unstable when the horizontal distance from the transmitting antenna becomes quite large, say greater than 10 km. This is due to the Sommerfeld integral tails problem which is totally abolished in the new formulation. It is also important to point out that for both the theoretical and experimental data, the slope for the path loss exponent between 1 km and 10 km is about 30 dB per decade, which was expected from the theoretical analysis using the saddle point method in [9]- [10]. The slope between 10 km and 100 km is 40 dB per decade, as predicted by the Norton ground wave for the far field. This illustrates that an accurate electromagnetic macro modeling of the environment is sufficient to predict the path loss as evidenced by the comparison between theory and experiment. This macro modeling is facilitated through the use of the new formulation by giving more numerically stable results. Use of an electromagnetic

macro model makes sense as the image generated by the transmitting antenna located over an imperfect ground is a semi-infinite line source and an optical analogue will reveal that such a source does not cast shadows [9]- [10]. This is illustrated in the thought experiment of Chapter 1.

The same numerical analysis of Fig. 6.1 Comparison between the experimental (Okumura et al.) and theoretical predictions (Schelkunoff and Sommerfeld formulations) computed through a macro model for predicting propagation path loss in an urban environment at: (a) 453 MHz, (b) 922 MHz, (c) 1920 MHz is shown in Fig. 6.1-(b) for 922 MHz (with 130 dB added to the theoretical data) and in Fig. 6.1-(c) for 1920 MHz (with 125 dB added to the theoretical data, note that those numbers include the adjustment of the reference from 1 V/m to 1 μ V/m). For these two frequencies the plots in Fig. 6.1-(b) and (c) are not with perfect match with the experiment because in our simulations, at these two frequencies, we used simply a half wave dipole as the transmitter whereas Okumura et al. used a highly directive antenna like a parabolic reflector whose dimensions were not reported in their paper. Next we illustrate the nature of the propagation mechanism over a two layer medium.



(a) 453 MHz



(b) 922 MHz

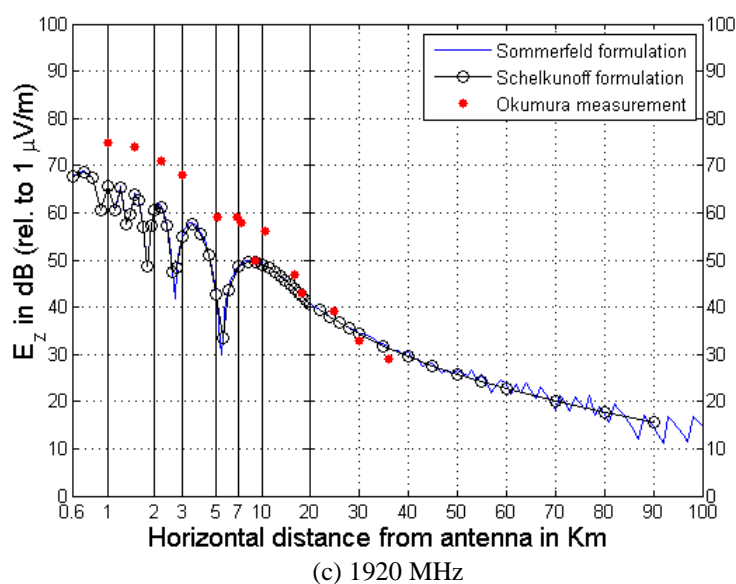


Fig. 6.1 Comparison between the experimental (Okumura et al.) and theoretical predictions (Schelkunoff and Sommerfeld formulations) computed through a macro model for predicting propagation path loss in an urban environment at: (a) 453 MHz, (b) 922 MHz, (c) 1920 MHz

6.2 A Distinction between Various Types of Surface Waves

First we start by describing the properties of a surface wave and observe how it differs from the other type of ground waves and then illustrate those principles using numerical computations based on the Schelkunoff formulation proposed in this dissertation.

As has been pointed out by Schelkunoff [28] the word “*Surface waves*” conveys *different meanings to different individuals. Hence, some “noise” in communication between us is unavoidable. As long as the noise level is relatively low, we manage to understand each other reasonably well. When the noise level becomes high, serious misunderstandings are inevitable, and needless as well as wasteful controversies may arise. Such a situation has arisen in electromagnetics in connection with the so-called “surface waves”*. As stated by Schelkunoff [28], Dr. James R. Wait, the Chairman of a working group formed during the URSI General Assembly in Boulder, Colorado,

compiled a list of 11 types of waves which at some time or another has been described by various writers as a surface wave. The list is presented in Table 1, which deals with propagation of plane waves in semi-infinite, nonmagnetic, non-dissipative media, separated by a plane boundary.

Table 1

1. *Zenneck Surface Wave (interface at half-space)*
2. *Sommerfeld Surface Wave (dipole radiating over a conducting half-space)*
3. *Norton Surface Wave (distant fields produced by a dipole radiating over a conducting half-space)*
4. *Sommerfeld Axial Surface Wave (imperfectly conducting cylindrical wire)*
5. *Harms-Goubau Axial Surface Wave (a dielectric coated wire)*
6. *Plane Trapped Surface Wave (dielectric coated plane conductor, corrugated surface, or other inductive boundaries)*
7. *Cylindrical Trapped Surface Wave (same as above in cylindrical form)*
8. *Plane Quasi-Trapped Surface Wave (stratified conductor when the surface impedance has both a resistive and inductive component)*
9. *Cylindrical Quasi-Trapped Surface Wave (same as above in cylindrical form)*
10. *Azimuthal Surface Waves (on dielectric coated and corrugated cylinders and spheres for propagation in the azimuthal direction)*
11. *Composite Axial–Azimuthal Surface Wave (same as above when propagation has a component in both the axial and azimuthal directions)*

According to Schelkunoff, the waves listed in 1-4 of Table 1, will propagate when there are only two planar semi-infinite media. The presence of a coating or a corrugation is considered to be a third medium beside the media above the plane boundary, considered to be air, and the one below the coating which is another medium. Hence, in this classification of Schelkunoff of all the various types of waves outlined in Table 1, only the first four of these waves can propagate over only a two semi-infinite planar medium. The other waves require either a coating or a corrugation to propagate.

According to Schelkunoff [28], the first four of these waves are not surface waves in the classical sense defined first by Lord Rayleigh. Wave types 5-11 are trapped waves and in the classical sense, the term “surface wave” applies only to those types 5-11 of all those eleven types of waves mentioned in Table 1 as they can be shown to exist without an explicit presence of an incident wave and are zeroes of the denominator of (7) often termed the ‘poles’.

We first describe what Schelkunoff meant by a surface wave in the classical sense. Then we illustrate that for this two layer problem, the total reflected fields do not indicate presence of a surface wave. In addition, we illustrate that the reflected fields are primarily affected by the Brewster zeros and therefore their variations will be expected to be independent of frequency of operation. Hence these fields are associated with radiating waves and not surface waves which by definition do not radiate.

A surface wave is generally guided by a boundary of two dissimilar media and has a phase velocity smaller than the velocity of light [28], [58]. For the propagation of a wave over two planar media as we have discussed in this dissertation, the planar interface does not support a surface wave [28]. In addition, there is no radiation from a surface

wave [58]. The fields associated with such a wave, perpendicular to the direction of propagation are evanescent in nature as one moves away from the planar boundary. As the frequency increases, the wave is more confined to the interface. The evanescent nature of the wave thus also varies with frequency. This is a very important property of a surface wave and thus it differs from a radiated wave where the evanescent nature in the transverse direction is generally independent of frequency [28]. Thus a Zenneck or a Sommerfeld wave over a two layer surface are not surface waves as the variation of the fields in the transverse direction are essentially independent of frequency. Also, the phase velocity of a Zenneck or a Sommerfeld wave is faster than the speed of light. In addition, the evanescent nature of the fields orthogonal to the direction of propagation does not vary with frequency, even though the phase constant changes with frequency.

In addition, it is well known that when a TM wave is incident at the two media at the Brewster's angle, then there will be no reflection and that the incident wave will penetrate into the second medium without reflection. And this phenomenon of total transmission will occur independent of frequency whereas the presence of a surface wave will display a high dependence of the field strength as a function of frequency. As the frequency increases the fields of the surface wave will be more confined to the planar boundary. We will illustrate these points when we deal with propagation of radio waves over earth and visualize in what form is the energy being carried.

We now demonstrate that only the Zenneck/Sommerfeld wave type and not a surface wave in the classical sense [28], [58] propagates over a two medium problem. This is illustrated not only by evaluating (1) by an accurate numerical electromagnetics code using the Schelkunoff formulation but also confirmed by experiments carried out

even in the Terahertz region, confirming nonexistence of high frequency surface waves [30].

First to illustrate that the propagation in the Okumura et al. experiment which is due to a Sommerfeld wave is not a surface wave we plot the decay of the fields along the vertical z -direction at a fixed distance from the transmitting antenna. As we have seen that for a surface wave this vertical attenuation of the fields should be a function of frequency whereas for a Zenneck wave or a Sommerfeld wave the vertical decay of the fields is independent of frequency. We consider a half wave dipole radiating over an urban ground. The transmitting antenna is located 10 m above the ground plane. We plot the variation of the magnitude of the **reflected field only** as a function of z for a fixed distance of $\rho = 100$ m from the ground up to a height of 100 m as seen in the plot of Fig. 6.2. It is seen that even though the frequency changes from 453 MHz, to 906 MHz and then to 1350 MHz, the magnitude of the decay of the fields in the vertical direction to the planar air-earth interface remain practically the same. As there is no appreciable variation of the fields even though the frequency changed by a factor of three, indicates that the term surface wave should not be associated with the Zenneck or the Sommerfeld/Norton type of waves as correctly suggested by Schelkunoff [28]. This also applies to the waves propagating over a two-layer medium like radio wave propagation in an urban environment. Also, in the plot of Fig. 6.2 for the absolute value of the reflected fields indicate a dip at 40 m from the source. Considering urban ground which has an $\epsilon_r = 4$, the Brewster's angle is given by $\tan^{-1}(\sqrt{4}) = 63.4^\circ$. However because of the presence of the conductivity the Brewster's angle will be complex and also the reflection coefficient will not be exactly zero.

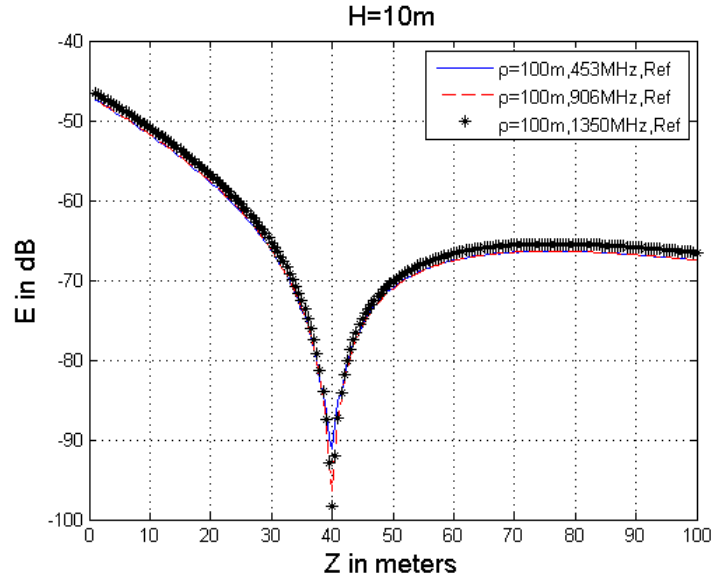


Fig. 6.2 Plot of the transverse component of the reflected fields at 100 m from the source.

From the geometry of the problem, it is seen that the angle subtended by the antenna with respect to the ground will be given by $\tan^{-1}(10/20) = 26.56^\circ$. Therefore, the angle with respect to the vertical is $90^\circ - 26.56^\circ = 63.44^\circ$, indicating that the dip in the field strength is occurring near the Brewster angle of 63.4° . In summary, the plot of the reflected field strength from the dipole over an imperfect ground reflects the strong influence of the Brewster angle which is due to a zero of the reflection coefficient. The plot also demonstrates the practical invariance of the reflected fields as a function of frequency which is also true for the Brewster's angle as it is also independent of frequency. Finally, the effect of the pole is not seen in Fig. 6.2. The conclusion that is easily reached is that for propagation over urban ground the surface wave phenomenon is nonexistent. Therefore, this plot confirms that the reflected field is a Zenneck–Sommerfeld type of a radiating wave strongly influenced by the Brewster zero of the reflection coefficient.

6.3 Absence of Surface Waves/Plasmons at Terahertz Frequencies

We further illustrate the absence of surface waves for propagation in a two layer media using both an accurate numerical analysis based on Schelkunoff integrals and experimental data measured by other researchers [30]- [31] in the THz region. In this case, the second medium has a negative ϵ , and so the goal is to see if the surface waves exist in the final solution of the reflected fields from the boundary. We observe this phenomenon from both a theoretical standpoint and measurement data [30] carried out by other researchers.

We illustrate the absence of surface waves in the reflected fields when a THz wave is propagating over an Aluminum sheet. This experiment was carried out by Jeon and Grischowsky at THz frequencies [30]. The basic block diagram of the experiment is illustrated in Fig. 6.3 where a wave at 0.4 THz is launched over an Aluminum sheet. The propagation of the direct wave is prevented by placing a screen and in addition making a dent on the Aluminum sheet so that only the wave guided by the surface will be propagated. The authors of the paper then measured the attenuation of the transmitted THz wave by a detector. The amplitude of the current in the detector decreased from 34 pA to 5.1 pA when the distance of the detector was varied from 14 cm to 98 cm. To estimate the propagation path loss exponent for this scenario we assume the field to vary

as $E \propto \frac{A}{R^p}$; or equivalently $34 = \frac{A}{(14)^p}$ and $5.1 = \frac{A}{(14+84)^p}$, where A is the

proportionality constant.

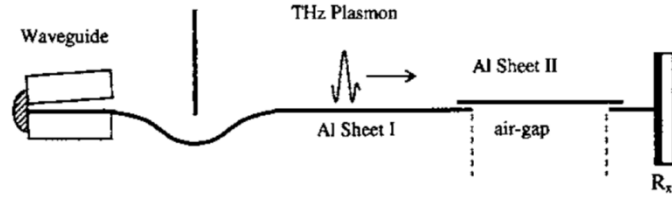


Fig. 6.3 Measurement setup of the work presented in [30] in search of the surface waves at THz frequency.

The solution for p is then obtained as $p=0.98$ or $p \approx 1$. Therefore the path loss exponent (This will be related to power and hence proportional to $|E|^2$ and therefore in this case will vary as $1/R^2$) is 2 indicating that this transmitted field beyond the Aluminum partition is generated from a point source, representing a spherical wave and it is not a surface wave, as the field varies as $1/R^p \rightarrow 1/R$.

Now if we apply the Schelkunoff formulation to analyze this same problem with $\epsilon_r = -33000$, and $\sigma = 3.54 \times 10^7$ mhos/m for Aluminum at 0.4 THz (the same parameters assumed in [30]), with a source dipole placed 0.001 m from the Aluminum sheet and the field is observed at a height of 0.001 m as a function of the radial distance. The transverse component of the reflected electric field is now plotted from a distance of 10 cm to 10 m as shown in Fig. 6.4. The propagation path loss for the reflected field appears to be approximately 20 dB per decade near the source indicating that the path loss exponent is 2. This implies that the variation of the field strength with distance is exactly $1/R$ as predicted from the measurements. So, in this case the dominant propagation mechanism is through the Sommerfeld Ground wave and there are no surface waves in the reflected fields even though the dielectric constant for the aluminum sheet at THz frequency is negative.

Finally, in Fig. 6.5 the strength of the transverse component of the electric field is plotted as a function of the vertical distance at 0.4 THz for different locations for the radial distance. It is clearly seen that there are no evanescent nature in the reflected fields. It is also interesting to note that when the transverse components of the fields for the same scenario is calculated at 0.3 THz and depicted in Fig. 6.6, it is seen that there is very little difference between Fig. 6.5 and Fig. 6.6 indicating that there is a radiating field and no surface waves in the total solution of the problem as the variation of the transverse components of the electric field is independent of frequency! In addition, even if the metal is made of a perfect electric conductor (PEC), there is also no difference in the magnitude of the transverse components of the fields indicating that at THz frequencies this Aluminum metal act similar to a PEC even though its permittivity is negative. This confirms that there are no surface waves in the total solution at THz frequencies and the computed results obtained by the Schelkunoff formulation agree well with the experimental data further validating the theory.

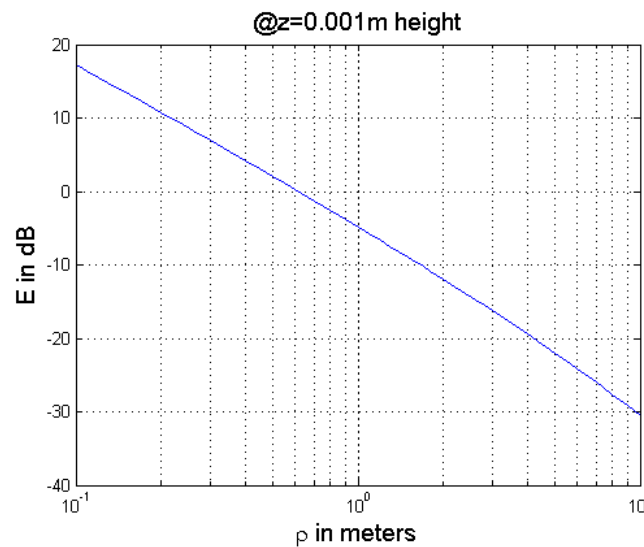


Fig. 6.4 Plot of the transverse component of the reflected fields as a function of the radial distance from the source.

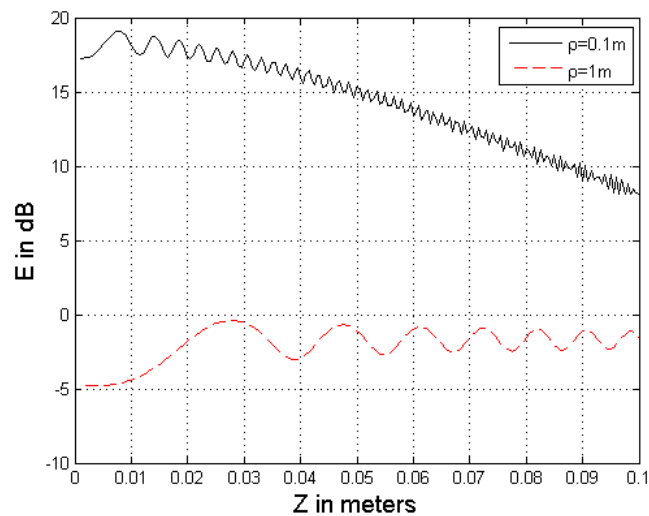


Fig. 6.5 Plot of the transverse component of the reflected fields as a function of the vertical distance from the interface at 0.4 THz.

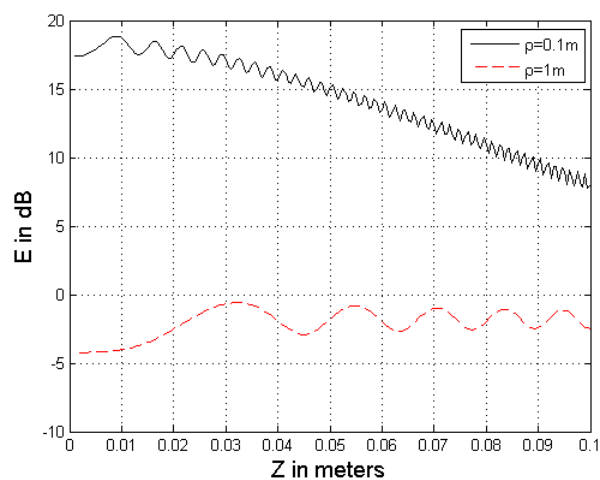


Fig. 6.6 Plot of the transverse component of the reflected fields as a function of the vertical distance from the interface at 0.3 THz.

7 Summary, Conclusion and Future Work

7.1 Summary and Conclusion

A spherical wave in the form e^{-jkr} / r can be decomposed into an infinite summation of cylindrical waves. The expressions of those cylindrical waves could be written in terms of either the horizontal or the vertical component of the propagation vector. Sommerfeld's original work made use of the summation in terms of the horizontal component of the propagation vector. The work presented in this dissertation aims to exploit the other representation which depends on the vertical component of the propagation vector. This representation was originally derived by Schelkunoff and hence we called it "the Schelkunoff representation" after his name.

In Chapters 2 and 3 of this dissertation, the original solution of Sommerfeld for the radiation of elementary dipoles mounted on top of infinite ground planes of arbitrary parameters was repeated based on the Schelkunoff representation of the spherical wave. The work presented in those chapters along with the five appendixes at the end of the dissertation give the full mathematical details that could have been done by Sommerfeld in case he started with the vertical component representation of the spherical wave. The characteristics of the numerical behavior of each representation were presented. The conclusion is that the solution based on Schelkunoff integrals totally abolish the numerical problem of Sommerfeld integral tails. This problem appears in the numerical solution of cases where the field and source points have large horizontal separation but both are very close to the ground plane. It is well known that in this case the Sommerfeld integral tails are not convergent because of the oscillatory behavior of the Bessel function

of the first kind $J_0(x)$. This problem was totally avoided in the Schelkunoff representation which is based on the monotonically decaying modified Bessel function of the second kind $K_0(x)$.

Since the Sommerfeld problem is more than hundred years old, therefore one can find a plethora of papers and contributions from many researchers all over the globe who wrote on the subject throughout the whole twentieth century. Some of those contributions were written before the advent of computers and some appeared after. Before the computers era all of the researchers were focusing on the analytical solution of Sommerfeld integrals, mainly, using Cauchy's complex integration theorem. The debate was whether this solution contained a surface wave or not. After the development of computers for scientific computation, most of the researchers were focusing on the numerical solution of Sommerfeld integrals and how to find mathematical ways to accelerate the convergence of those integrals. No effort was dedicated to question the source of the numerical problem, instead people were trying to find workarounds just to solve it. The different feature in the work presented in this dissertation is that the main work of Sommerfeld itself was questioned, the source of the numerical problem is understood and the alternative solution was given as explained in the previous paragraph. However, due to this debatable nature of the problem a complete chapter had to be dedicated for the theoretical comparison between Sommerfeld integrals and the new Schelkunoff integrals derived in this dissertation. The aim of Chapter 4 was not to settle the debate because it is almost impossible to do so. Instead we aimed in Chapter 4 to give a very clear idea to the reader about our stand point in the debate.

The claim that might arise against the new formulas derived in this dissertation was found to be based on the analytical solution of Sommerfeld integrals which include two branch cuts and one pole contributions. Our conclusion is that the pole in a two-media problem should not be included on the proper Riemann sheet. This is because:

- This pole does not give a solution which varies continuously with the physical parameters of the problem.
- This pole gives a field decay rate which was never reported in a real-life measurement.
- This pole was used by Sommerfeld to explain the propagation of Marconi's waves beyond the horizon. This was proven to be wrong after the discovery of the ionosphere.
- This pole is a pole of the reflection coefficient which is a function of two complex variables. This means that the Riemann sheets should be studied in two domains instead of one. This analysis is one of the unique contributions of this dissertation and is explained in Chapter 5.
- As proved by Collin in [3], if the pole is mathematically included, then there must be a saddle point contribution which totally cancels the pole contribution.

It is also concluded that one of the branch cut contributions gives the total correct solution of the problem while the other branch cut associated with the second medium gives a contribution that dies out exponentially as the height of either the field point or the source point increases. Thus, both formulations give identical results except for the case when the second branch cut contribution is not neglected which correspond

physically to the case where both the source and field points are very close to the interface.

Since a physical problem should only have one unique solution, thus we conclude that in this rare case where both the source and field points are very close to the interface either one of the formulation is wrong or both are wrong. This confusion can be settled by logical intuition. This is achieved by noticing a very important statement made by Sommerfeld [21, p. 239]: *“Hence if for $\bar{\Pi}$ we substitute e^{ikr} / r and determine the free constant in terms of the strength of the alternating current in the antenna, then according to Maxwell, we have in (4) the field radiated from the antenna, valid for all distances that are large compared to $\lambda = 2\pi / k$. For the immediate neighborhood of the antenna our description breaks down owing to the excessive idealization of our antenna model.”* This simply means that when the source point is very close to the interface, the primary stimulation to begin with is not developed as a spherical wave in the form e^{-jkr} / r . Therefore, the philosophy of representing this spherical wave in terms of cylindrical waves in any form simply breaks down because the spherical wave does not exist. It is just an approximation which is totally not valid in the vicinity of the source.

Based on those conclusions, Chapter 5 was dedicated to the study of the Sommerfeld elusive pole and its effect on the new area of research of plasmonics. The evolution of the term plasmonics was traced back to the middle of the twentieth century. A detailed literature review was given in Chapter 5 to show that there is no relation what so ever between surface plasmons and surface waves which are related to the elusive Sommerfeld pole. Finally in Chapter 6, some applications of the new formulations were given to prove the validity of the analysis presented in the dissertation. The new

formulation was used to duplicate the famous measurement data of Okumura [20]. Also, it was used to duplicate the results of a THz surface plasmon experiment [30] and analyze the existence/absence of surface waves in the radiated field from a dipole over an imperfect ground plane.

7.2 Future Work

There are some interesting topics of research that might be considered as an extension for the work presented in this dissertation. First, the consideration of a three layer problem where lateral waves needs to be considered instead of the elusive Sommerfeld surface waves. Second, the redesign of Burrow's experiment [26] in a lab environment should be considered. The only experiment that simulates the propagation in a two-media problem where the source and field points are very close to the interface is Burrow's experiment. However, this experiment was done in the 1930's which of course is limited to the accuracy of the measurement equipment available at that time. This experiment needs to be redone preferably in a lab environment while making use of the state of the art measurement equipment hopefully to settle down the Sommerfeld surface wave debate once and for all.

Appendix A: Proof of the Schelkunoff Identity

We will give a slightly different proof than that given by Schelkunoff in [13]. We will prove (2.6), while Schelkunoff proved (2.5). However, for simplicity, as Schelkunoff did, it is sufficient to show that the identity (2.6) holds for $z=0$, and since they are wave functions, then the identity will hold for any other value of z . The Sommerfeld integral is given by:

$$I_{som} = \int_0^{\infty} J_0(\lambda\rho) \frac{\lambda}{\sqrt{\lambda^2 - k^2}} d\lambda \quad (\text{A.1})$$

As indicated earlier, the integral (A.1) can be decomposed into two intervals:

$$\begin{aligned} I_{som} &= \int_k^{\infty} J_0(\lambda\rho) \frac{\lambda}{\sqrt{\lambda^2 - k^2}} d\lambda - j \int_0^k J_0(\lambda\rho) \frac{\lambda}{\sqrt{k^2 - \lambda^2}} d\lambda \\ &= A_{som} - jB_{som} \end{aligned} \quad (\text{A.2})$$

where A_{som} and B_{som} are the real and the negative of the imaginary parts of the Sommerfeld integral respectively. Starting with the real part:

$$A_{som} = \int_k^{\infty} J_0(\lambda\rho) \frac{\lambda}{\sqrt{\lambda^2 - k^2}} d\lambda \quad (\text{A.3})$$

Substituting $\lambda = \sqrt{t^2 + k^2}$, then $t = \frac{u}{\rho}$, we get

$$A_{som} = \frac{1}{\rho} \int_0^{\infty} J_0\left(\sqrt{u^2 + (k^2\rho)^2}\right) du \quad (\text{A.4})$$

Proceeding to the imaginary part which is given by:

$$B_{som} = \int_0^k J_0(\lambda\rho) \frac{\lambda}{\sqrt{k^2 - \lambda^2}} d\lambda \quad (\text{A.5})$$

Substituting $\lambda = \sqrt{k^2 - s^2}$, then $s = \frac{v}{\rho}$, we get

$$B_{som} = \frac{1}{\rho} \int_0^{k\rho} J_0\left(\sqrt{(k\rho)^2 - v^2}\right) dv \quad (\text{A.6})$$

It is required now to prove that the real and imaginary parts of Schelkunoff integrals are identical to those of Sommerfeld integrals given in (A.4) and (A.6).

Schelkunoff integral is given by:

$$I_{sch} = \frac{2}{\pi} \int_0^\infty K_0\left(\rho\sqrt{\xi^2 - k^2}\right) d\xi \quad (\text{A.7})$$

The integral in (A.7) can also be decomposed into two intervals as follows:

$$I_{sch} = \frac{2}{\pi} \int_0^k K_0\left(j\rho\sqrt{k^2 - \xi^2}\right) d\xi + \frac{2}{\pi} \int_k^\infty K_0\left(\rho\sqrt{\xi^2 - k^2}\right) d\xi \quad (\text{A.8})$$

$$\because K_0(jx) = -\frac{\pi}{2} N_0(x) - j\frac{\pi}{2} J_0(x) \quad (\text{A.9})$$

$$\begin{aligned} \therefore I_{sch} = & -\int_0^k N_0\left(\rho\sqrt{k^2 - \xi^2}\right) d\xi + \frac{2}{\pi} \int_k^\infty K_0\left(\rho\sqrt{\xi^2 - k^2}\right) d\xi \\ & - j \int_0^k J_0\left(\rho\sqrt{k^2 - \xi^2}\right) d\xi \end{aligned} \quad (\text{A.10})$$

where the real part is given by:

$$A_{sch} = -\int_0^k N_0\left(\rho\sqrt{k^2 - \xi^2}\right) d\xi + \frac{2}{\pi} \int_k^\infty K_0\left(\rho\sqrt{\xi^2 - k^2}\right) d\xi \quad (\text{A.11})$$

$$\therefore N_0(x) = -\frac{2}{\pi} \int_x^\infty \frac{\cos \tau}{\sqrt{\tau^2 - x^2}} d\tau \quad \& \quad K_0(x) = \int_0^\infty \frac{\cos \tau}{\sqrt{\tau^2 + x^2}} d\tau \quad (\text{A.12})$$

$$\begin{aligned} \therefore A_{sch} &= \frac{2}{\pi \rho} \left[\int_{\rho \xi = 0}^{\rho \xi = k \rho} \int_{\tau = \sqrt{(k \rho)^2 - (\rho \xi)^2}}^{\tau = \infty} + \int_{\rho \xi = k \rho}^{\rho \xi = \infty} \int_{\tau = 0}^{\tau = \infty} \right] \frac{\cos \tau d\tau}{\sqrt{\tau^2 - (k \rho)^2 + (\rho \xi)^2}} d\rho \xi \\ &= I_1 + I_2 \end{aligned} \quad (\text{A.13})$$

where I_1 and I_2 are as shown in Fig. A.1. Substituting using the transformation in (A.14), which is illustrated in Fig. A.1, we get:

$$\begin{aligned} \tau &= R \cos \psi, & \rho \xi &= R \sin \psi \quad \Rightarrow \\ R^2 &= \tau^2 + (\rho \xi)^2 \quad \& \quad d\tau d(\rho \xi) &= \rho d\tau d\xi = R dR d\psi \end{aligned} \quad (\text{A.14})$$

$$\Rightarrow A_{sch} = \frac{2}{\pi \rho} \int_{R=k\rho}^{R=\infty} \int_{\psi=0}^{\psi=\pi/2} \frac{\cos(R \cos \psi)}{\sqrt{R^2 - (k\rho)^2}} R dR d\psi \quad (\text{A.15})$$

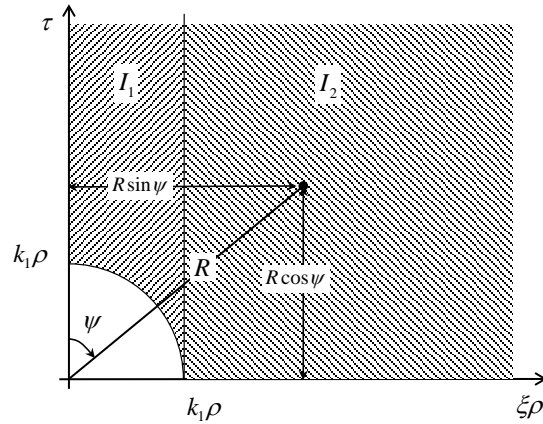


Fig. A.1. Transformation of variables used in (A.15).

$$\therefore J_0(R) = \frac{2}{\pi} \int_0^{\pi/2} \cos(R \cos \psi) d\psi \quad (\text{A.16})$$

$$\therefore A_{sch} = \frac{1}{\rho} \int_{k_1 \rho}^{\infty} \frac{J_0(R)}{\sqrt{R^2 - (k_1 \rho)^2}} R dR \quad (\text{A.17})$$

Substituting $R = \sqrt{u^2 + (k_1 \rho)^2}$, we get:

$$A_{sch} = \frac{1}{\rho} \int_0^{\infty} J_0(\sqrt{u^2 + (k\rho)^2}) du \quad (\text{A.18})$$

Finally, the imaginary part of the Schelkunoff integral is given by:

$$B_{sch} = \int_0^k J_0\left(\rho\sqrt{k^2 - \xi^2}\right) d\xi \quad (\text{A.19})$$

Substituting: $\xi = \frac{v}{\rho}$, we get:

$$B_{sch} = \frac{1}{\rho} \int_0^{k\rho} J_0\left(\sqrt{(k\rho)^2 - v^2}\right) dv \quad (\text{A.20})$$

Comparing (A.4) to (A.18) and (A.6) to (A.20), we conclude the validity of the identity (2.6). Also from (A.6) and (A.20), we conclude that:

$$\xi^2 = k^2 - \lambda^2 \quad (\text{A.21})$$

Equation (A.21) enforces our physical description which assumes λ to be the horizontal component of the propagation vector, and ξ corresponds to the vertical component, k_z , in (2.2).

Appendix B: Validation of the Vertical Dipole Formulation

In this appendix, it is required to prove the validity of the forms in (2.15). It is also required to find the reflection and transmission coefficients, namely $R(\zeta)$ and $T(\zeta)$.

$$\nabla^2 \Pi_{2z} = \nabla(\nabla \cdot \bar{\Pi}_{2z}) - \nabla \times \nabla \times \bar{\Pi}_{2z} \quad (\text{B.1})$$

$$\Rightarrow \nabla^2 \Pi_{2z} = \hat{a}_z \left[\frac{\partial^2}{\partial z^2} \Pi_{2z} + \frac{1}{\rho} \frac{\partial}{\partial \rho} \left(\rho \frac{\partial}{\partial \rho} \Pi_{2z} \right) \right] \quad (\text{B.2})$$

$$\because \frac{\partial^2}{\partial z^2} \Pi_{2z} = -\xi_2^2 \Pi_{2z} \quad (\text{B.3})$$

$$\begin{aligned} \& \frac{1}{\rho} \frac{\partial}{\partial \rho} \left(\rho \frac{\partial}{\partial \rho} \Pi_{2z} \right) = \frac{2}{\pi} \int_0^\infty T(\xi) (\xi_2^2 - k_2^2) \cdot \\ & \left[\frac{K'_0 \left(\rho \sqrt{\xi_2^2 - k_2^2} \right)}{\rho \sqrt{\xi_2^2 - k_2^2}} + K_0'' \left(\rho \sqrt{\xi_2^2 - k_2^2} \right) \right] \cos(\xi_2 z - \xi h) d\xi \end{aligned} \quad (\text{B.4})$$

Using the properties of the modified Bessel function of the second type [23], namely:

$$K_0(z) = \frac{K'_0(z)}{z} + K_0''(z) \quad (\text{B.5})$$

$$\begin{aligned} \therefore \nabla^2 \Pi_{2z} &= \frac{2}{\pi} \int_0^\infty T(\xi) (-\xi_2^2 + \xi_2^2 - k_2^2) K_0 \left(\rho \sqrt{\xi_2^2 - k_2^2} \right) \cos(\xi_2 z - \xi h) d\xi \\ \Rightarrow \nabla^2 \Pi_{2z} &= -k_2^2 \Pi_{2z} \end{aligned} \quad (\text{B.6})$$

Therefore, Π_{2z} satisfies the wave equation in medium (2). Examining the boundary conditions in (2.16) implies to:

$$\begin{aligned} \frac{\partial}{\partial z} \Pi_{1z} &= \frac{2}{\pi} \int_0^{\infty} [-\xi] K_0 \left(\rho \sqrt{\xi^2 - k_1^2} \right) \sin(\xi(z-h)) d\xi \\ &+ \frac{2}{\pi} \int_0^{\infty} [-\xi R(\xi)] K_0 \left(\rho \sqrt{\xi^2 - k_1^2} \right) \sin(\xi(z+h)) d\xi \end{aligned} \quad (\text{B.7})$$

$$\frac{\partial}{\partial z} \Pi_{2z} = \frac{2}{\pi} \int_0^{\infty} [-\xi_2 T(\xi)] K_0 \left(\rho \sqrt{\xi_2^2 - k_2^2} \right) \sin(\xi_2 z - \xi h) d\xi \quad (\text{B.8})$$

$$\therefore \frac{\partial}{\partial z} \Pi_{1z} = \frac{\partial}{\partial z} \Pi_{2z} \quad \text{at } z=0 \quad (\text{B.9})$$

$$\begin{aligned} \therefore \frac{2}{\pi} \int_0^{\infty} [-\xi + \xi R(\xi)] K_0 \left(\rho \sqrt{\xi^2 - k_1^2} \right) \sin(-\xi h) d\xi \\ = \frac{2}{\pi} \int_0^{\infty} [-\xi_2 T(\xi)] K_0 \left(\rho \sqrt{\xi_2^2 - k_2^2} \right) \sin(-\xi h) d\xi \end{aligned} \quad (\text{B.10})$$

For the above equation to be satisfied at all values of ρ ,

$$\sqrt{\xi^2 - k_1^2} = \sqrt{\xi_2^2 - k_2^2} \Rightarrow \xi_2^2 = \xi^2 - k_1^2 + k_2^2 \quad (\text{B.11})$$

which is the phase matching condition; since the integration is done over the vertical (normal to the boundary) component of the propagation vector. Furthermore, to be satisfied at all values of ρ :

$$-\xi + \xi R(\xi) = -\xi_2 T(\xi) \quad (\text{B.12})$$

One more equation is still needed to find the expressions for $T(\xi)$ and $R(\xi)$. This equation comes from the remaining boundary condition (2.17):

$$\Pi_{1z} = \varepsilon \Pi_{2z} \quad \text{at } z=0 \quad (\text{B.13})$$

$$\begin{aligned}
& \therefore \frac{2}{\pi} \int_0^{\infty} [1 + R(\xi)] K_0 \left(\rho \sqrt{\xi^2 - k_1^2} \right) \cos(\xi h) d\xi \\
& = \frac{2}{\pi} \int_0^{\infty} [\varepsilon T(\xi)] K_0 \left(\rho \sqrt{\xi^2 - k_2^2} \right) \cos(\xi h) d\xi
\end{aligned} \tag{B.14}$$

The above equation again implies the phase matching condition, and gives one more equation in $T(\xi)$ and $R(\xi)$:

$$1 + R(\xi) = \varepsilon T(\xi) \tag{B.15}$$

Solving the two equations (B.12) and (B.15) gives:

$$R(\xi) = \frac{\varepsilon \xi - \sqrt{\xi^2 - (1 - \varepsilon)k_1^2}}{\varepsilon \xi + \sqrt{\xi^2 - (1 - \varepsilon)k_1^2}} \tag{B.16}$$

$$T(\xi) = \frac{2\xi}{\varepsilon \xi + \sqrt{\xi^2 - (1 - \varepsilon)k_1^2}} \tag{B.17}$$

It is interesting to note that (B.16) and (B.17) can be achieved by substituting (A.21) in the functions originally given by Sommerfeld in his formal solution, shown below [1]:

$$R(\lambda) = \frac{\varepsilon \sqrt{\lambda^2 - k_1^2} - \sqrt{\lambda^2 - k_2^2}}{\varepsilon \sqrt{\lambda^2 - k_1^2} + \sqrt{\lambda^2 - k_2^2}} \tag{B.18}$$

$$T(\lambda) = \frac{2\sqrt{\lambda^2 - k_1^2}}{\varepsilon \sqrt{\lambda^2 - k_1^2} + \sqrt{\lambda^2 - k_2^2}} \tag{B.19}$$

However, it is important to get the expressions as shown in this appendix since the integrals include inhomogeneous waves which are hard to predict their associated reflection coefficients.

Appendix C: Validation of the Horizontal Dipole Formulation

In this appendix, it is required to prove the validity of the forms in (3.13), (3.17)-(3.20). It is sufficient to do it for one of the two media. If we choose medium (2), the vector potential is assumed to be:

$$\vec{\Pi}_2 = \Pi_{2x} \hat{a}_x + \Pi_{2z} \hat{a}_z \quad (\text{C.1})$$

In this section, the proof is given in cylindrical coordinates. This decision was taken to prove the validity of the assumed forms for any horizontal dipole (parallel to the x - y plane). However, without loss of this generality, the dipole is assumed to be x -oriented as shown in Fig. 1, where for any other horizontal dipole which makes an angle φ_0 from the x -axis, it would be sufficient just to replace the term φ by $(\varphi - \varphi_0)$ in the rest of the proof.

In cylindrical coordinates the vector potential is given by:

$$\vec{\Pi}_2 = \cos \varphi \Pi_{2x} \hat{a}_\rho - \sin \varphi \Pi_{2x} \hat{a}_\varphi + \Pi_{2z} \hat{a}_z \quad (\text{C.2})$$

It is required to prove that:

$$\nabla^2 \vec{\Pi}_2 + k_2^2 \vec{\Pi}_2 = 0 \quad (\text{C.3})$$

where
$$\nabla^2 \vec{\Pi}_2 = \nabla(\nabla \cdot \vec{\Pi}_2) - \nabla \times \nabla \times \vec{\Pi}_2 \quad (\text{C.4})$$

In cylindrical coordinates, the vector Laplace operator is defined as:

$$\begin{aligned}
\nabla^2 \vec{\Pi}_2 = & \hat{a}_\rho \left(\nabla^2 \cos \varphi \Pi_{2x} + \frac{2}{\rho^2} \frac{\partial}{\partial \varphi} \sin \varphi \Pi_{2x} - \frac{\cos \varphi}{\rho^2} \Pi_{2x} \right) \\
& + \hat{a}_\varphi \left(-\nabla^2 \sin \varphi \Pi_{2x} + \frac{2}{\rho^2} \frac{\partial}{\partial \varphi} \cos \varphi \Pi_{2x} + \frac{\sin \varphi}{\rho^2} \Pi_{2x} \right) \\
& + \hat{a}_z (\nabla^2 \Pi_{2z})
\end{aligned} \tag{C.5}$$

From the ρ -component:

$$\nabla^2 \cos \varphi \Pi_{2x} = \frac{1}{\rho} \frac{\partial}{\partial \rho} \left(\rho \frac{\partial}{\partial \rho} \cos \varphi \Pi_{2x} \right) + \frac{1}{\rho^2} \frac{\partial^2}{\partial \varphi^2} \cos \varphi \Pi_{2x} + \frac{\partial^2}{\partial z^2} \cos \varphi \Pi_{2x} \tag{C.6}$$

where the first term of (C.6) is given by:

$$\begin{aligned}
\frac{1}{\rho} \frac{\partial}{\partial \rho} \left(\rho \frac{\partial}{\partial \rho} \cos \varphi \Pi_{2x} \right) &= \frac{2}{\pi} \cos \varphi \int_0^\infty T(\xi) (\xi^2 - k_2^2) \cdot \\
&\cdot \left(K_0''(\rho \sqrt{\xi^2 - k_2^2}) + \frac{K_0'(\rho \sqrt{\xi^2 - k_2^2})}{\rho \sqrt{\xi^2 - k_2^2}} \right) \cos(\xi_2 z - \xi h) d\xi
\end{aligned} \tag{C.7}$$

$$\because K_0(x) = K_0''(x) + \frac{K_0'(x)}{x} \tag{C.8}$$

$$\begin{aligned}
\therefore \frac{1}{\rho} \frac{\partial}{\partial \rho} \left(\rho \frac{\partial}{\partial \rho} \cos \varphi \Pi_{2x} \right) &= \frac{2}{\pi} \cos \varphi \int_0^\infty T(\xi) (\xi^2 - k_2^2) \\
&K_0(\rho \sqrt{\xi^2 - k_2^2}) \cos(\xi_2 z - \xi h) d\xi
\end{aligned} \tag{C.9}$$

The second term of (C.6) is given by:

$$\frac{1}{\rho^2} \frac{\partial^2}{\partial \varphi^2} \cos \varphi \Pi_{2x} = \frac{-\cos \varphi}{\rho^2} \Pi_{2x} \tag{C.10}$$

and the last term of (C.6) is given by:

$$\frac{\partial^2}{\partial z^2} \cos \varphi \Pi_{2x} = \frac{2}{\pi} \cos \varphi \int_0^\infty T(\xi) (-\xi^2) K_0(\rho \sqrt{\xi^2 - k_2^2}) \cos(\xi_2 z - \xi h) d\xi \tag{C.11}$$

The second term of the ρ -component in (C.5) is defined as:

$$\frac{2}{\rho^2} \frac{\partial}{\partial \varphi} \sin \varphi \Pi_{2x} = \frac{2 \cos \varphi}{\rho^2} \Pi_{2x} \quad (\text{C.12})$$

Adding all the equations (C.9)-(C.12) and substituting in the ρ - component of (C.5), then comparing the result to (3.18):

$$\Rightarrow \nabla^2 \cos \varphi \Pi_{2x} + \frac{2}{\rho^2} \frac{\partial}{\partial \varphi} \sin \varphi \Pi_{2x} - \frac{\cos \varphi}{\rho^2} \Pi_{2x} = -k_2^2 \cos \varphi \Pi_{2x} \quad (\text{C.13})$$

Similarly; from the φ -component of (C.5):

$$\begin{aligned} \nabla^2 (-\sin \varphi \Pi_{2x}) &= \frac{1}{\rho} \frac{\partial}{\partial \rho} \left(\rho \frac{\partial}{\partial \rho} (-\sin \varphi \Pi_{2x}) \right) \\ &+ \frac{1}{\rho^2} \frac{\partial^2}{\partial \varphi^2} (-\sin \varphi \Pi_{2x}) + \frac{\partial^2}{\partial z^2} (-\sin \varphi \Pi_{2x}) \end{aligned} \quad (\text{C.14})$$

where the first term of (C.14) is given by:

$$\begin{aligned} \frac{1}{\rho} \frac{\partial}{\partial \rho} \left(\rho \frac{\partial}{\partial \rho} (-\sin \varphi \Pi_{2x}) \right) &= \frac{2}{\pi} (-\sin \varphi) \int_0^\infty T(\xi) (\xi^2 - k_2^2) \cdot \\ &\cdot \left(K_0''(\rho \sqrt{\xi^2 - k_2^2}) + \frac{K_0'(\rho \sqrt{\xi^2 - k_2^2})}{\rho \sqrt{\xi^2 - k_2^2}} \right) \cos(\xi_2 z - \xi h) d\xi \end{aligned} \quad (\text{C.15})$$

Using (C.8) in (C.15), we get:

$$\begin{aligned} \frac{1}{\rho} \frac{\partial}{\partial \rho} \left(\rho \frac{\partial}{\partial \rho} (-\sin \varphi \Pi_{2x}) \right) &= \frac{2}{\pi} (-\sin \varphi) \int_0^\infty T(\xi) (\xi^2 - k_2^2) \\ &K_0(\rho \sqrt{\xi^2 - k_2^2}) \cos(\xi_2 z - \xi h) d\xi \end{aligned} \quad (\text{C.16})$$

The second term of (C.14) is given by:

$$\frac{1}{\rho^2} \frac{\partial^2}{\partial \varphi^2} (-\sin \varphi \Pi_{2x}) = \frac{\sin \varphi}{\rho^2} \Pi_{2x} \quad (\text{C.17})$$

and the last term of (C.14) is given by:

$$\frac{\partial^2}{\partial z^2} (-\sin \varphi \Pi_{2x}) = \frac{2}{\pi} (-\sin \varphi) \int_0^\infty T(\xi) (-\xi^2) K_0(\rho \sqrt{\xi^2 - k_2^2}) \cos(\xi_2 z - \xi h) d\xi \quad (\text{C.18})$$

The second term of the φ -component in (C.5) is defined as:

$$\frac{2}{\rho^2} \frac{\partial}{\partial \varphi} \cos \varphi \Pi_{2x} = \frac{-2 \sin \varphi}{\rho^2} \Pi_{2x} \quad (\text{C.19})$$

Adding all the equations (C.16)-(C.19) and substituting in the φ - component of (C.5), then comparing the result to (3.18):

$$\Rightarrow -\nabla^2 \sin \varphi \Pi_{2x} + \frac{2}{\rho^2} \frac{\partial}{\partial \varphi} \cos \varphi \Pi_{2x} + \frac{\sin \varphi}{\rho^2} \Pi_{2x} = k_2^2 \sin \varphi \Pi_{2x} \quad (\text{C.20})$$

Finally, from the z -component of (C.5):

$$\nabla^2 \Pi_{2z} = \frac{1}{\rho} \frac{\partial}{\partial \rho} \left(\rho \frac{\partial}{\partial \rho} \Pi_{2z} \right) + \frac{1}{\rho^2} \frac{\partial^2}{\partial \varphi^2} \Pi_{2z} + \frac{\partial^2}{\partial z^2} \Pi_{2z} \quad (\text{C.21})$$

The first term of (C.21) is given by:

$$\begin{aligned} \frac{1}{\rho} \frac{\partial}{\partial \rho} \left(\rho \frac{\partial}{\partial \rho} \Pi_{2z} \right) &= \frac{2}{\pi} \cos \varphi \int_0^\infty T_z(\xi) (\xi^2 - k_2^2) \cdot \\ &\cdot \left(\frac{K_1'(\rho \sqrt{\xi^2 - k_2^2})}{\rho \sqrt{\xi^2 - k_2^2}} + K_1''(\rho \sqrt{\xi^2 - k_2^2}) \right) \sin(\xi_2 z - \xi h) d\xi \end{aligned} \quad (\text{C.22})$$

while the second term of (C.21) can be written as:

$$\begin{aligned}
\frac{1}{\rho^2} \frac{\partial^2}{\partial \varphi^2} \Pi_{2z} &= \frac{-1}{\rho^2} \Pi_{2z} \\
&= \frac{2}{\pi} \cos \varphi \int_0^\infty T_z(\xi) \left(\frac{-1}{\rho^2} \right) K_1(\rho \sqrt{\xi^2 - k_2^2}) \sin(\xi_2 z - \xi h) d\xi
\end{aligned} \tag{C.23}$$

and the last term of (C.21) is given by:

$$\begin{aligned}
\frac{\partial^2}{\partial z^2} \Pi_{2z} &= -\xi_2^2 \Pi_{2z} \\
&= \frac{2}{\pi} \cos \varphi \int_0^\infty T_z(\xi) (-\xi_2^2) K_1(\rho \sqrt{\xi^2 - k_2^2}) \sin(\xi_2 z - \xi h) d\xi
\end{aligned} \tag{C.24}$$

Adding (C.22)-(C.24), we get:

$$\begin{aligned}
\nabla^2 \Pi_{2z} &= \frac{2}{\pi} \cos \varphi \int_0^\infty T_z(\xi) \cdot \left\{ (\xi^2 - k_2^2) \cdot \right. \\
&\quad \left(\frac{K_1'(\rho \sqrt{\xi^2 - k_2^2})}{\rho \sqrt{\xi^2 - k_2^2}} + K_1''(\rho \sqrt{\xi^2 - k_2^2}) - \frac{K_1(\rho \sqrt{\xi^2 - k_2^2})}{\rho^2 (\xi^2 - k_2^2)} \right) \\
&\quad \left. - \xi_2^2 K_1(\rho \sqrt{\xi^2 - k_2^2}) \right\} \sin(\xi_2 z - \xi h) d\xi
\end{aligned} \tag{C.25}$$

Utilizing some properties of the modified Bessel function of the second kind [23]:

$$\therefore K_1'(x) = -K_0(x) + \frac{-K_1(x)}{x} \tag{C.26}$$

$$\therefore K_1''(x) = -K_0'(x) - \left[\frac{xK_1'(x) - K_1(x)}{x^2} \right] \tag{C.27}$$

$$\therefore K_1(x) = -K_0'(x) \tag{C.28}$$

$$\therefore K_1''(x) = K_1(x) - \frac{K_1'(x)}{x} + \frac{K_1(x)}{x^2} \tag{C.29}$$

$$\Rightarrow \frac{K_1'(x)}{x} + K_1''(x) - \frac{K_1(x)}{x^2} = K_1(x) \tag{C.30}$$

Substituting (C.30) in (C.25) and comparing to (3.20), we get:

$$\Rightarrow \nabla^2 \Pi_{2z} = \frac{2}{\pi} \cos \varphi \int_0^{\infty} T_z(\xi) \cdot \left\{ (\xi^2 - k_2^2) \cdot K_1(\rho \sqrt{\xi^2 - k_2^2}) - \xi^2 K_1(\rho \sqrt{\xi^2 - k_2^2}) \right\} \sin(\xi_2 z - \xi h) d\xi \quad (\text{C.31})$$

$$\text{i.e. } \nabla^2 \Pi_{2z} = -k_2^2 \Pi_{2z} \quad (\text{C.32})$$

Using (C.13), (C.20) and (C.32) in (C.5) and comparing to (C.2), we get:

$$\begin{aligned} \nabla^2 \vec{\Pi}_2 &= \hat{a}_\rho \left(-k_2^2 \cos \varphi \Pi_{2x} \right) + \hat{a}_\varphi \left(k_2^2 \sin \varphi \Pi_{2x} \right) + \hat{a}_z \left(-k_2^2 \Pi_{2z} \right) \\ &= -k_2^2 \vec{\Pi}_2 \end{aligned} \quad (\text{C.33}) \quad \text{Q.E.D.}$$

Appendix D: Sommerfeld Formulation for Horizontal Dipoles

In this appendix, the original solution of Sommerfeld for the horizontal case is shown for the sake of comparison. The forms of the solutions assumed by Sommerfeld were [21]:

$$\Pi_{1x}^{prim} = \int_0^{\infty} J_0(\lambda\rho) e^{-|z-h|\sqrt{\lambda^2-k_1^2}} \frac{\lambda}{\sqrt{\lambda^2-k_1^2}} d\lambda = \frac{e^{-jk_1r_1}}{r_1} \quad (D.1)$$

$$\Pi_{1x}^{sec} = \int_0^{\infty} R(\lambda) J_0(\lambda\rho) e^{-(z+h)\sqrt{\lambda^2-k_1^2}} \frac{\lambda}{\sqrt{\lambda^2-k_1^2}} d\lambda \quad (D.2)$$

$$\Pi_{2x}^{sec} = \int_0^{\infty} T(\lambda) J_0(\lambda\rho) e^{z\sqrt{\lambda^2-k_2^2}-h\sqrt{\lambda^2-k_1^2}} \frac{\lambda}{\sqrt{\lambda^2-k_1^2}} d\lambda \quad (D.3)$$

$$\Pi_{1z}^{sec} = \cos\varphi \int_0^{\infty} R_z(\lambda) J_1(\lambda\rho) e^{-(z+h)\sqrt{\lambda^2-k_1^2}} \frac{\lambda}{\sqrt{\lambda^2-k_1^2}} d\lambda \quad (D.4)$$

$$\Pi_{2z}^{sec} = \cos\varphi \int_0^{\infty} T_z(\lambda) J_1(\lambda\rho) e^{z\sqrt{\lambda^2-k_2^2}-h\sqrt{\lambda^2-k_1^2}} \frac{\lambda}{\sqrt{\lambda^2-k_1^2}} d\lambda \quad (D.5)$$

From the boundary conditions, we can define the functions:

$$R(\lambda) = \frac{\sqrt{\lambda^2-k_1^2} - \sqrt{\lambda^2-k_2^2}}{\sqrt{\lambda^2-k_1^2} + \sqrt{\lambda^2-k_2^2}} \quad (D.6)$$

$$T(\lambda) = \frac{2}{\varepsilon} \frac{\sqrt{\lambda^2-k_1^2}}{\sqrt{\lambda^2-k_1^2} + \sqrt{\lambda^2-k_2^2}} \quad (D.7)$$

$$R_z(\lambda) = \frac{-2\lambda\sqrt{\lambda^2-k_1^2}}{k_1^2} \frac{\sqrt{\lambda^2-k_1^2} - \sqrt{\lambda^2-k_2^2}}{\varepsilon\sqrt{\lambda^2-k_1^2} + \sqrt{\lambda^2-k_2^2}} \quad (D.8)$$

$$T_z(\lambda) = \frac{-2\lambda\sqrt{\lambda^2 - k_1^2}}{k_2^2} \frac{\sqrt{\lambda^2 - k_1^2} - \sqrt{\lambda^2 - k_2^2}}{\varepsilon\sqrt{\lambda^2 - k_1^2} + \sqrt{\lambda^2 - k_2^2}} \quad (\text{D.9})$$

Following a procedure like what is shown in Chapter 3, one can write the electric field expressions as:

$$E_x = k_1^2(g_0 - g_1 + g_{sH}^{Som}) + \frac{\partial}{\partial x} \left(\frac{\partial}{\partial x} (g_0 - g_1 + g_3^{Som}) \right) \quad (\text{D.10})$$

$$E_y = \frac{\partial}{\partial y} \left(\frac{\partial}{\partial x} (g_0 - g_1 + g_3^{Som}) \right) \quad (\text{D.11})$$

$$E_z = k_1^2 \frac{\partial}{\partial x} g_2^{Som} + \frac{\partial}{\partial z} \left(\frac{\partial}{\partial x} (g_0 - g_1 + g_3^{Som}) \right) \quad (\text{D.12})$$

where g_0 and g_1 are defined in (3.26), while g_{sH}^{Som} , g_2^{Som} and g_3^{Som} are defined as: (The superscript “Som” stands for Sommerfeld formulation)

$$g_{sH}^{Som} = \int_0^\infty \frac{2\sqrt{\lambda^2 - k_1^2}}{\sqrt{\lambda^2 - k_1^2} + \sqrt{\lambda^2 - k_2^2}} J_0(\lambda\rho) e^{-(z+h)\sqrt{\lambda^2 - k_1^2}} \frac{\lambda}{\sqrt{\lambda^2 - k_1^2}} d\lambda \quad (\text{D.13})$$

$$g_2^{Som} = \int_0^\infty \frac{2\sqrt{\lambda^2 - k_1^2}}{k_1^2} \cdot \frac{\sqrt{\lambda^2 - k_1^2} - \sqrt{\lambda^2 - k_2^2}}{\varepsilon\sqrt{\lambda^2 - k_1^2} + \sqrt{\lambda^2 - k_2^2}} J_0(\lambda\rho) e^{-(z+h)\sqrt{\lambda^2 - k_1^2}} \frac{\lambda}{\sqrt{\lambda^2 - k_1^2}} d\lambda \quad (\text{D.14})$$

$$g_3^{Som} = \int_0^\infty \frac{2\sqrt{\lambda^2 - k_1^2}}{\varepsilon\sqrt{\lambda^2 - k_1^2} + \sqrt{\lambda^2 - k_2^2}} J_0(\lambda\rho) e^{-(z+h)\sqrt{\lambda^2 - k_1^2}} \frac{\lambda}{\sqrt{\lambda^2 - k_1^2}} d\lambda \quad (\text{D.15})$$

Appendix E: Derivation of the Boundary Conditions for the Horizontal Dipole Case

In this appendix, the derivation of the expressions (3.21)-(3.24) is shown based on the boundary conditions (3.8)-(3.11).

Substituting (3.17)-(3.19) in (3.8) at $z = 0$ and for all values of ρ gives:

$$\sqrt{\xi^2 - k_1^2} = \sqrt{\xi_2^2 - k_2^2} \Rightarrow \xi_2^2 = \xi^2 - k_1^2 + k_2^2 \quad (\text{E.1})$$

and
$$1 + R(\xi) = \varepsilon T(\xi) \quad (\text{E.2})$$

Equation (E.1) is the phase matching condition; since the integration is done over the vertical (normal to the boundary) component of the propagation vector. Substituting (3.17)-(3.19) in (3.9) at $z = 0$ and for all values of ρ gives:

$$-\xi + \xi R(\xi) = -\varepsilon \xi T(\xi) \quad (\text{E.3})$$

Solving (E.2) and (E.3) simultaneously gives the expressions in (3.21) and (3.22).

Substituting (3.19)-(3.20) in (3.10) at $z = 0$ gives:

$$R_z(\xi) = -\varepsilon T_z(\xi) \quad (\text{E.4})$$

To apply the boundary condition in (3.11), the following expressions are useful:

$$\frac{\partial}{\partial z} \Pi_{1z}^{\text{sec}} = \frac{2}{\pi} \cos \varphi \int_0^{\infty} \xi R_z(\xi) K_1(\rho \sqrt{\xi^2 - k_1^2}) \cos(\xi(z+h)) d\xi \quad (\text{E.5})$$

$$\frac{\partial}{\partial z} \Pi_{2z}^{\text{sec}} = \frac{2}{\pi} \cos \varphi \int_0^{\infty} \xi_2 T_z(\xi) K_1(\rho \sqrt{\xi_2^2 - k_2^2}) \cos(\xi_2 z - \xi h) d\xi \quad (\text{E.6})$$

$$\frac{\partial}{\partial x} \Pi_{2x}^{\text{sec}} = \frac{2}{\pi} \cos \varphi \int_0^{\infty} -\sqrt{\xi^2 - k_2^2} T(\xi) K_1(\rho \sqrt{\xi^2 - k_2^2}) \cos(\xi_2 z - \xi h) d\xi \quad (\text{E.7})$$

$$\frac{\partial}{\partial x} \Pi_{1x}^{\text{prim}} = \frac{2}{\pi} \cos \varphi \int_0^{\infty} -\sqrt{\xi^2 - k_1^2} K_1(\rho \sqrt{\xi^2 - k_1^2}) \cos(\xi(z - h)) d\xi \quad (\text{E.8})$$

$$\frac{\partial}{\partial x} \Pi_{1x}^{\text{sec}} = \frac{2}{\pi} \cos \varphi \int_0^{\infty} -\sqrt{\xi^2 - k_1^2} R(\xi) K_1(\rho \sqrt{\xi^2 - k_1^2}) \cos(\xi(z + h)) d\xi \quad (\text{E.9})$$

Using (E.5)-(E.9) in (3.11) gives:

$$\xi R_z(\xi) - \xi_2 T_z(\xi) = -\sqrt{\xi^2 - k_2^2} T(\xi) + \sqrt{\xi^2 - k_1^2} (1 + R(\xi)) \quad (\text{E.10})$$

Solving (E.4) and (E.10) simultaneously and using (E.1)-(E.3) give the expressions in (3.23) and (3.24).

References

- [1] A. Sommerfeld, "Propagation of waves in wireless telegraphy," *Annalen Der Physik*, vol. 28, pp. 665-736, 1909.
- [2] A. Banos, *Dipole Radiation in the Presence of a Conducting Half-Space*, Oxford, England: Pergamon Press, 1966.
- [3] R. Collin, "Hertzian dipole radiating over a lossy earth or sea: some early and late 20th-century controversies," *Antennas and Propagation Magazine, IEEE*, vol. 46, no. 2, pp. 64-79, April 2004.
- [4] B. Van Der Pol, "Theory of the reflection of the light from a point source by a finitely conducting flat mirror, with an application to radiotelegraphy," *Physica*, vol. 2, pp. 843-853, 1935.
- [5] A. Goldsmith, *Wireless Communications*, Cambridge University Press, 2005.
- [6] K. Fujimoto, *Mobile Antenna Systems Handbook*, Third Edition ed., Artech House, 2008.
- [7] T. Kaiser, "When will smart antennas be ready for the market? Part I," *Signal Processing Magazine, IEEE*, vol. 22, no. 2, pp. 87-92, March 2005.
- [8] F. Rayal, "Why have smart antennas not yet gained traction with wireless network operators?," *Antennas and Propagation Magazine, IEEE*, vol. 47, no. 6, pp. 124-126, Dec 2005.
- [9] T. Sarkar, W. Dyab, M. Abdallah, M. Salazar-Palma, M. Prasad, S. W. Ting and S. Barbin, "Electromagnetic Macro Modeling of Propagation in Mobile Wireless Communication: Theory and Experiment," *Antennas and Propagation Magazine, IEEE*, vol. 54, no. 6, pp. 17-43, December 2012.
- [10] T. K. Sarkar, W. M. G. Dyab, M. N. Abdallah, M. Salazar-Palma, M. V. S. N. Prasad, S. Barbin and S. W. Ting, "Physics of propagation in a cellular wireless communication environment," *URSI Radio Sci. Bulletin*, vol. 343, December 2012.
- [11] S. Schelkunoff, *Electromagnetic waves*, New York, NY USA: D. Van Nostrand, 1943.
- [12] G. Tyras, *Radiation and Propagation of electromagnetic waves*, New York, NY USA: Academic Press, 1969.
- [13] S. A. Schelkunoff, "Modified Sommerfeld's integral and its applications," *Proc. Inst. Radio Engr.*, vol. 24, no. 10, pp. 1388-1398, 1936.
- [14] K. Michalski, "Extrapolation methods for Sommerfeld integral tails," *Antennas and Propagation, IEEE Transactions on*, vol. 46, no. 10, pp. 1405-1418, Oct 1998.
- [15] M. Yuan and T. Sarkar, "Computation of the Sommerfeld Integral tails using the matrix pencil method," *Antennas and Propagation, IEEE Transactions on*, vol. 54, no. 4, pp. 1358-1362, April 2006.

- [16] R. Golubovic, A. Polimeridis and J. Mosig, "Efficient Algorithms for Computing Sommerfeld Integral Tails," *Antennas and Propagation, IEEE Transactions on*, vol. 60, no. 5, pp. 2409-2417, May 2012.
- [17] M. Yuan, Y. Zhang, A. De, Z. Ji and T. Sarkar, "Two-Dimensional Discrete Complex Image Method (DCIM) for Closed-Form Green's Function of Arbitrary 3D Structures in General Multilayered Media," *Antennas and Propagation, IEEE Transactions on*, vol. 56, no. 5, pp. 1350-1357, May 2008.
- [18] L. F. Shampine, "Vectorized adaptive quadrature in MATLAB," *J. Comp. Appl. Math.*, vol. 211, pp. 131-140, 2008.
- [19] J. R. Mosig and F. E. Gardiol, "Analytical and numerical techniques in the Green's function treatment of microstrip antennas and scatterers," *Proc. Inst. Elec. Eng. H Microw., Opt. Antennas*, vol. 130, no. 2, pp. 175-182, 1983.
- [20] T. Okumura, E. Ohmori and K. Fukuda, "Field strength and its variability in VHF and UHF land mobile service," *Rev. Elect. Commun. Lab.*, vol. 16, no. 9-10, pp. 825-873, 1968.
- [21] A. Sommerfeld, *Partial differential equations in physics*, New York: Academic Press, 1964.
- [22] T. Sarkar, "Analysis of arbitrarily oriented thin wire antennas over a plane imperfect ground," *AEU*, vol. 31, no. 11, pp. 449-457, 1977.
- [23] M. Abramowitz and I. A. Stegun, *Handbook of Mathematical Functions*, vol. Series #55, Mineola, NY USA: National Bureau of Standards, 1965.
- [24] T. Kahan and G. Eckart, "On the Existence of a Surface Wave in Dipole Radiation over a Plane Earth," *Proceedings of the IRE*, vol. 38, no. 7, pp. 807-812, July 1950.
- [25] J. A. Kong, *Electromagnetic wave theory*, Cambridge, Massachusetts: EMW Publishing, 2005.
- [26] C. Burrows, "The Surface Wave in Radio Propagation over Plane Earth," *Radio Engineers, Proceedings of the Institute of*, vol. 25, no. 2, pp. 219-229, Feb 1937.
- [27] J. R. Wait, "Asymptotic theory for dipole radiation in the presence of a lossy slab lying on a conducting half-space," *Antennas and Propagation, IEEE Transactions on*, vol. 15, no. 5, pp. 645-648, September 1967.
- [28] S. Schelkunoff, "Anatomy of "Surface waves"," *Antennas and Propagation, IRE Transactions on*, vol. 7, no. 5, pp. 133-139, December 1959.
- [29] D. Sarid and W. Challener, *Modern introduction to surface plasmons: Theory, mathematic modeling and applications*, Cambridge University Press, 2010.
- [30] T.-I. Jeon and D. Grischkowsky, "THz Zenneck surface wave (THz surface plasmon) propagation on a metal sheet," *Applied Physics Letters*, vol. 88, no. 6, pp. -, 2006.
- [31] T.-I. Jeon, J. Zhang and D. Grischkowsky, "THz Sommerfeld wave propagation on a single metal wire," *Applied Physics Letters*, vol. 86, no. 16, pp. -, 2005.
- [32] D. Schumacher, C. Rea, D. Heitmann and K. Scharnberg, "Surface plasmons and Sommerfeld-Zenneck waves on corrugated surfaces:: Application to high-Tc superconductors," *Surface Science*, vol. 408, no. 3, pp. 203-211, 1998.

- [33] R. H. Ritchie, "Plasma Losses by Fast Electrons in Thin Films," *Phys. Rev.*, vol. 106, pp. 874-881, Jun 1957.
- [34] R. H. Ritchie, "Plasma losses by fast electrons in thin films," *ISI Current Contents*, vol. 3, 12 January 1985.
- [35] R. H. Ritchie and H. B. Eldridge, "Optical Emission from Irradiated Foils. I," *Phys. Rev.*, vol. 126, pp. 1935-1947, Jun 1962.
- [36] R. Ritchie, "Surface plasmons in solids," *Surface Science*, vol. 34, no. 1, pp. 1-19, 1973.
- [37] J. A. Stratton, *Electromagnetic theory*, New York: McGraw-Hill Book Company, 1941.
- [38] A. Otto, "Excitation of nonradiative surface plasma waves in silver by the method of frustrated total reflection," *Zeitschrift fur Physik*, vol. 216, no. 4, pp. 398-410, 1968.
- [39] H. Raether, *Surface plasmons on smooth and rough surfaces and on gratings*, Springer-Verlag Berlin Heidelberg, 1988.
- [40] T. W. Ebbesen, H. J. Lezec, H. F. Ghaemi, T. Thio and P. A. Wolff, "Extraordinary optical transmission through sub-wavelength hole arrays," *Nature*, vol. 391, no. 6668, pp. 667-669, Feb 1998.
- [41] L. Martin-Moreno, F. J. Garcia-Vidal, H. J. Lezec, K. M. Pellerin, T. Thio, J. B. Pendry and T. W. Ebbesen, "Theory of Extraordinary Optical Transmission through Subwavelength Hole Arrays," *Phys. Rev. Lett.*, vol. 86, no. 6, pp. 1114-1117, Feb 2001.
- [42] H. Lezec and T. Thio, "Diffracted evanescent wave model for enhanced and suppressed optical transmission through subwavelength hole arrays," *Opt. Express*, vol. 12, no. 16, pp. 3629-3651, Aug 2004.
- [43] G. Gay, O. Alloschery, B. V. de Lesegno, J. Weiner and H. J. Lezec, "Surface Wave Generation and Propagation on Metallic Subwavelength Structures Measured by Far-Field Interferometry," *Phys. Rev. Lett.*, vol. 96, p. 213901, Jun 2006.
- [44] J. Zenneck, "Propagation of Plane Electromagnetic Waves along a Plane Conducting Surface and Its Bearing on the Theory of Transmission in Wireless Telegraphy," *Annalen Der Physik*, vol. 23, pp. 846-866, 1907.
- [45] S. A. Maier, S. R. Andrews, L. Martin-Moreno and F. J. Garcia-Vidal, "Terahertz Surface Plasmon-Polariton Propagation and Focusing on Periodically Corrugated Metal Wires," *Phys. Rev. Lett.*, vol. 97, p. 176805, Oct 2006.
- [46] G. Goubau, "Surface Waves and Their Application to Transmission Lines," *Journal of Applied Physics*, vol. 21, no. 11, pp. 1119-1128, Nov 1950.
- [47] J. A. Deibel, K. Wang, M. Escarra, N. Berndsen and D. M. Mittleman, "The excitation and emission of terahertz surface plasmon polaritons on metal wire waveguides," *Comptes Rendus Physique*, vol. 9, no. 2, pp. 215-231, 2008.
- [48] M. Nagel, A. Michalski, T. Botzem and H. Kurz, "Near-field investigation of THz surface-wave emission from optically excited graphite flakes," *Opt. Express*, vol. 19, no. 5, pp. 4667-4672, Feb 2011.

- [49] S. Li, M. M. Jadidi, T. E. Murphy and G. Kumar, "Terahertz surface plasmon polaritons on a semiconductor surface structured with periodic V-grooves," *Opt. Express*, vol. 21, no. 6, pp. 7041-7049, Mar 2013.
- [50] M. Kuttge, J. G. Rivas, J. Saxler, P. Bolivar and H. Kurz, "Terahertz surface plasmon polaritons on metal and semiconductor surfaces," in *Infrared and Millimeter Waves, 2004 and 12th International Conference on Terahertz Electronics, 2004. Conference Digest of the 2004 Joint 29th International Conference on*, 2004.
- [51] J. Zhang, L. Zhang and W. Xu, "Surface plasmon polaritons: physics and applications," *Journal of Physics D: Applied Physics*, vol. 45, no. 11, p. 113001, 2012.
- [52] C. Caloz, C.-J. Lee, D. Smith, J. Pendry and T. Itoh, "Existence and properties of microwave surface plasmons at the interface between a right-handed and a left-handed media," in *Antennas and Propagation Society International Symposium, 2004. IEEE*, 2004.
- [53] A. Ishimaru, *Electromagnetic Wave Propagation, Radiation, and Scattering*, Englewood Cliffs, New Jersey, 1991.
- [54] L. Wang, J.-X. Cao, Y. Lv, L. Liu, T.-Y. Niu and Y.-C. Du, "Experimental study of surface-wave-assisted microwave transmission through a single subwavelength slit," *Journal of Applied Physics*, vol. 105, no. 9, pp. -, 2009.
- [55] A. Sihvola, J. Qi and I. Lindell, "Bridging the Gap Between Plasmonics and Zenneck Waves," *Antennas and Propagation Magazine, IEEE*, vol. 52, no. 1, pp. 124-136, Feb 2010.
- [56] R. Gordon, "Surface plasmon nanophotonics: A tutorial," *IEEE Nanotechnology magazine*, September 2008.
- [57] A. R. Djordjevic, M. B. Bazdar, T. K. Sarkar and R. F. Harrington, *AWAS version 2.0: Analysis of Wire Antennas and Scatterers, Software and User's Manual*, Norwood, MA, USA: Artech House, 2002.
- [58] H. E. M. Barlow, "Surface Waves: A proposed definition," *Proceedings of the IEE - Part B: Electronic and Communication Engineering*, vol. 107, no. 33, p. 240, 1960.
- [59] G. Goubau, "Waves on interfaces," *Antennas and Propagation, IRE Transactions on*, vol. 7, no. 5, pp. 140-146, December 1959.
- [60] S. Enoch and N. Bonod, *Plasmonics: From basics to advanced topics*, Springer-Verlag Berlin Heidelberg, 2012.

Biography

NAME OF AUTHOR: Walid Mohamed Galal Dyab

PLACE OF BIRTH: Alexandria, Egypt

DATE OF BIRTH: September 17, 1981

GRADUATE AND UNDERGRADUATE SCHOOLS ATTENDED:

Alexandria University, Alexandria, Egypt

DEGREES AWARDED:

Master of Science in Electrical Engineering, 2007

Bachelor of Science in Electrical Engineering, 2003

AWARDS AND HONORS:

IEEE Antennas and Propagation Society Doctoral Research Award, Nov2012

Syracuse University Graduate Fellowship Award, 2009, 2010, 2011

PROFESSIONAL EXPERIENCE:

Teaching Assistant, Department of Electrical Engineering, Syracuse University, Syracuse NY, USA, 2012-2014

Teaching and Research Assistant, Faculty of Information Engineering and Technology, German University in Cairo (GUC), Cairo, Egypt, 2006-2009

Technical Support Engineer, Alcatel, 2005-2006

Teaching Assistant, Department of Electrical Engineering, Alexandria Institute of Technology (AIT), Alexandria, Egypt 2003-2005